APPLICATION OF MECHANISTIC ENZYMOLOGY IN IDENTIFYING INHIBITORS OF CRITICAL ENZYMES FROM HUMAN PATHOGENS

A Dissertation

by

DEMETRIOS HARRY KOSTOMIRIS

Submitted to the Graduate and Professional School of
Texas A&M University
in partial fulfillment of the requirements for the degree of

DOCTOR OF PHILOSOPHY

Chair of Committee,	Jorge Cruz-Reyes
Committee Members,	Thomas D. Meek
	Tadhg P. Begley
	Frank M. Raushel
Head of Department,	Joshua A. Wand

August 2021

Major Subject: Biochemistry

ABSTRACT

The single-celled pathogens *Mycobacterium tuberculosis* and *Trypanosoma cruzi* are the causative agents of the human diseases tuberculosis and Chagas disease, respectively. In an effort to develop potentially new treatments for both of these diseases we have utilized an understanding of enzyme mechanisms to guide the identification and development of potential inhibitors for critical enzymes of these two pathogens.

In chapter II the work towards developing/discovering inhibitors of the D-alanine:D-alanine ligase enzyme from *M. tuberculosis* (*Mt*Ddl) is detailed. *Mt*Ddl is a target for the antibiotic D-cycloserine (DCS), the use of which is limited, in part, due to side-effects associated with the drug. The goal of this study was to determine if alternative D-alanine-like molecules could inhibit the function of this enzyme *in vitro*. The inhibitory effect of a small library of D-alanine analogs was evaluated. *Mt*Ddl was found to have a high degree of ligand selectivity; however two compounds that mimic the catalytic intermediates were characterized by kinetic and biochemical methods. The results of this study showed that both of these compounds exhibit similar inhibitory potency to DCS. Additionally, evidence for DCS phosphorylation was provided by positional isotope exchange, supporting a mechanism of inhibition which contradicts previous studies.

In chapter III the study of a hypoxanthine-guanine phosphoribosyltransferase (HGPRT) enzyme from *T. cruzi* is discussed. Due to the role of HGPRTs in purine salvage, these enzymes are promising targets for the development of new treatments for Chagas disease. In this study we have found that *T. cruzi* CL Brener strain possesses a pair of functionally identical genes encoding enzymes with HGPRT activity *in vitro*. One of these enzymes was further characterized and was found to be rate-limited by product release, which prevented accurate measurement of kinetic isotope effects. Potential transition-state analogs were tested against the enzyme and the most potent of which were found to bind with low nanomolar affinity. Analysis of the structure-activity relationship of the putative transition-state analog inhibitors provided convincing evidence for a chemical mechanism involving an S_N1-like transition-state.

ACKNOWLEDGEMENTS

I would like to thank my research advisor, Dr. Thomas D. Meek, for providing guidance and support. I would also like to thank my committee members: Dr. Tadhg P. Begley, Dr. Frank M. Raushel, and Dr. Jorge Cruz-Reyes, for providing me with thoughtful discussions and advice. Finally, I would like to thank my colleagues and friends for making the time during my study enjoyable.

CONTRIBUTORS AND FUNDING SOURCES

Contributors

This work was supervised by a thesis committee consisting of Professor Thomas D. Meek of the Department of Biochemistry and Biophysics, Professor Jorge Cruz-Reyes of the Departments of Biochemistry and Biophysics and Genetics, Professor Frank M. Raushel of the Departments of Chemistry and Biochemistry and Biophysics, and Professor Tadhg P. Begley of the Department of Chemistry.

In Chapter II the plasmid containing the gene for *Mycobacterium tuberculosis* D-alanine:D-alanine ligase was provided by Professor Luiz Pedro S. de Carvalho

In Chapter III Dr. Ardala Katzfuss designed the plasmids for the heterologous expression of *Tryanosoma cruzi* HGPRT enzymes, *Trypanosoma brucei brucei* adenine phosphoribosyltransferase, and *Saccharomyces cerevisiae* adenine deaminase. Dr. Katzfuss also performed the initial expression and purification tests for HGPRTs, and expressed and purified adenine deaminase. Professors Vern Schramm and Peter Tyler provided putative transition-state analog inhibitors. Professor Vern Schramm provided radiolabeled AMPs. Ryan Bringenberg characterized allopurinol kinetics and co-performed KIE and radiosynthesis.

Funding Sources

This work was funded by the Department of Biochemistry and Biophysics Startup fund and the National Institutes of Health [R01 AI127807-01A1].

NOMENCLATURE

3A2OBP	3-amino-2-oxybutylphosphonate
ADP	Adenosine 5’-diphosphate
AG	Arabinogalactan
AMP	Adenosine 5’-monophosphate
APRT	Adenine phosphoribosyltransferase
ATP	Adenosine 5’-triphosphate
Da	Dalton
D-Ala-P	D-alanyl-phosphonate (1-aminoethylphosphonate)
DCS	D-cycloserine
Ddl	D-alanine:D-alanine ligase
EA	Enzyme-substrate binary complex
EA^*	Enzyme-(radiolabeled)substrate binary complex
EAB	Enzyme-substrate-substrate ternary complex
HGPRT	Hypoxanthine-guanine phosphoribosyltransferase
Hx	Hypoxanthine
I	Inhibitor
IMP	Inosine 5’-monophosphate
KIE	Kinetic isotope effect
mAGP	Mycolyl-arabinogalactan-peptidoglycan
MDR	Multi-drug resistant

OPRT	Orotate phosphoribosyltransferase
P	First product released from enzyme
P^*	Radiolabeled first product released from enzyme
PG	Peptidoglycan
PIX	Positional Isotope Exchange
PNP	Purine nucleoside phosphorylase
PRPP	5-Phospho-α-D-ribose 1-diphosphate
TB	Tuberculosis
TcMUC	*Trypanosoma cruzi* mucins
TSAI	Transition-state analog inhibitor
UDP	Uridine 5'-diphosphate
UDP-GlcNAc	Uridine 5'-diphosphate *N*-acetylglucosamine
UDP-MurNAc/Glyc	Uridine 5'-diphosphate *N*-(acetyl/glycolyl)muramic acid
UMP	Uridine 5'-monophosphate
XDR	Extensively drug-resistant

TABLE OF CONTENTS

Page

LIST OF FIGURES

Page

LIST OF TABLES

Page

CHAPTER I

INTRODUCTION

Background Information for Chapter II

Tuberculosis and the causative agent Mycobacterium tuberculosis

Tuberculosis, the disease caused by infection of the bacterium *Mycobacterium tuberculosis*, has plagued humanity since the Stone Age[1]. The emergence of tuberculosis in humans predates agriculture, in contrast to many other infectious diseases that endanger public health, which are zoonotic in origin. Although *M. tuberculosis* was first identified by Robert Koch in the late 1800s; well into the 21st century the disease still burdens humanity, with an estimated 10 million new infections and over 1 million tuberculosis-associated deaths in 2019 alone[2].

The primary route of tuberculosis (TB) infection is through the inhalation of airborne sputum droplets containing the bacillus, from individuals with active TB. Once the droplets are inhaled, they are able to travel to the lungs where the pathogen starts the initial point of infection. Infection of the alveoli initiates an immune response that leads to endocytosis of *M. tuberculosis* by alveolar macrophages. *M. tuberculosis* that has been incorporated into the phagosomes of the alveolar macrophages are able to survive the potentially hostile environment through inhibition of both phagosome acidification[3, 4] and fusion of the phagosome with lysosomes[5]. Instead of being destroyed, *M. tuberculosis* divides in the phagosome and actively inhibits macrophage apoptosis in order to preserve the sanctuary provided by the host macrophage [6, 7].

Activation of the T-cells leads to the formation of caseous granulomas: cellular necrotic regions surrounded by macrophages. The tuberculosis bacilli remain at the center of the granuloma, where starved of oxygen, they enter a dormant metabolic state [8]. It is this latent infection that is by far the most prevalent, affecting roughly a quarter of the world's population [9]. Latent infections have a 5-10% chance to develop into an active infection, in which the granuloma is dissolved, allowing oxygen to reach the bacilli. With oxygen, *M. tuberculosis* is able to multiply rapidly, spread to other regions of the respiratory track, and be exhaled in respiratory droplets [8].

The current first-line drugs available for the treatment of tuberculosis are: isoniazid, rifampicin, ethambutol, and pyrazinamide (**Figure I-1**). Isoniazid and isoniazid co-administration rifampicin are the two regiments that are recommend for treating latent infections[10], while all four first-line drugs are used in combination for treating active tuberculosis[11]. Treatment of drug-resistant tuberculosis is more complicated, involving the use of second-line antibiotics.

Ethambutol inhibits the formation of the mycolyl-arabinogalactan-peptidoglycan complex (mAGP), an essential part of the cell wall for Mycobacterium. It is believed that ethambutol exerts its bacteriostatic effect though inhibition of arabinosyl transferase, and enzyme involved in the polymerization of arabinan [12, 13]. Isoniazid also inhibits the synthesis of mAGP. Isoniazid is first activated by the catalase-peroxidase enzyme

KatG, forming an electrophilic intermediate compound which then inactivates InhA, a fatty-acid synthase protein involved in the synthesis of mycolic acids [14, 15]. Activated isoniazid binds to the InhA-NADH complex and forms and adduct with NADH, creating a tight-binding inhibitor of the enzyme[16-19]. Rifampicin inhibits bacterial transcription by binding to the bacterial DNA-dependent RNA polymerase and preventing transcript elongation [20, 21]. The mechanism of action for pyrazinamide is currently debated. Pyrazinamide is converted into the active compound, pyrazinoic acid, by Mycobacterial pyrazinamidase[22]. A recent work suggests that binding of pyrazinoic acid to aspartate decarboxylase, an enzyme required for Coenzyme A synthesis, leads to the destruction of aspartate decarboxylase by caseinolytic protease[23].

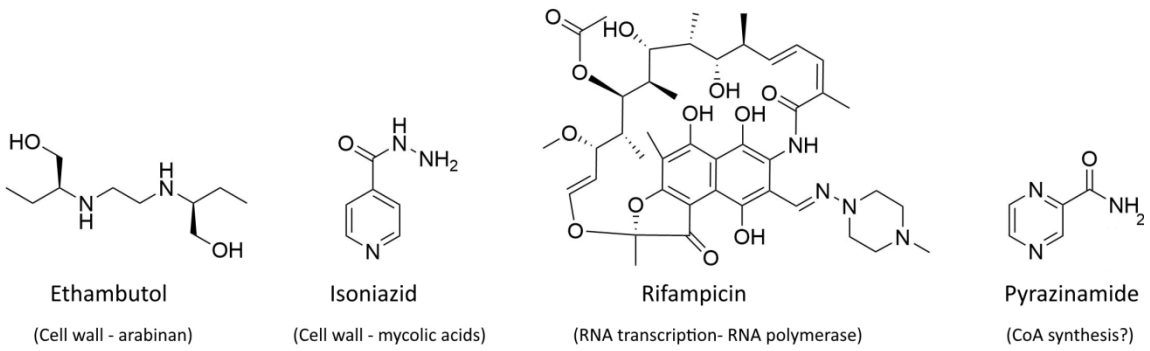

Figure I-1. First-line drugs for treating tuberculosis. Biological pathways associated with antibacterial properties shown in parenthesis.

Overview of Mycolyl-Arabinogalactan-Peptidoglycan Structure

The structural features of the cell wall of *M. tuberculosis* are dominated by a central cell wall core complex referred to as the mycolyl-arabinogalactan-peptidoglycan (mAGP) complex. The mAGP is divided in to three distinct sections (**Figure I-2**): peptidoglycan (PG), arabinogalactan (AG), and the mycolic acids. Peptidoglycan is positioned just outside of the inner membrane of the *Mycobacterial* cells and is a polymer composed largely of alternating, repeating units of β(1→4)-linked *N*-acetylglucosamine (GlcNAc) and *N*-substituted muramic acid (Mur). There are at least two major differences in the PG of *Mycobacterium* spp. when compared to model prokaryotes such as *E. coli.* One difference is in the muramic acid residues: *M. tuberculosis* PG contains classical *N*-acetylmuramic acids (MurNAc) as well as non-classical *N*-glycolylmuramic acids (MurNGlyc)[24]. The significance of the presence of MurNGlyc in the PG of some *Mycobacterium* species is not well understood; as the gene responsible for the oxidation of MurNAc is dispensable for *M. smegmatis* growth *in vitro[25]*. However, mutants of *M. smegmatis* deficient in MurNGlyc display an increase sensitivity to both β-lactam and lysozyme treatment, suggesting that *N*-glycolylation may play a role in stabilizing the structure of PG[25]. The second major difference is in the cross-linking between peptidoglycan strands. *M. tuberculosis* PG contains the typical D,D-(3→4) crosslinking between *meso*-diaminopimelic acid (mDAP) and D-alanine, and atypical L,D-(3→3) crosslinking between two mDAP residues [26, 27].

Arabinogalactan is the intermediate layer of the mAGP complex; anchored to the PG layer and in turn the anchor for the mycolic layer. AG is connected to the C-6 of MurNAc/Glyc by a special linker moiety. The structure of the linker moiety was found to be a diglycosylphosphoryl bridge: -L-Rha-α(1→3)-D-GlcNAc-(1→P). The phosphate is covalently attached to C-6 of MurNAc/Glyc residues from PG, forming a phosphodiester, and the rhamnose residue is connected to galactose of AG through an α(1→4) glycosidic bond[28]. AG is composed of arabinan and galactan polymers, the sugars of which are both exclusively in the furanose form [29, 30]. The galactan polymers are linear, composed of mainly alternating 5- and 6- linked β galactose, connecting to arabninan by 5,6-linked branching points[31].

Earlier studies have suggested that three arabinan chains are connected to a single galactan chain[32], however more recent evidence has suggested that the AG polymer of *M. tuberculosis* is composed of an approximately 23-mer galactan linked to two arabinan chains of approximately 26 residues[33]. In contrast to the linear nature of galactan, the arabinan chains are doubly branched [33] with branching introduced by 3,5- linked arabinose and linear segments composed of 5-linked arabinose[31]. The terminal and penultimate arabinose residues of arabinan are connected to the mycolic acids through a ester linkage on C-5[34].

Mycolic acids are long chain α-alkyl-β-hydroxy fatty acids generally between 70 and 90 carbons in length, and are a major component of the pseudo-outer membrane of *Mycobacterium* spp.

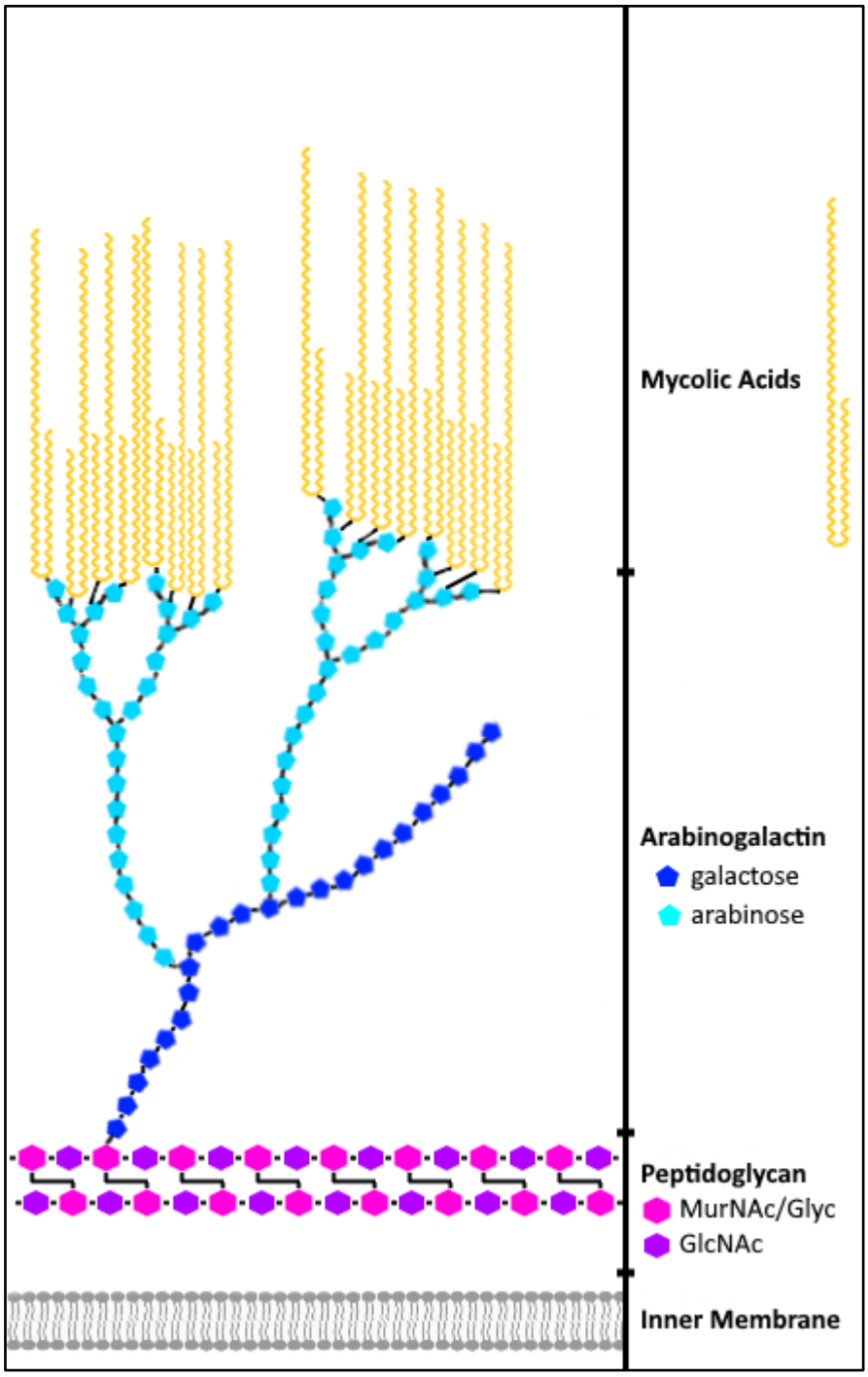

Figure I-2. Cartoon representation of the mycolyl-arabinogalactan-peptidoglycan complex. Linker moiety not shown.

There are three distinct types of mycolic acids found in *M. tuberculosis* cells: alpha, methoxy, and keto. The relative abundance of the different mycolic acids appears to be highly influenced by culturing conditions[35].

Synthesis of Peptidoglycan

Most of what is known about peptidoglycan synthesis in *M. tuberculosis* is inferred from the study of model organism, such as *E. coli*. The biosynthetic pathway is divided into two main sections: the synthesis of the repeating units of peptidoglycan, which occurs in the cytosol and the polymerization and crosslinking of nascent peptidoglycan, which occurs outside of the inner membrane. The synthesis of peptidoglycan, depicted in (**Figure I-3**), starts with the molecule uridine-5'-diphosphate *N*-acetylglucosamine (UDP-GlcNAc), a product of the hexosamine branch of glycolysis. The enzyme encoded by the gene murA (UDP-*N*-acetylglucosamine 1-carboxyvinyltransferase) catalyzes the first committed step of peptidoglycan synthesis: the transfer of phosphoenolpyruvate to C3 of the GlcNAc moiety of UDP-GlcNAc to form uridine 5'-diphosphate *N*-acetyl-3-O-(1-carboxyvinyl)-glucosamine (UDP-enoylpyruvyl-GlcNAc)[36, 37]. It is worth noting that murA is the target of the naturally occurring antibiotic fosfomycin, which inactivates the enzyme through alkylation of an active site cysteine residue [36, 38, 39].

The product of the gene murB (UDP-*N*-acetylenolpyruvylglucosamine reductase) carries out the second step: the NADPH-dependent reduction of UDP-enoylpyruvyl-GlcNAc to form uridine 5'-diphosphate *N*-acetylmuramic acid (UDP-MurNAc)[40, 41]. The

presence of *N*-glycolyl modified muramic acid, which is unusual in bacterial cell walls, is believed to be due to hydroxylation catalyzed by the gene product of namH. Raymond and colleagues have demonstrated that strains of *M. Smegmatis* deficient in namH (ΔnamH) lacked both detectable levels of *N*-glycolylated peptidoglycan precursor molecules and UDP-MurNAc hydroxylase activity in cellular extracts [25]. However a direct study of the gene product, putatively an iron-sulfur containing hydroxylase, has yet to be done for *M. smegmatis* or the *M. tuberculosis* homolog, Rv3818.

MurC-F encode for cytosolic, ATP-dependent ligases which consecutively add L-alanine, D-glutamate, *meso*-2,6-diaminopimelate (*m*DAP), and D-alanyl-D-alanine, respectively[42-45]. The mechanism for the Mur ligases is believed to involve an acyl-phosphate intermediate[46], analogous to the mechanism for D-alanine:D-alanine ligase, which is described in detail in the next subsection. The dipeptide substrate of murF, D-alanyl-D-alanine, is synthesized by the D-alanine branch of the pathway. This branch contains two enzymes: alanine racemase, encoded by the gene alr, and D-alanine:D-alanine ligase (Ddl), encoded by the gene ddl. Alanine racemase catalyzes the interconversion of L-alanine and D-alanine[47], while Ddl catalyzes the ATP-dependent ligation of two D-alanine residues into the dipeptide D-alanyl-D-alanine[48]. The end product from the action of the Mur ligases is uridine 5'-diphosphate *N*-(acetyl/glycolyl)muramic acid (UDP-MurNAc/Glyc pentapeptide), also known as the Park nucleotide.

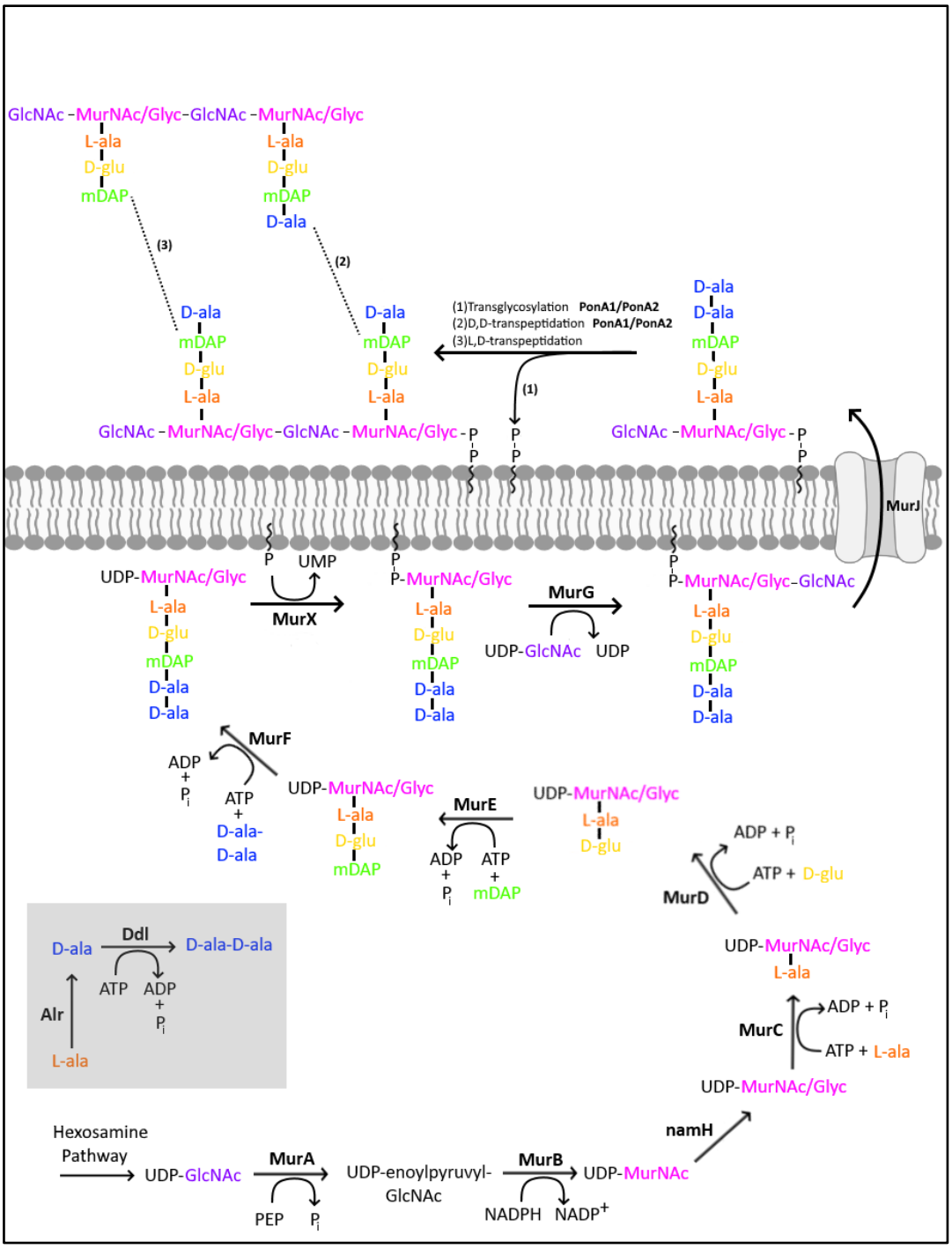

Figure I-3. Simplified scheme of peptidoglycan synthesis in *Mycobacterium tuberculosis*. D-alanine branch of pathway shown in grey box. UDP-GlcNAc: uridine 5'-diphosphate *N*-acetylglucosamine, UDP-MurNAc/Glyc: uridine 5'-diphosphate *N*-(acetyl/glycolyl)muramic acid.

Park nucleotide is the substrate for the gene product of murX (sometimes called mraY; phospho-*N*-acetylmuramoyl-pentapeptide-transferase), which catalyzes the transfer of MurNAc/Glyc pentapeptide from UDP to decaprenyl phosphate, forming decaprenyl diphosphate-MurNAc/Glyc, also known as Lipid I. An important distinction in *Mycobacterium* spp. is the use of decaprenyl phosphate (C50) as the lipid carrier[49, 50], as opposed to undecaprenyl phosphate (C55) which is predominant in other bacteria[51]. The study of murX *in vitro* is largely limited, apparently due to the difficulty of studying the membrane associated enzyme [52-54]. Lipid I is then in turn the substrate for the product of murG (UDP-*N*-acetylglucosamine:*N*-acetylmuramyl-pentapeptide- pyrophosphoryl-undecaprenol *N*-acetylglucosamine transferase), which catalyzes the transfer of GlcNAc from UDP-GlcNAc to Lipid I; forming the complete, carrier-bound subunit of peptidoglycan, Lipid II [55, 56].

Lipid II is translocated from the inner leaflet of the inner cell membrane to the outer leaflet by a flippase. The identity of the flippase is somewhat contentious. MurJ was initially identified by Ruiz as the Lipid II flippase by a bioinformatics approach (supported also by a limited amount of biochemical and genetic data)[57], however this result was challenged by Mohammadi *et al* who presented evidence for the role of FtsW in membrane translocalization of reconstituted vesicles[58]. More recent work by Ruiz's group, in which an elegant *in vivo* radiological flippase assay was developed, provided strong evidence for the role of MurJ as the lipid II flippase[59]. Additionally

Taguchi *et al* have since demonstrated a role of FtsW in peptidoglycan polymerization[60].

Once on the outside of the inner membrane, the peptidoglycan subunits are polymerized into nascent peptidoglycan polymers and cross-linked by transpeptidation. In *Mycobacterium* the class A penicillin binding proteins: PonA1 and PonA2, are bifunctional enzymes which catalyze both the transglycosylation (polymerization), and the D,D-transpeptidation (3→4) of peptidoglycan[61, 62]. *M. tuberucolosis* encodes several suspected L,D-transpeptidases (3→3), the most studied of which are LdtMt1 and LdtMt2.

Characteristics and Inhibitors of D-Alanine:D-Alanine Ligases

D-alanine:D-alanine ligase (Ddl) is a member of the ATP-grasp family, a family of enzymes defined by the ATP-grasp fold; which is comprised of two α + β domains that "grasp" molecules of ATP. A common reaction intermediate for members of the ATP-grasp family are acyl-phosphates, which are generated by reaction of a carboxylate group of a substrate molecule with a phosphate group of ATP. Ddl was first characterized in detail by Francis C. Neuhaus, who published a series of studies on the enzyme from *Streptococcus faecalis*[1] in the 1960s. The results of these studies appear to be generally applicable to all Ddl enzymes studied to date and are summarized herein.

[1] Currently referred to as *Entercoccus faecalis*. The old classification is used in this text to maintain consistency with the literature referenced.

1) The enzymatic reaction requires divalent metals such as Mg^{2+} or Mn^{2+} and ATP. ADP phosphate, and D-alanyl-D-alanine are products of the reaction 2) The enzyme is highly specific for substrates with the "D-" configuration and a higher degree of specificity is observed for the "donor site" (site that corresponds to the N-terminus D-alanine) than the "acceptor site" (the site that corresponds to the C-terminus D-alanine) [63, 64]. 3) Binding of both "donor" and "acceptor" D-alanine is characterized by distinct Michaelis constants[65]. 4) Ddl is inhibited by the antibiotic D-cycloserine.

More detailed characterization of the enzyme appeared later. Initial velocity studies of the enzyme from *Salmonella typhimurium*[66] (1990) and *M. tuberculosis*[67] (2013) provided evidence for an ordered ter-ter kinetic mechanism for Ddls in which the order of substrate binding is ATP, D-alanine (donor), and D-alanine (acceptor); the order of release of product is phosphate, D-alanyl-D-alanine, and ADP. However, it should be noted that for both enzymes the lack of an uncompetitive pattern for phosphate product inhibition versus ATP substrate, with saturating amounts of D-alanine, is not consistent with a strictly ordered product release. Indeed, phosphate was shown to catalyze molecular isotope exchange of radiolabeled D-alanine into D-alanyl-D-alanine in the absence of nucleotide[66], providing further evidence for some degree of randomness in product release. Positional isotope exchange experiments provided evidence for the formation of the acyl-phosphate intermediate during catalysis[66], which had eluded direct capture. From this finding the chemical mechanism (**Figure I-4**) for Ddl catalysis was proposed as starting with a nucleophilic attack of the donor D-alanine carboxylate

group, forming the activated acyl-phosphate and ADP. The reactive acyl-phosphate is then attacked by the amino group of the acceptor D-alanine, which ultimately forms the amide bond of the dipeptide and phosphate. Later studies of *E. coli* Ddl and the *Entercoccus faecium* vancomycin resistant (depsipeptide-forming) Ddl variant enzyme, demonstrated that the formation of the acyl-phosphate is rapid, occurring several orders-of-magnitude faster than the overall catalytic rate (k_{cat})[68]. A structural study of the enzyme from *Thermus thermophilus*[69] has illustrated the conformational changes of Ddl during catalysis, which suggest that the active site of the enzyme closes upon formation of the quaternary complex (E-ATP-D-ala-D-ala), presumably to exclude water from the active site, which could otherwise react with the reactive acyl-phosphate intermediate generated during catalysis.

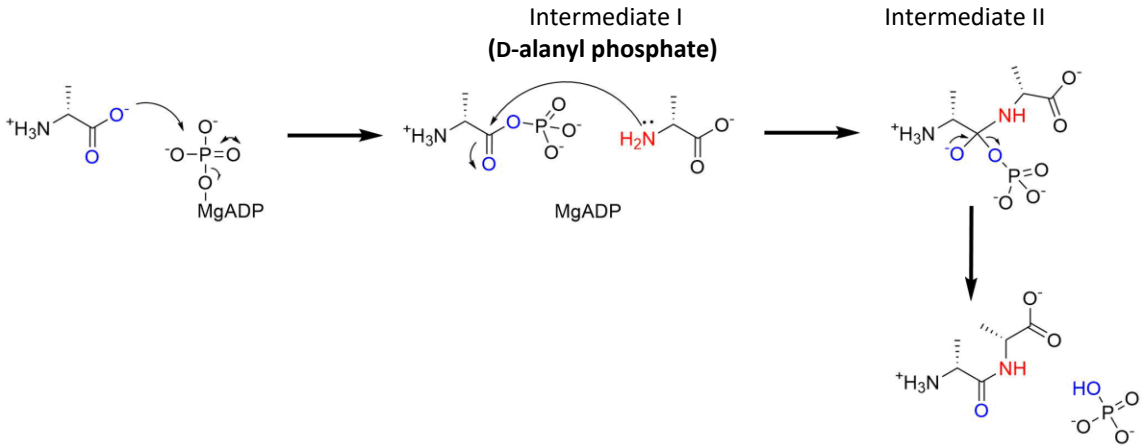

Figure I-4. Proposed chemical mechanism of *Mt*Ddl [66]. The carboxylic group of the first D-alanine attacks the γ-phosphate of MgATP, forming the activated acyl-phosphate intermediate and MgADP. The amino group of the second D-alanine attacks the activated carboxylic group, resulting in the formation of the dipeptide D-alanyl-D-alanine and phosphate.

There has been much work done on identifying inhibitors of Ddl enzymes, the bulk of which can be broadly classified in one of the following categories: D-cycloserine analogs, phosphonate and phosphinate compounds, and heterocycles. D-cycloserine (DCS) and related analogs [64] are perhaps the most important group of Ddl inhibitors, as D-cycloserine is a second-line treatment for tuberculosis[70]. DCS inhibits both *M. tuberculosis* alanine racemase and Ddl *in vitro*, however it is currently debated which enzyme is the major target *in vivo*. Metabolomic studies have suggested that the major target is Ddl[71, 72], while genetic screening of DCS resistant mutations[73, 74] and the finding that D-alanine supplementation reverses DCS growth inhibition[75], contradict the conclusion of the metabolomic studies. *In vitro* inhibition of *M. tuberculosis* Ddl by DCS is rapidly reversible, with a dissociation constant reported to be on the order of 10^{-6} – 10^{-5} M[76, 77]. Recently, structural and isotopic studies of clinically irrelevant Ddls[78, 79] have presented compelling evidence for DCS phosphorylation in the active site during inhibition; it is also likely that a similar phosphorylation event occurs during inhibition of the clinically relevant *M. tuberculosis* Ddl. Inhibition of *M. tuberculosis* alanine racemase on the other hand is essentially irreversible, with DCS forming an adduct with PLP in the active site of the enzyme[80]. Derivatives of DCS, such as β-aminoxy-D-alanine and cyclothreonine, were found to be less potent in inhibiting the enzyme from *S. faecalis* than DCS[64].

The early reports of phosphonate inhibitors found that both 1-aminoethylphosphonic acid and 2-aminophosphonic acid were capable of inhibiting the activity of Ddl enzymes

from the gram-negative *Pseudomonas aeruginosa* and the gram-positive *S. faecalis*[81]. Further development of the phosphonates by researchers at Merck led to the synthesis of the phosphinate inhibitors[82]. The phosphinate inhibitors (**Figure I-5**) are presumably mimics of the tetrahedral intermediate (Intermediate II, **Figure I-4**) formed during

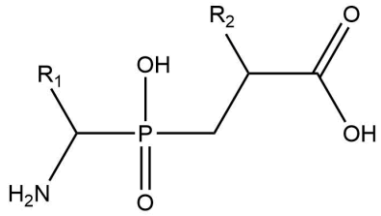

Figure I-5. General structure of (alkyl)phosphinate inhibitors developed by Parsons et al. [82]

catalysis ,and are among the most potent inhibitors of the enzyme to date. The most effective of the inhibitors were found to bind so tightly to the enzyme that the inhibition of the enzyme is essentially irreversible[82]. At the time it was speculated that the phosphinate group of the inhibitors (or inactivators) were phosphorylated by ATP in the active site; analogous to the ATP-dependent inhibition of glutamine synthetase by phosphinothricin[83] and methionine sulfoximine[84], which were previously reported. Biochemical evidence for the phosphorylation of the phosphinate (and presumably 1-aminoethylphosphonate) were published shortly after by Duncan and Walsh[85], which was later followed by both NMR[86] and structural[87] evidence that phosphinate analogs were phosphorylated by the enzyme. Although the phosphinate compounds were found to be potent inhibitors of Ddl enzymes *in vitro*, they fell short *in vivo*, presumably due to lack of uptake mechanisms for dipeptides with a D,D configuration. Derivatives of the alkylphosphinate compounds were also developed by Merck:

phosphonates and phosphonamidate analogs of the acyl-phosphate intermediate (intermediate I, **Figure I-1**). Such derivatives were found to be of similar potency as DCS *in vitro*, however, like the alkylphosphinates they were found to be poorly active *in vivo*[88]. Similar failings of *in vivo* potency were also presented by phosphonamidate analogs of the scaffold in **Figure I-5**[89].

More recent work on the discovery of Ddl inhibitors have utilized *in silico* docking as a starting point in inhibitor design. Researchers in Slovenia have identified several heterocyclic compounds with modest *in vitro* inhibitory potential [90, 91]. Although most of the compounds tested were less potent than DCS against purified enzyme, one compound, an ellipticine derivative (**Figure I-6**), was found to be comparable to DCS both *in vitro* and *in vivo* (*E. coli and S. aureus*)[91]. In contrast to the two groups of inhibitors discussed above, which bind primarily to the D-alanine pockets, the ellipticine derivative is competitive versus ATP.

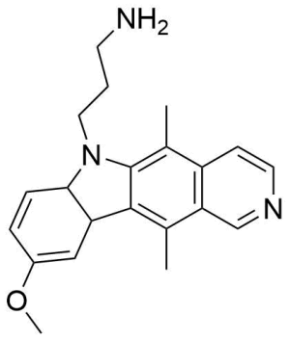

Figure I-6. Ellipticine derivative identified by Kovač *et al* [91]as both a Ddl inhibitor and bactericidal agent.

Background Information for Chapter III

Chagas Disease

Chagas Disease, also known as American trypanosomiasis, is caused by the protozoa parasite *Trypanosoma cruzi*. Considered by the World Health Organization to be a neglected tropical disease, Chagas Disease is endemic to Latin American where it disproportionally affects individuals living in poverty or who are otherwise marginalized [92, 93]. It is believed that approximately 6-7 million people are currently infected with *T. cruzi*. In endemic regions, *T. cruzi* is primarily transmitted to people from Triatomine insects (also known as kissing bugs) which feed on vertebrate blood and serve as the disease vector for *T. cruzi* infection [94]. *T. cruzi* replicates in the digestive tract of the insect, where it is ultimately excreted in the feces. When feeding Triatomines have a tendency to defecate; contact of *T. cruzi*-infested feces with mucosal membranes or breaks in the epidermis allow for the initial infection. Other routes of infection include the ingestion of food and drink contaminated with *T. cruzi* infested feces, consumption of undercooked meat of infected animals, organ transplantation, blood transfusion, and congenital transmission [94-98].

Chagas Disease in humans is divided into two distinct phases: the initial, acute disease and the chronic disease. After initial vector-borne infection by *T. cruzi*, the incubation period for the disease is typically 1-2 weeks. Following incubation, parasitemia is high, with *T. cruzi* microscopically visible in blood samples. Symptoms of the acute disease are generally mild, with most patients being asymptomatic. Occasionally swelling of the

skin (chagoma) or eyelid (Romaña's sign), caused by inflammation at the point of entry, is visible [97, 99].

Two to three months post-infection, the chronic phase of the disease begins, in which any symptoms developed during the acute infection and parasitemia are diminished. Between 60 and 70% of individuals will remain asymptomatic but seropositive for anti-trypanosomal antibodies, in what is known as the indeterminate chronic disease. On the other hand, the remaining 30-40% of individuals will develop the determinate chronic disease, characterized by damage to organs of the cardiovascular and/or digestive tract. Chronic Chagas disease of the cardiovascular system leads to the enlargement and weakening of the heart muscles, and ultimately results in heart failure[96, 99].

There are two drugs approved for the treatment of Chagas disease: the nitrofuran, nifurtimox and the nitroimidazole, benznidazole (**Figure I-7**). The mechanism of action for both drugs is believed to be similar: free radicals are generated by the drugs, which in turn, leads to damage of the trypanosomal DNA [100, 101]. Both drugs are highly efficacious in treating the acute stage of the disease, curing 80% or more of patients [95]. However neither drug is effective at curing the disease in adults once it has progressed to the chronic state, nor is there clear evidence that treatment of the chronic disease leads to a more favorable disease progression [102-104]. Although benznidazole is generally the preferred treatment because it is better tolerated than nifurtimox[95], the drug still remains quite toxic- leading to a high amount of treatment abandonment[96, 105].

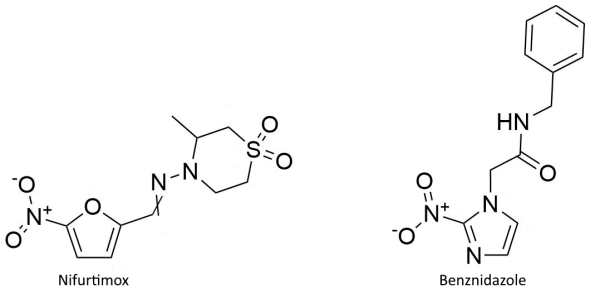

Figure I-7. Drugs approved for treatment of Chagas disease.

Although no vaccine for Chagas disease exist, disease control- in the form of blood screening and the use of insecticides, has resulted in a significant reduction is disease burden in endemic areas[106].

Trypanosoma cruzi

T. cruzi is a parasitic flagellated protozoa that infects a wide range of vertebrates, including humans. Belonging to the class kinetoplastea, *T. cruzi* possesses the unique structure called the kinetoplast: mitochondrial DNA that is composed of thousands of interlocked small circular DNA molecules, located within the single mitochondria of the cell[107]. Gene regulation in trypanosomes occurs at the post-transcriptional level and involves unique features not found in most other eukaryotes. Genes are transcribed as long polycistronic transcripts, which are then processed into the individual genes by *trans*-splicing. In the *trans*-splicing process, short, capped RNA transcripts called splice leaders (SLs) are transcribed in addition to the large polycistron transcripts. SLs are *trans*-spliced to individual genes of the polycistronic transcript in a process that is coupled to polyadenylation, forming the mature mRNA genes [108, 109].

T. cruzi has a complicated lifecycle, with substantial morphological differentiation occurring in both the vector and host cycles of infection. There are three major forms of *T. cruzi* during the infection cycle: trypomastigotes (metacyclic and bloodstream), epimastigotes, and amastigotes. Trypomastigotes and epimastigotes are long and slender in shape. In both of these forms the flagellum starts at the kinetoplast. In trypomastigotes the kinetoplast is positioned towards the posterior of the cell and the flagellum runs the length of the cell, towards the anterior side where it protrudes out. In epimastigotes, the kinetoplast is more centrally positioned, with the flagellum running approximately half the cell before protruding. In contrast to epimastigotes and trypomastigotes, amastigotes are small and round, with no visible flagellum. Trypomastigotes are the infective developmental forms while epimastigotes and amastigotes are the reproductive forms. [110, 111].

Infection cycle in vertebrates (**Figure I-8**) begins when metacyclic trypomastigotes enter the host through the contact of broken skin or mucosal membranes with *T. cruzi* infested feces. Metacyclic trypomastigotes that enter the host invade the cells near the point of entry. Entry into the host cell is achieved, in part, due to a stage-specific, 82 kDa surface glycoprotein known as gp82. Manque *et al* have found that stable expression of the metacyclic trypomastigote-specific protein gp82 in epimastigotes results in HeLa cell adhesion and activation of Ca^{2+} mobilization, two features required for cellular invasion [112, 113]. One route of *T. cruzi* trypomastigotes entry into host cells is believed to occur through a process in which parasite-host cell interactions cause damage to the cell

membrane. The cell membrane response of the host cells ultimately leads to endocytosis of the parasite through ceramide-enriched endosomes [114]. *T. cruzi* is internalized inside of a transient structure called the parasitophorous vacuole, which fuses with lysosomes inside the host cell [115]. Lysosomes are redirected to the parasitophorous vacuole through interactions with host cell microtubule networks [116].

Pessoa *et al* [117] has found that *T. cruzi* metacyclic trypomastigotes undergo the process of differentiation into amastigotes prior to escape from the parasitophorous vacuole, suggesting that maturation of the vacuole leads to parasite development. *T.cruzi* is then able to lyse the vacuole, from which it is released into the cytoplasm and replicates intracellularly through binary fission [118]. Several days after infection the amastigotes differentiate into trypomastigotes which again enter the bloodstream [119]. The newly emerged trypomastigotes can infect additional cells, and repeat the replicative cycle or enter the Triatomine vector during feeding of the insect. Inside of the gut of the insect, *T. cruzi* differentiates into epimastigotes, which are the main replicative form during the invertebrate portion of the parasitic lifecycle. The epimastigotes migrate to the hindgut where they differentiate into metacyclic trypomastigotes which in turn are excreted in the feces, repeating the cycle of infection [96]. The differentiation of epimastigotes into metacyclic trypomastigotes is believed to be triggered due to changes in nutrient levels when migrating into the hindgut [120].

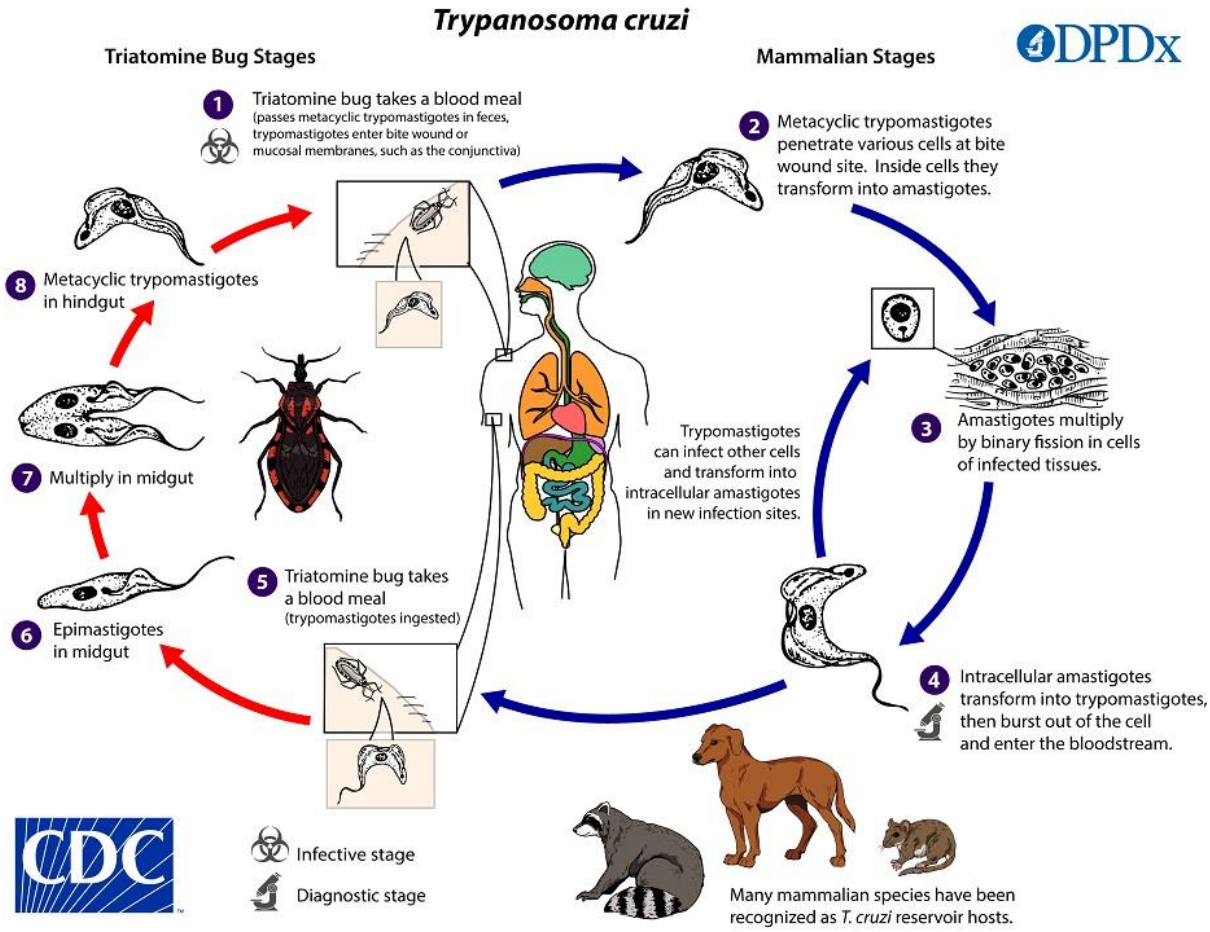

Figure I-8. Lifecycle of *T. cruzi*. From reference [94]

Although *T. cruzi* is shielded from the immune system of vertebrates during intracellular replication, extracellular trypomastigotes are essential for the infection of new cells. As a result, *T. cruzi* has developed an arsenal of immune-evasion mechanisms. Many of the genes associated with antigenic escape exist in the genome as large, multigene families. Two of these important multigene families are the *trans*-sialidases and the mucins. *Trans*-sialidases (TSs), which account for roughly 1400 genes in *T. cruzi* [121], are glycosylphosphatidylinositol-anchored enzymes that catalyze the transfer of sialic acid

groups from the host to the parasite's surface glycoconjugates, such as mucins [122-124]. The transfer of sialic residues from the host to parasite is the main, if not only, route for sialyation of parasitic glycoconjugates [125]. This process is rapid, with trypomastigotes developing a sialic-specific epitope within seconds following exposure to sialic-donating serum [126]. One of the roles for the sialyation of parasitic surface proteins appears to be the suppression of the alternative complement pathway. Tomlinson *et al* [127] have shown that sialic-deficient trypomastigotes were more susceptible to serum lysis than trypomastigotes that retained surface sialyation. Additionally de-sialylated trypomastigotes were found to have higher levels of the major complement protein, C3, while sialylated trypomastigotes had a higher conversion of C3b fragments into lytically inactive forms.

Mucins are the third largest gene family, of which there are roughly 860 genes [121]. *T. cruzi* mucins (TcMUC) are highly glycosylated glycosylphosphatidylinositol-anchored surface proteins, and are a major component of the cell surface. As previously noted, TcMUC are the main acceptor of sialic acids from TS activity. The sialylated glycans are linked to TcMUC through *O*-glycosylation via *N*-GlcNAc [128, 129]. The expression of TcMUC is highly variable, depending on developmental stage of the parasite. Freitas-Junior *et al* examined the expression of TcMUC genes across the developmental stages of *T. cruzi* [130]. They have found that a group (I) of TcMUCs with $KP_{(1-2)}T_{(6-8)}$ repeats (a motif found commonly in mammalian mucins) was highly expressed in cell-derived trypomastigotes. A second group (II) of TcMUC, in which the internal domain is highly

heterogeneous, was found to be expressed in variable amounts during all developmental stages. However, examination of trypomastigote-derived mucins by Buscaglia *et al* [131] indicated that group II is the dominant TcMUC on the cell surface. The discrepancy between the two studies may be due to translational regulation, bias during purification, or preferential shedding of group I TcMUC. The highly sialylated TcMUC of the trypomastigotes appear to have a significant role in protecting the parasite from the host immune system. Pereira-Chioccola *et al* [132] have demonstrated a protective role of sialylated mucins; *T. cruzi* lysis by patient-derived anti-α-galactose antibodies was reduced in *T. cruzi* containing sialylated mucins, presumably by preventing aggregation of TcMUC that results in membrane destabilization. The N-terminus of both group I and II TcMUC contain regions of hypervariability [133]. It has been speculated that, given the position of the hypervariable region on the N-terminus of group I and II TcMUC (away from parasitic cell membrane), these regions play a role in early immunoevasion. Indeed, small fragments of the hypervariable region were found to elicit an immunogenic response from serum derived from infected mice, rabbits, and humans (chronic disease). The immunogenic response in mice was found to increase as the infection progressed, with no reactivity detected a few weeks after infection to increased activity (and cross-reactivity) at later points (>50 days) [134].

Purine Metabolism in T. cruzi

Overview of *de novo* and salvage pathways

In many forms of life the synthesis of purines can be accomplished by one of two routes. In the *de novo* pathway (**Figure I-9**) IMP is assembled from simpler molecules such as formate, carbon dioxide, and amino acids. The first step (**1)** of the *de novo* pathway, the formation of 5-phosphoribosyl-1-amine (PRA), is the committed step for *de novo* purine synthesis. Some of the enzymes for steps **(2)**, **(5),** and **(7)** belong to the ATP-grasp family, and likely catalyze C-N bond formation through attack of the γ-phosphate of ATP by the carbonyl oxygen of the carbon-donating substrate [135-137]. Many of the steps are catalyzed by single, mulifunctional enzymes. For example, in humans metabolic steps (**2)**, (**3)**, and (**5)** are catalyzed by a single trifunctional enzyme [136], steps (**6**) and (**7**) are catalyzed by a bifunctional enzyme [138], and the last two steps, (**9**) and (**10**), are catalyzed by a bifunctional enzyme [139]. Synthesis of purines by the *de novo* route is costly: 4 molecules of ATP (5 for some species [140]), 2 amino groups from glutamine, 2 formyl moeities from N^{10}-formyltetrahydrofolate, 1 amino group from aspartate, and a molecule of carbon dioxide for every molecule of inosine-5'-monophosphate (IMP) formed.

In contrast, the salvage pathway (**Figure I-10**) provides a means for the inexpensive interconversion of preformed purine rings. The enzymes responsible for interconversion of the nucleotides (steps **8**, **9**, **10**, **11**, **12**, and **13**) are shared with the *de novo* pathway.

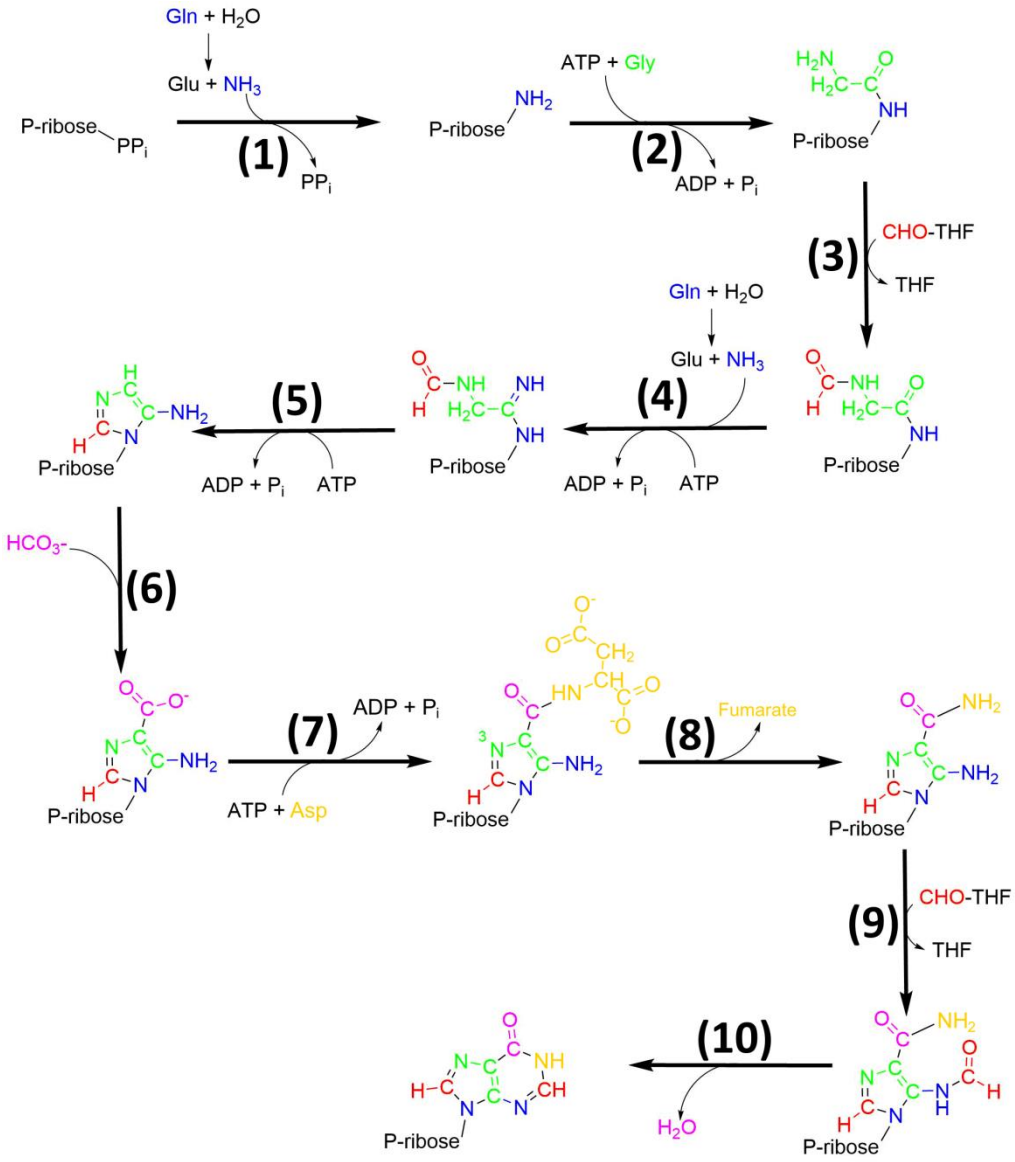

Figure I-9. Formation of IMP in the d*e novo* pathway of purine synthesis. The first step **(1)** of the *de novo* pathway is the formation of 5-phosphoribosyl-1-amine (PRA) from PRPP and glutamine-derived ammonium; a reaction catalyzed by amidophosphoribosyltransferase. **(2)** Glycine is added to the amino group of PRA by the enzyme phosphoribosylamine-glycine ligase. **(3)** Formyl from CHO-THF is transferred to the amino group of the glycine residue by phosphoribosylglycinamide formyltransferase. (**4)** Glutamine-derived ammonium is added to the carboxylate group of the glycine residue by phosphoribosylformylglycinamidine synthase. (**5)** 5-aminoimidazole ribotide synthetase catalyzes the ATP-dependent cyclization. **(6)** Bicarbonate is transferred to what was the α-carbon of glycine by phosphoribosylaminoimidazole carboxylase. **(7)**

Phosphoribosylaminoimidazolesuccinocarboxamide synthase catalyzes the ligation of aspartate to the carboxylate moiety of bicarbonate. **(8)** Adenylosuccinate lyase catalyzes the elimination of fumarate. **(9)** The second molecule of aldehyde is added by phosphoribosylaminoimidazolecarboxamide formyltransferase. **(10)** IMP synthase catalyzes the second cyclization, forming IMP.
CHO-THF: N^{10}-formyltetrahydrofolate, P-ribose: ribose-5-phosphate

IMP is considered to be a branching point in the interconversion pathways, from which either GMP or AMP can be formed. Cells that lack *de novo* synthesis must import rely on the salvage of purines from their enviroment. Nucleotides are generally not transported into cells, however nucleosides and nucleobases are. Nucleosides can be converted into nucleotides through either 5'-phosphorylation by nucleoside kinases (**2**) or conversion into nucleobases by nucleoside hydrolases (**3)** and/or phosphorylases (**4**) followed by *N*- ribosylation by phosphoribosyltransferases (**1**). In turn, imported nucleobases can be converted into nucleotides directly by phosphoribosyltransferases (**1**) or by subsequent action of nucleosides phosphorylases (**4**) and nucleoside kinases (**2**). Purines can be removed by oxidation into uric acid by xanthine oxidase, which is the terminal product in humans and other primates. Other organisms, however, can further oxidize uric acid into5-hydroxyisourate through urate oxidase [141, 142].

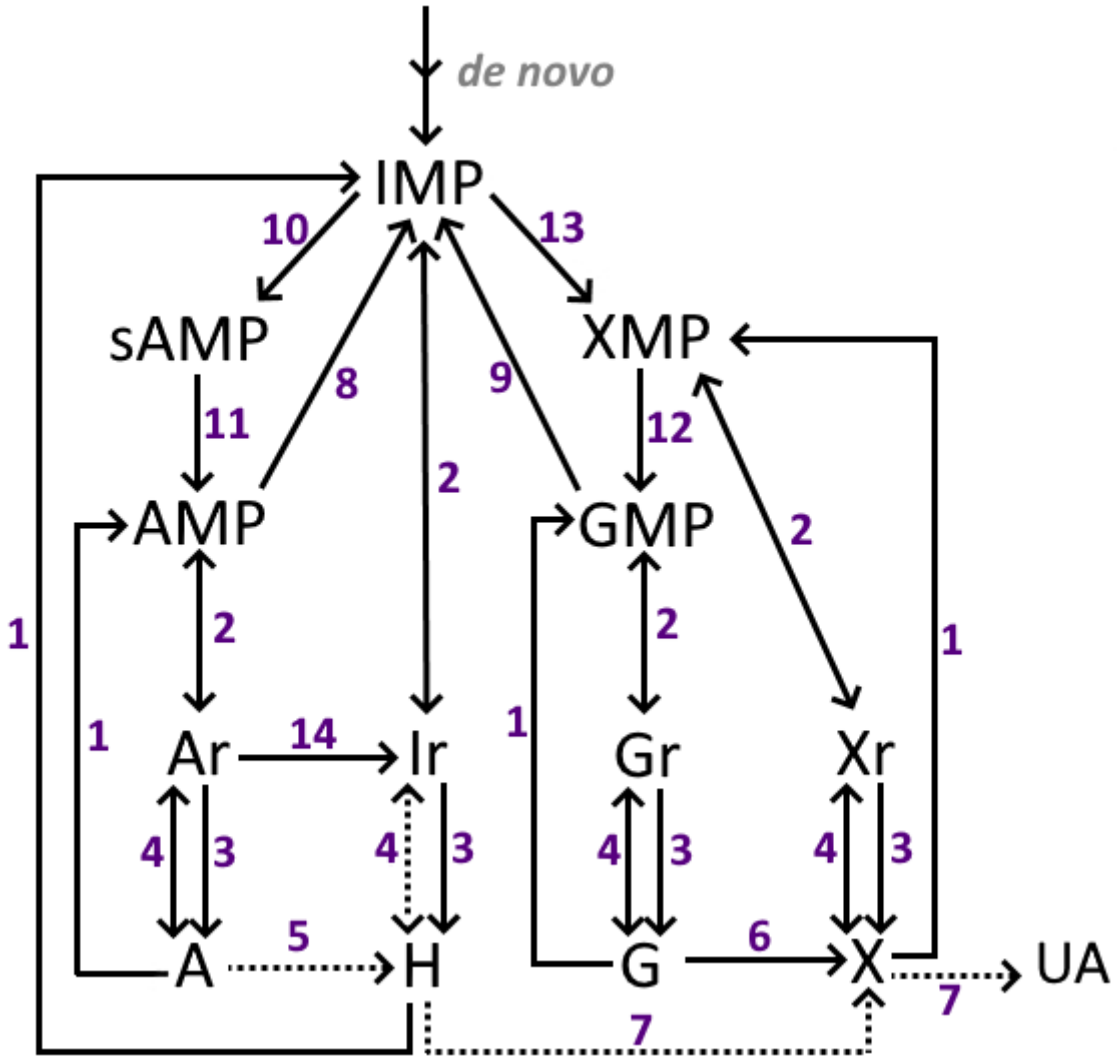

Figure I-10. Scheme of salvage pathway integrated with purine catabolism and *de novo* synthesis. (**1**) phosphoribosyltransferases, (**2**) nucleoside kinases, (**3**) nucleoside hydrolases, (**4**) nucleoside phosphorylases, (**5**) adenine deaminase, (**6**) guanine deaminase, (**7**) xanthine oxidase, (**8**) AMP deaminase, (**9**) GMP reductase, (**10**) adenylosuccinate synthetase, (**11**) adenylsuccinate synthetase, (**12**) GMP synthetase, (**13**) IMP dehydrogenase, (**14**) adenosine deaminase. For simplicity, co-factors and co-substrates not shown. Dotted lines represent functions that are absent in *T. cruzi*. **IMP**: inosine-5'-monophosphate, **sAMP**: N^6-succinyl-adenosine-5'-monophosphate, **AMP**: adenosine-5'-monphosphate, **XMP**: xanthosine-5'-monophosphate, **GMP**: guanosine-5'-monphosphate, **Ar:** adenosine, **Ir:** inosine, **Gr**: guanosine, **Xr**: xanthosine, **A**: adenine, **H**: hypoxanthine, **G**: guanosine, **X**: xanthine, **UA**: uric acid.

Limited purine metabolism in *T.cruzi*

T. cruzi, like most other parasitic protozoa, are believed to be purine auxotrophs [143]. The lack of a functional *de novo* pathway is supported by several pieces of evidence. Early work by Fernandes and Castellani found that incorporation of ^{14}C-glycine into nucleotides is much less efficient than incorporation of ^{14}C-adenine for *T. cruzi* epimastigotes [144]. Follow up work by Gutteridge and Gaborak[145] provided more details into purine (and pyrimidine) metabolism in *T. cruzi*. The major findings of this work are summarized: 1) trypomastigotes, epimastigotes, and amastigotes efficiently incorporate radiolabeled adenine, guanine, and hypoxanthine, and to a lesser extent, the radiolabeled nucleosides: guanosine and adenosine. 2) Incorporation of ^{14}C-labelled orotate, glycine, and bicarbonate into adenine or guanine was not significantly detected for all three developmental stages. Formate incorporation into adenine and guanine was detected, to an extent, for trypomastigotes, but not epimastigotes nor amastigotes. These results were supported by experiments conducted by Ceron *et al*, who showed that in *T. cruzi* ^{14}C-guanine and ^{14}C-adenine could incorporate into DNA and RNA, while ^{14}C-glycine could only be incorporated into proteins[146]. Similar results were found once again by Berens *et al* [147], in which radiolabeled glycine, serine, and formate were not significantly incorporated into adenosine or guanosine nucleotides. Additionally, the supplementation of at least one purine nucleobase (hypoxanthine, adenine, guanine, or xanthine) or nucleoside is required for cell division of *T. cruzi* [147]. Taken together, these results demonstrate that *T. cruzi* possesses no significant means for *de novo* purine synthesis, but instead, has a robust and efficient means for purine salvage.

Several features of the purine salvage pathway in *T. cruzi* are notable. The lack of adenine to hypoxanthine conversion, and hypoxanthine to xanthine/urate conversion suggests a lack of adenine deaminase and xanthine oxidase activity, respectively (functions **5** and **7, Figure I-10**). The lack of adenosine to inosine conversion suggested a deficiency of adenosine deaminase activity [147], however later work found low activity in cell-free extracts from *T. cruzi* epimastigotes [148] (function **14**, **Figure I-10**). Additionally, the apparent lack of inosine phosphorolysis in cellular extract suggests a lack of inosine phosphorylase activity [148, 149] (dotted function **4**, **Figure I-10**).

Purine transport in Trypanosomatids

What is known about purine transport in *T. cruzi* is largely inferred from studies of the related Trypanosomatids, particularly *Leishmania spp.* and *Trypanosoma brucei spp.* In typical experiments the import of radioactive nucleobases and/or nucleosides is probed. Often to distinguish the function of multiple transporters, mutant cell lines resistant to toxic purine analogs were developed. More advanced studies have since examined the uptake of purines in frog (*Xenopus*) oocytes injected with specific transporter cRNA. This has allowed for more controlled experiments than those provided by generating resistance mutants (issue reviewed in [150]). To date, all known purine transporters in *Leishmania spp.* and *T. brucei spp.* are members of the equilibrative nucleoside transporter (ENT) family, homologous to human ENT1 and ENT2[151-153]. Studies of *L. donovani* purine transporters (NT1.1, NT1.2, NT2) suggest that these transporters are

proton-symporters; presumably allowing the parasite to concentrate purines inside their own cells, outcompeting the host cells [151]. A relationship between proton-motive force and adenosine transport for *T. brucei brucei* (procyclic form) was also noted [154] , suggesting that the use of concentrative symporters may be a general strategy of parasitism by parasitic Trypanosomatids. The study of *T. cruzi* transporters is much more limited. *T. cruzi* cells deficient in tubercidin (7-deazaadenine, a toxin for Eukaryotic cells) uptake, were also found to be deficient in thymidine, but not adenosine or inosine uptake. The uptake of tubercidin by "wild-type" cells was also found to be strongly inhibited by thymidine, uridine, and cytidine, but not guanosine or inosine. Taken together, these results suggest that there are at least two transport processes in *T. cruzi*: one for pyrimidine nucleosides (and tubercidin) and another for purine nucleosides [155].

CHAPTER II

ANALOGS OF D-ALANINE AND CATALYTIC INTERMEDIATES AS INHIBITORS OF D-ALANINE:D-ALANINE LIGASE FROM *MYCOBACTERIUM TUBERCULOSIS*

Introduction

Globally, tuberculosis remains the leading cause of death from a single infectious disease, contributing to over 1 million deaths in 2019 alone.[2] The antibiotic D-cycloserine (DCS) is currently a second-line treatment for infections of *Mycobacterium tuberculosis,* the causative agent of tuberculosis. The limited use of DCS in treating extensively drug resistant (XDR) and multi-drug resistant (MDR) infections is in part due to the severity of neurological effects associated with the drug[156, 157]. Owing to the structural similarity of DCS to D-alanine, DCS has been shown to be a potent inhibitor of both alanine racemase[158] and D-alanine-D-alanine ligase (Ddl)[67, 77, 159] *in vitro*. Despite inhibition of two enzymes in the same pathway, metabolomic studies [71, 72] suggest that Ddl is the primary target of DCS *in vivo*.

Ddl catalyzes the formation of the dipeptide D-alanyl-D-alanine, which is incorporated as the C-terminus of the pentapeptide of nascent peptidoglycan found in bacterial cell walls. The mechanism of Ddl catalysis is thought to involve an initial transfer of the γ-phosphate from MgATP to the carboxylic group of D-alanine, forming an acyl-phosphate [66, 68] (**Figure I-4**). This reactive, enzyme-bound D-alanyl phosphate intermediate is then apparently attacked by the amino group of the second D-alanine

substrate which displaces the phosphate, thereby forming the D-alanyl-D-alanine product, phosphate, and MgADP. In kind, Ddl catalyzes phosphorylation of DCS to produce an apparent mimic of D-alanyl phosphate [78, 79], contributing to the inhibitory potency of this antibiotic.

Similar phosphorylation events were also observed for phosphinate analogs of D-alanyl-D-alanine, which are potent inhibitors of gram-negative and gram-positive Ddls *in vitro*[85, 160], as well as inhibitors of glutamine synthetase such as methionine sulfoximine and phosphinothricin [83, 84]. These findings suggest that the enzyme-catalyzed phosphorylation of other substrate analogues may be a broadly applicable strategy to enable mechanism-based inhibition/inactivation of ligases that utilize acyl-phosphate intermediates to ultimately form amide bonds.

Despite the limited success of previous work, little effort has since focused on investigating small molecules that structurally resemble the natural substrate, D-alanine. In this work, we examine the inhibitory potential of a small library of compounds that are analogs of D-alanine and/or related intermediates in the catalytic cycle. The results of our library screen show that the enzyme possesses a high degree of D-alanine substrate specificity, however mimics of the presumptive catalytic intermediates were found to be of similar potency do the antibiotic DCS.

Materials and Methods

Materials

D-alanine, phosphoenolpyruvate, pyruvate kinase, L-lactate dehydrogenase, taurine, isobutyric acid, 1-aminoethylphosphonic acid, D-cycloserine, nicotinamide adenosine dinucleotide reduced, nicotinamide adenosine dinucleotide phosphate, magnesium chloride, adenosine triphosphate, hexokinase, D-glucose, adenosine diphosphate, and glucose-6-phosphate dehydrogenase were purchased from Sigma Aldrich/Sigma Millipore (Burlington, MA). 4-(2-hydroxyethyl)-1-piperazineethanesulfonic acid (HEPES), D-alanyl-D-alanine, and R(+)-2-chloropropionic acid were purchased from ChemImpex (Wood Dale, Il). 1-aminoethanesulfonic acid and 1-aminocyclopropane carboxylic acid were purchased from TCI (Tokyo, Japan). 3-[(3-cholamidopropyl)dimethylammonio]-1-propanesulfonate (CHAPS) was purchased from Gold Biotechnology (St Louis, MO), β-alanine was purchased from AK Scientific (Union City, CA), Trifluoroalanine was purchased from CombiBlocks (San Diego, CA), 1-(3-methoxyisoxazol-5-yl)ethan-1-amine was purchase from Astatech (Bristol, PA), 1-(oxetan-3-yl)ethan-1-amine was purchased from Advanced Chemblocks Inc (Burlingame, CA) and 3-amino-2-oxybutyl-phosphonate was synthesized by FCH Group (Chernigov, Ukraine). These chemicals were used without further purification.

Preparation of [γ-^{18}O]ATP

[γ-^{18}O]ATP was provided by WuXi (Shanghai, China) by coupling of the mono(tri-*n*-butylammonium) salt (*13*) of [$^{18}O_4$]phosphate, prepared from PCl_5 and [^{18}O]H_2O (*14*),

with ADP-morpholidate (*15*). The resulting tris(triethylammonium salt) of [γ-$^{18}O_4$]ATP was found to be >96% pure by high-performance liquid chromatography and with a molecular weight of 818.75 amu as determined by mass spectrometry. Further quantification of the product [γ-^{18}O]ATP was ascertained from measurement of a sample by its absorbance at 259 nm for total adenine content, and also by enzymatic conversion of ATP to ADP by use of the hexokinase/glucose 6-phosphate dehydrogenase coupling enzyme system as described (*16*). Samples were found to consist of ≥93% ATP. Analysis of the integrals of γ-phosphate resonance of the [γ-$^{18}O_4$]ATP by ^{31}P-nmr indicated that the substitution pattern of ^{18}O atoms in the γ-phosphate group was: [γ-$^{18}O_4$], 74%; [γ-$^{18}O_3{}^{16}$O], 26%.

MtDdl Expression and Purification

A plasmid encoding an N-terminal His_6-tagged *Mycobacterium tuberculosis* D-alanine:D-alanine ligase was a generous gift from Prof. Luiz Pedro S. de Carvalho[11]. The plasmid was transformed into *E. coli* Bl21(DE3), and grown to mid-log phase in Luria Broth containing 30 μg/mL kanamycin at 37 °C. 0.2 mM Isopropyl β-D-1-thiogalactopyranoside (IPTG) was added to the cultures, and cell growth continued for approximately 16 hours at 18 °C. Cells were then collected by centrifugation, and resuspended in Ni-NTA buffer A (20 mM triethanolamine (pH 7.8), 300 mM NaCl, 50 mM imidazole), and Roche cOmplete EDTA-free protease inhibitor cocktail was added (1 tablet per 1L of cell culture). The re-suspended cells were lysed by sonication (30 cycles at approximately 14.5% duty cycle), and lysate was then clarified by

centrifugation at 25,000 x(g) for 1 hour. Clarified cell lysate (approximately 94 mLs) was then loaded on to a GE HisTrap FF Crude 5-mL column pre-equilibrated in Ni-NTA buffer A. The column was then washed with 5% of Ni-NTA buffer B (20 mM triethanolamine (pH 7.8), 300 mM NaCl, 500 mM imidazole) in Ni-NTA buffer A for 10 column volumes, followed by a linear gradient from 5% to 100% Ni-NTA buffer B over 20 column volumes. A single peak observed at $OD_{280\ nm}$ eluted from the column, for which the corresponding fractions were pooled together, and concentrated to 4 mL using a 15-mL Amicon centrifuge concentrator with 10,000 MWCO. The concentrated protein of approximately 4 mL was then loaded on to a HiLoad 26/600 200 PG gel filtration column pre-equilibrated with buffer composed of 50 mM HEPES (pH 7.3), 80 mM KCl, 10 mM $MgCl_2$. Fractions corresponding to the approximate molecular weight of homodimeric Ddl (77 kDa) were pooled, concentrated, and glycerol was then added to a final concentration of 40% (v/v), prior to flash-freezing and storage at -80 °C.

Kinetic Assays in the Forward Direction

Unless otherwise specified, all kinetic data was collected using a SpectraMax M2 plate reader (Molecular Devices, San Jose, CA). The biosynthetic reaction catalyzed by *Mt*Ddl was assayed using the pyruvate kinase-lactate dehydrogenase coupled-enzyme format in which the product MgADP was measured as the formation of NAD^+ by its change in absorbance at 340 nm, under the following conditions: 100 mM HEPES (pH 7.3), 10 mM KCl, 20 mM $MgCl_2$, 1 mM CHAPS, 2 mM phosphoenolpyruvate, 300 μM NADH, and approximately 50 U/mL of both PK and L-LDH. Assays were conducted at

30 °C in a 96-well microplate (Greiner Bio-One UV-Star) by measurement of changes in absorbance at 340 nm. Reaction mixtures for initial velocity studies (0.25 mLs) contained 0.25 – 5.0 mM MgATP when assayed at higher concentrations of D-alanine, which was varied between 2-100 mM. Reactions were initiated by the addition of Ddl to a final concentration of 26-100 nM to determine the kinetic parameters for the higher-affinity D-alanine site; the initial velocity was also measured when D-alanine was varied at lower concentrations (0.05-2.0 mM). The reactions contained a fixed concentration of 5 mM of MgATP, and Ddl was added to a final concentration of 40-525 nM to initiate the reaction. Initial velocities were determined from linear time courses of absorbance data at 340 nm.

Initial velocity data obtained from assays at higher concentrations (2-100 mM) of D-alanine were measured in duplicate, and fitted to (**eq. 2.1**) which describes a sequential bi-substrate mechanism, for which *v* is the initial velocity, E_t is the total enzyme concentration, k_{cat} is the turnover number, K_{ia} is the dissociation constant for MgATP, K_a is the Michaelis constant of MgATP, K_b is the Michaelis constant of the lower affinity D-alanine, A is the concentration of MgATP, and B is the concentration of D-alanine. The results from three separate experiments were averaged to determine the reported kinetic parameters.

$$\frac{v}{E_t} = \frac{k_{cat}AB}{K_{ia}K_b + K_aB + K_bA + AB} \tag{2.1}$$

Initial velocity measurements obtained at lower concentrations of D-alanine (0.05-2.0 mM) were acquired in duplicate and fitted to (**eq. 2.2)** [65], for which apparent values of

k_{cat} and the K_M for the lower-affinity D-alanine were fixed by using the kinetic parameters (k_{cat} and $K_{D\text{-}ala,2}$) obtained when assayed at higher D-alanine concentrations.

$$\frac{1}{v} = \frac{K_a K_b}{k_{cat}}\left(\frac{1}{A^2}\right) + \frac{K_b}{k_{cat}}\left(\frac{1}{A}\right) + \frac{1}{k_{cat}} \quad (2.2)$$

For (**eq. 2.2**), K_a is the Michaelis constant for the higher affinity D-alanine, K_b is the Michaelis constant for the lower affinity D-alanine and A is the concentration of D-alanine.

Kinetic assays in the Reverse Direction

The reverse reaction catalyzed by Ddl was measured using the hexokinase-glucose-6-phosphate dehydrogenase enzyme-coupling assay in which product MgATP is measured as the formation of NADPH by its change in absorbance at 340 nm. The final assay conditions were 25 U/mL hexokinase, 15 U/mL glucose-6-phosphate dehydrogenase, 2 mM glucose, 0.3 mM $NADP^+$ in buffer containing 100 mM HEPES (pH 7.3), 10 mM KCl, 20 mM $MgCl_2$. The concentration of *Mt*Ddl was varied at 12.8 - 820 nM. The apparent Michaelis constant for phosphate was determined at fixed concentrations of 5 mM MgADP and 500 μM D-alanyl-D-alanine, and the apparent Michaelis constant for D-alanyl-D-alanine was determined at fixed concentrations of 5 mM MgADP and 10 mM phosphate.

Inhibition Studies

Inhibition of the forward reaction was examined under conditions identical to those of the forward kinetic assay. Isobutyric acid (**1**), 2-chloropropionic acid (**2**), D-alanine (**9**),

and taurine (**10**) were varied between 2-100 mM in assay mixtures containing 53 nM Ddl, 7.3 mM D-alanine, and 5 mM MgATP. All other compounds were evaluated in assay mixtures containing 40-45 nM Ddl, 3.9 mM D-alanine, and 5 mM MgATP. The concentration ranges used for other compounds were: (R)-1-(1H-tetrazol-5-yl)ethanamine (**5,** 55-880 μM), 1-(oxetan-3-yl)ethan-1-amine (**8,** 55-880 μM), 1-aminoethanesulfonic acid (**6,** 0.25-2 mM), 1-(3-methoxyisoxazol-5-yl)ethan-1-amine (**7,** 0.125-2.0 mM), 1-aminocyclopropane carboxylic acid (**4,** 0.063-1.0 mM), trifluoroalanine (**3,** 0.063-1 mM), and D-cycloserine (**13,** 12.5-200 μM).

When the effect of inhibition was examined on the steady-state rates the following equation was used to fit data:

$$\frac{v_s}{v_0}\,(\%) = \frac{100}{1 + \frac{I}{IC_{50}}} \quad \text{which for a competitive inhibitor:} \quad IC_{50} = K_i\left(1 + \frac{S}{K_M}\right) \qquad (2.3)$$

Where I is the concentration of inhibitor and IC_{50} is the apparent inhibitor concentration to reduce catalytic activity by 50%, S and K_M are the respective fixed concentration and apparent Michaelis constant of D-alanine.

Time-dependent inhibition

Kinetic time courses of the time-dependent inhibition of *Mt*Ddl by 0-880 μM 1-aminoethylphosphonate (D-Ala-P; **Table 2, compound 11**) was measured under conditions essentially identical to the kinetic assay described above, in which the concentrations of D-alanine and MgATP were fixed at 3.9 mM and 5 mM, respectively.

The reaction was initiated by the addition of *Mt*Ddl to a final concentration of 7 nM in a 1 mL cuvette. Formation of the MgADP product was measured by monitoring the absorbance at 340 nm via the coupled enzyme assay. Inhibition data were fitted to (**eq. 2.3**) in which v_s is the steady-state rate, v_0 is the initial rate, and k_{obs} is the apparent rate constant for conversion of v_0 to v_s at each concentration of D-Ala-P. Data from replotting of k_{obs} vs. [D-Ala-P] were fitted to (**eq. 2.4)** to provide the inhibition parameter $k_{inact}/K_{i,app}$. The inhibition constant (K_i^*) was determined by fitting the steady-state data as a competitive inhibitor versus D-alanine[1].

$$Product = v_s t + \frac{(V_0 - V_s)}{k_{obs}}(1 - e^{-k_{obs} * t}); \quad (2.4)$$

$$k_{obs} = I\left(\frac{k_{inact}}{K_{i,app}}\right) + k_{rev}\,; \quad for\ a\ competitive\ inhibitor\ K_{i,app} = K_i(1 + \frac{S}{K_M}) \quad (2.5)$$

A scheme for time-dependent inhibition is shown in (**Figure II-1**).

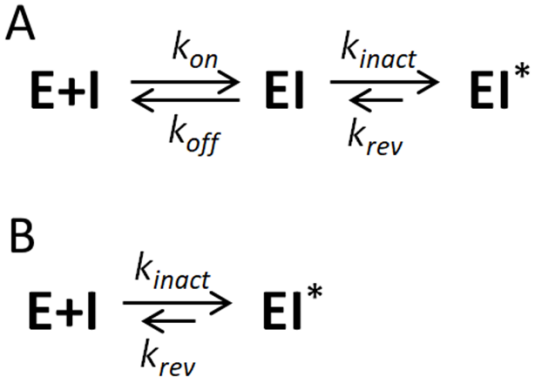

Figure II-1. Scheme representing mechanisms of time-dependent inhibition. A) Inhibitor binds to enzyme forming the EI complex, followed by slow conformation

changes or covalent modification to form EI*. Both the inactivation rate (k_{inact}) and the rate of inactivation reversal (k_{rev}) are much slower than the establishment of EI, which is determined by [I]k_{on} and k_{off}. **B)** This mechanism represents a rare case where the initial binding of inhibitor to enzyme is slow.

Inhibition of Ddl by 3-amino-2-oxybutylphosphonate was assessed by measuring the formation of MgATP by the reverse reaction at varied concentrations of inhibitor. The conditions were essentially identical to the reverse reaction assay using final concentrations of 5 mM MgADP, 700 μM D-alanyl-D-alanine, and 10 mM phosphate, unless specified otherwise. Data of the formation of product were fitted to **(eq. 2.4),** and data from the replot of k_{obs} vs. [3A2OBP] were fitted to (**eq. 2.5)** to provide the inhibition parameter $k_{inact}/K_{i,app}$.

Evaluation of reversibility of enzyme-inhibitor complexed by rapid-dilution

Recovery of enzymatic function following pre-incubation with D-alanine analogues was evaluated after rapid-dilution of the pre-incubated samples into reaction mixtures. For D-Ala-P, samples containing 3 μM Ddl and either 0 or 5 mM MgATP and 0 or 1530 μM D-Ala-P were incubated at 30 °C for 1 hour. Pre-incubation samples containing enzyme, MgATP, and D-Ala-P were then rapidly diluted 50-fold into reaction mixtures to a final volume of 250 μL, and activity of the biosynthetic reaction was measured as described above. For 3A2OBP, 20 μM of *Mt*Ddl was incubated with either 0 or 5 mM MgADP containing either 0 or 800 μM 3A2OBP (four separate conditions) for 1 hour at room temperature. Incubation samples were then rapidly diluted 50-fold into reaction mixtures to a final volume of 150 μL. Enzyme activity for the reverse direction was

measured as described above. For both compounds, the extent of recovery of enzyme activity was determined by examination of kinetic time courses and by fitting of the resulting data to (**eq. 2.4**).

Effects of addition of variable D*-alanine on protein tryptophan fluorescence.* Changes in tryptophan fluorescence during catalysis were measured by monitoring the change in fluorescence of the *Mt*Ddl-MgATP complex upon addition of D-alanine. Data were collected on a KinTek AutoSF-120 stopped-flow instrument (KinTek Corporation, Snow Shoe, PA) in which one syringe contained 3 μM enzyme, 3 mM MgATP, in assay buffer; while the other syringe contained variable concentrations of D-alanine, and 3 mM MgATP in assay buffer. The excitation wavelength was 290 nm, and the emission was collected by a 320-nm broad cutoff filter. Protein fluorescence data were collected as 500 points acquired in 0.5 seconds, and the resulting data described by an exponential "burst" of fluorescence were fitted to (**eq. 2.6**), in which Y_{max} and Y_{min} are the respective maximal and minimal values of fluorescence, and k_{obs} is the transient rate constant.

$$Fluorescence = (Y_{max} - Y_{min})(1 - e^{-k_{obs}*t}) + Y_{min} \quad (2.6)$$

The values of k_{obs} were replotted against the concentration of D-alanine and fitted to (**eq. 2.7**)

$$k_{obs} = \frac{k_{for} * D-alanine}{K_M + D-alanine} + k_{back} \quad (2.7)$$

Where k_{for} is the rate constant for the formation of the fluorescently-enhanced species and k_{back} is the rate constant for the break-down of the fluorescently-enhanced species.

Perturbation of protein tryptophan fluorescence with varied 3-amino-2-oxybutylphosphonate.

Changes in protein tryptophan fluorescence were calculated by measuring the endpoint fluorescence. Protein fluorescence data was collected in 20-µL reaction mixtures in black 384-well low-volume microplates containing 11.5 µM Ddl and 3 mM MgADP in assay buffer. Measurements were obtained by excitation at a wavelength of 280 nm, with emission captured between the wavelengths of 360-400 nm using a 325-nm cutoff filter. The effects on protein fluorescence upon binding of 3-amino-2-oxybutylphosphonate were quantified by fitting the area under the curve (AUC) for the emission spectra to (**eq. 2.8**)

$$AUC = AUC_{Max}\left(\frac{-b-\sqrt{b^2-4ac}}{2a}\right) + AUC_{Min} \quad where\ a = 1,\ b = -(E_t + K_I + I_t),\ c = E_t * I_t \quad (2.8)$$

Positional Isotope Exchange

20 µM *Mt*Ddl was incubated with either 15 µM 1-aminoethylphosphonate, 15 µM D-cycloserine, or water in assay buffer (100 mM HEPES (7.3), 20 mM $MgCl_2$, 10 mM KCl, 1 mM CHAPS), also containing 0.5 U/mL phosphoenolpyruvate carboxylase, 1 mM phosphoenolpyruvate, and 3 mM [γ-$^{18}O_4$]ATP. At the time points indicated, 400 µL of the reaction mixture was added to 100 µL of 500 mM EDTA. 450 µL of the EDTA-

quenched sample was then added to 50 µL of D_2O, and the ^{31}P NMR spectra were collected with the following parameters on a Bruker Avance III 400 Mhz NMR spectrophotometer: 512 scans, 50 ppm spectral width, and -12 ppm offset. NMR spectra were processed with Bruker TopSpin 3.6.2 software. The acquired chemical shifts (in ppm) were calibrated so that the chemical shift for added sodium phosphate was set at 0 ppm. The relative areas (integrals) for the $^{16}O_1{}^{18}O_3$ and $^{18}O_4$ species of the γ-phosphate ATP were calculated using peak deconvolution. Fractional $^{18}O_4$ was fitted to a simple exponential decay of the form:

$$Fraction\ {}^{18}O_4 = (Y_{Max} - Y_{Min})(e^{k*t}) + Y_{Min} \quad (2.9)$$

Where Y_{Max} is the Y-intercept (initial fraction of [γ-$^{18}O_4$]-ATP), Y_{Min} is the equilibrium fraction of [γ-$^{18}O_4$]-ATP, and *k* is the observed rate of conversion from [γ-$^{18}O_4$]-ATP to [γ-$^{16}O^{18}O_3$]-ATP.

Results and Discussion

Kinetics of MtDdl

The kinetic mechanisms of the D-alanine:D-alanine ligase have previously been reported for the orthologous enzyme from *Salmonella typhimurium*[66] as well as the enzyme from *M. tuberculosis*[67]. For both enzymes the kinetic mechanism was found to be ordered ter-ter with the order of substrate binding as MgATP, D-Ala_1, and D-Ala_2, followed by the ordered release of the products, phosphate, D-alanyl-D-alanine dipeptide, and MgADP. At high concentrations of D-alanine (>1 mM), the kinetic data (**Figure II-2 A**) fitted well (global R^2 >0.98) to (**eq. 2.1**) which describes a simplified ordered bi-

substrate mechanism. An intersecting initial velocity pattern of the reciprocal plot for $1/v$ vs. 1/[D-alanine] with varied concentrations of MgATP is expected for when the Michaelis constants for the two D-alanine substrates are dissimilar- as the catalytic rate is apparently unimolecular with regard to D-alanine (**Figure II-2 A, inset**). At lower concentrations of D-alanine (**Figure II-2 B**) the double-reciprocal plot of $1/v$ vs. 1/[D-alanine] with saturating MgATP was apparently parabolic, as expected for the binding of two D-alanine molecules which are reversibly connected. Fitting of these data to (**eq. 2.2)** is consistent with having a squared term in the denominator. The kinetic constants for the forward reaction (**Table II-1**) are consistent with previous studies [67], with the exception of the apparent Michaelis constant for the donor D-alanine$_1$, which was roughly five-fold higher under our conditions.

For the reverse reaction (**Table II-1**), the apparent Michaelis constant for phosphate is comparable to what was previously reported for the enzyme from *S. typhimurium* [66]. However, the apparent Michaelis constant for the dipeptide is at least one order-of-magnitude higher for the enzyme from *M. tuberculosis* under our conditions, and no significant substrate inhibition was observed at concentrations of D-alanyl-D-alanine up to 1.6 mM (**Figure II-2 C**).

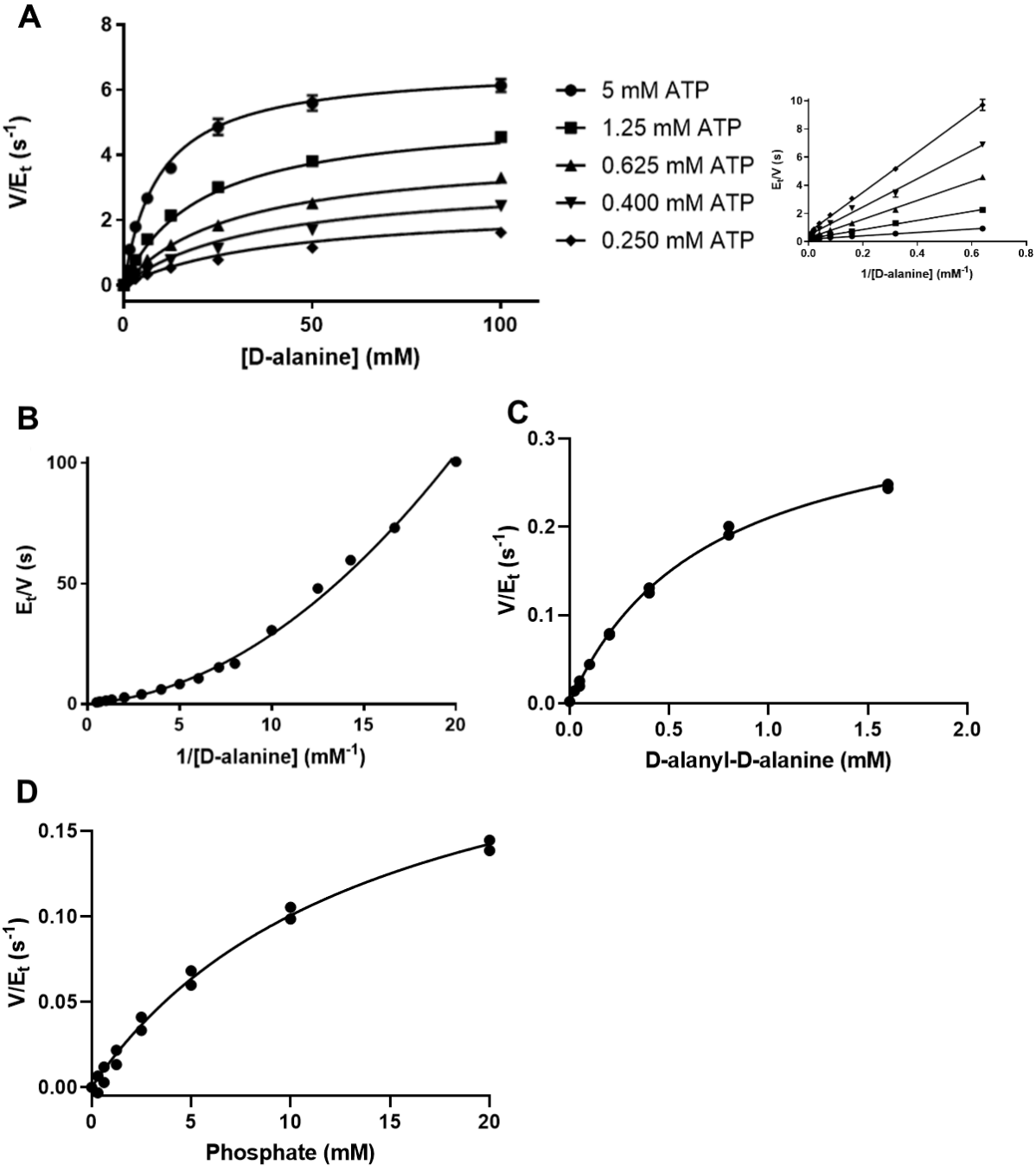

Figure II-2. Initial velocity studies of MtDdl. A) Representative data for *Mt*Ddl assayed at higher concentrations (2-100 mM) of D-alanine. Inset shows the double reciprocal plot of 1/v vs [1/D-alanine]. **B)** *Mt*Ddl assayed at lower concentrations (0.05-2 mM) of D-alanine. Reverse reaction of *Mt*Ddl rate at varied concentrations of **C)** D-alanyl-D-alanine dipeptide or at varied concentrations of **D)** phosphate.

Table II-1. Kinetic constants of *Mt*Ddl

Kinetic parameter	Value
Forward	
$\underline{k_{cat,forward}}$	6.9 ± 0.6 s^{-1}
$K_{M,MgATP}$	0.46 ± 0.09 mM
$K_{M,D\text{-}ala2}$	3.9 ± 0.8 mM
$K_{M,app,D\text{-}ala1}$	0.409 ± 0.006 mM
Reverse	
$K_{M,app,phosphate}$	14 ± 2 mM
$K_{M,app,D\text{-}alanyl\text{-}D\text{-}alanine}$	0.70 ± 0.03 mM

Enzyme conformational changes from substrate binding

Changes in the intrinsic tryptophan fluorescence of enzymes as the result of substrate and/or inhibitor binding has been previous demonstrated for *Mt*Ddl[67], the chemically-related ligase glutamine synthetase[161], and unrelated proteins such as isocitrate lyase[162]. It is thought that perturbations in the intrinsic fluorescence can be largely attributed to changes in the micro-environment of individual tryptophan residues. In the case of *Mt*Dd;, W210 and W347 are positioned proximal to active site loops and are good candidates for the observed fluorescent perturbations(PDB ID: 3LWB)[76]. The putative chemical mechanism of *Mt*Ddl likely requires the exclusion of water from the active site during catalysis to prevent hydrolysis of the D-alanyl phosphate intermediate, which would result in the nonproductive hydrolysis of ATP. Therefore it is anticipated that loop closure, which may be observable by measuring changes in tryptophan fluorescence, precedes catalytic steps. Indeed, Kitamura and colleagues have shown

progressive active site closure and conformational changes associated with substrate binding to *Thermus thermophilus* Ddl [69]. Perturbations in the intrinsic fluorescence were measured at several concentrations of the substrate D-alanine (**Figure II-3 A**). The fluorescent signal rapidly increased to a limiting value and was well described by a single exponential fit (**eq. 2.6**). The fit of the observed rate (k_{obs}) as a function of D-alanine yielded a forward rate of 20 ± 1 s^{-1} with an apparent Michaelis constant of K_M = 2.3 ± 0.5 mM (**Figure II-3 B**). The Michaelis constant for $D_{ala,2}$ determined by this method is comparable to the kinetic determination of the Michaelis constant for the substrate (2.3 ± 0.5 mM vs 3.9 ± 0.8 mM). The transient rate of 20 ± 1 s^{-1} is faster than the rate determined for catalysis (k_{cat} 6.9 ± 0.6 s^{-1}), which is consistent with the suggestion that the observed changes in tryptophan fluorescence occur during conformational changes that precede catalysis.

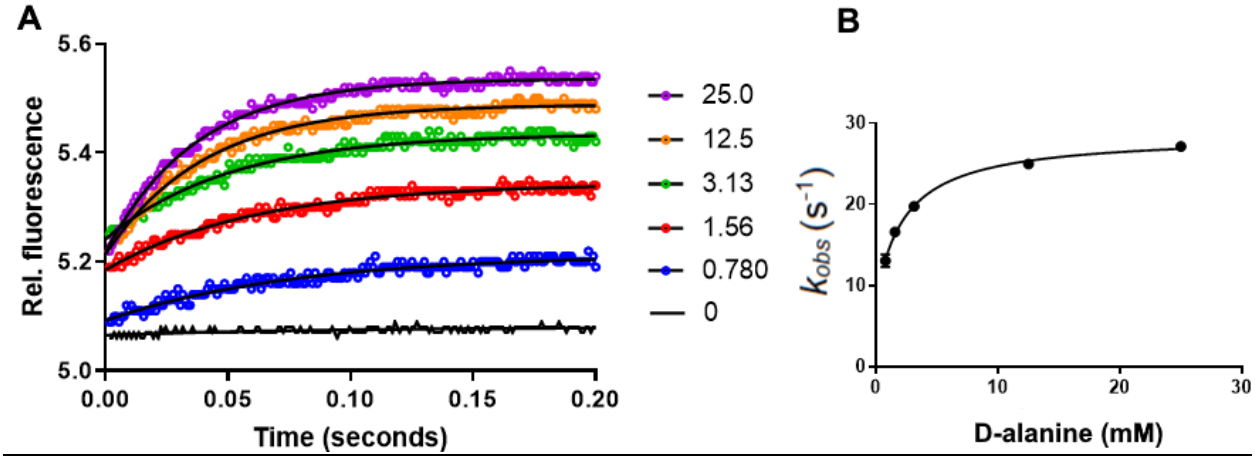

Figure II-3. Binding of D-alanine to *Mt*Ddl-MgATP complex. **A)** Intrinsic tryptophan fluorescence of binding of 3 μM Ddl, 3 mM MgATP, and 0-25 mM D-alanine. **B)** Replot of transient kobs vs. D-alanine calculated from data in A and fitted to (**eq. 1.7**)

This observation is however in stark contrast to previous work[68] which has found that the transient rate was much faster than the catalytic rate for *E. coli* DdlB and *Enterococcus faecium* VanA enzymes, which results in a "burst" in formation of product ADP when monitoring the reaction using pre-steady-state techniques. In contrast, the pre-steady-state/catalytic rate ratio of approximately 3 for MtDdl would imply that product release is limiting to a much lower degree than other Ddl orthologous, and would predict that no "burst" of ADP formation would be detected during pre-steady-state kinetic analysis. The effect of D-Ala-P on the intrinsic tryptophan fluorescence was also examined. However due to the much slower rate of inactivation compared to catalysis, photobleaching became a complicating factor, and reliable data could not be acquired (**APPENDIX C**).

Evaluation of analogues of D-alanine as potential MtDdl inhibitors.

We have investigated the inhibitory potential of a small library of compounds with structures that mimic aspects of substrate and/or reaction intermediates for the biosynthetic reaction of *Mt*Ddl. Unfortunately and surprisingly, few of these compounds showed significant inhibition under our conditions, despite modest structural changes relative to the substrate D-alanine (**Table II-2**). Perhaps the most illustrative of the results is the lack of apparent inhibition arising from only small changes in the sidechain, such as substitution of the methyl group of D-alanine with a trifluoromethyl group (**3**) or a cyclopropyl group (**4)**. Substitution of the carboxyl group of D-alanine with the

bioisosteres, including a tetrazole (**5**), an oxetane (**8**), or an 3-methoxyisoxazole (7) group in kind provided analogues of D-alanine which did not exert inhibition at the concentrations tested.

Replacement of the carbonyl group with tetrahedral sulfonates (**6, 10)** also demonstrated no significant inhibition. In addition, replacement of the amino group with methyl (**1**) or chloro (**2**), and methylene increase to the amino-carboxylate distance, as exemplified by β-alanine (**9**), showed no significant inhibition at 10 mM. The observation of high selectivity for chemical groups that mimic the sidechain and α-amino group of D-alanine is in line with what has previously reported for orthologous enzymes[48, 66]. Although the formation of analog-D-alanine and D-alanyl-analog products was not directly assessed in this study, the lack of significant changes in the rate of ATP hydrolysis over a wide range of compound concentrations (compounds **3-10)** renders the possibility for the formation of such products unlikely, as a poor substrate competing for catalysis would inhibit the formation of MgADP.

Table II-2. Analogs of D-alanine. Biological substrate D-alanine boxed; **11** – 1-aminoethylphosphonate (D-Ala-P); **12**- 3-amino-2-oxybutylphosphonate (3A2OBP); **13**- D-cycloserine (DCS)

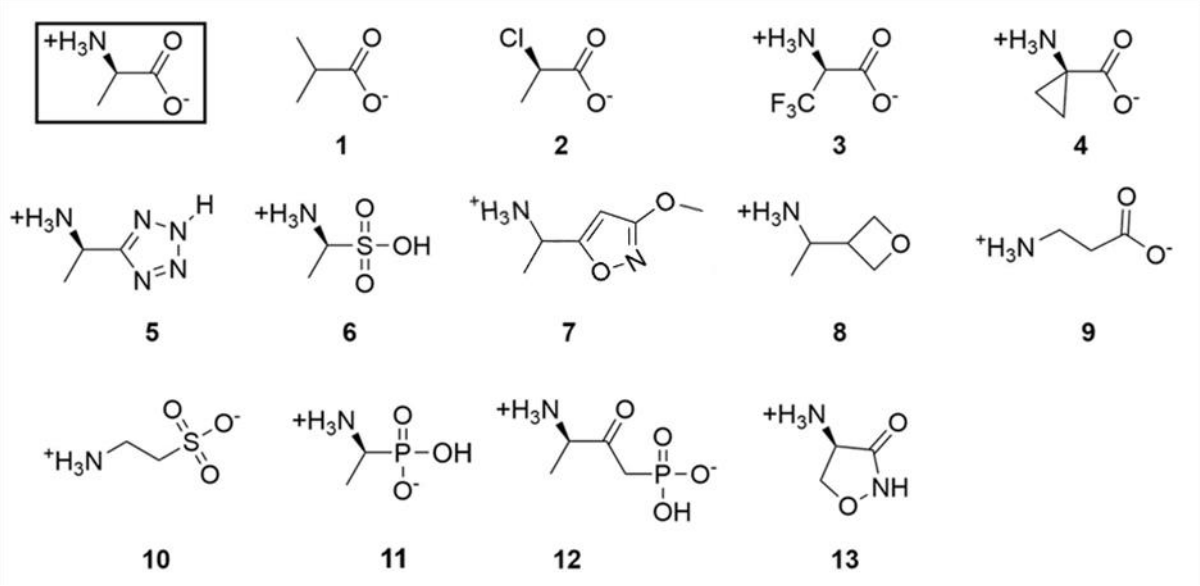

Inactivation by 1-aminoethylphosphonate (D-Ala-P)

We investigated whether or not 1-aminoethylphosphinate (D-Ala-P; compound **11** in **Table** II-2) could afford mechanism-based inhibition of *Mt*Ddl for several reasons: 1) the inactivation of *S. typhimurium* Ddl by D-Ala-P has been studied in detail[85], 2) the mechanism of inactivation likely proceeds through a phosphorylation event analogous to the biosynthetic mechanism in which the phosphonate is expected to be phosphorylated[85], and 3) the compound is commercially available. Similar to the inactivation of *S. typhimurium* Ddl [85], *Mt*Ddl was inactivated by D-Ala-P in a time-dependent manner (**Figure II-4 A**). The observation of time-dependent inhibition is

often diagnostic of a two-step mechanism in which initial binding of the enzyme and inhibitor is relatively weak and rapid, followed by a slower chemical step and/or conformational change that results in an overall higher affinity enzyme-inhibitor interaction. The replot of k_{obs} values, which relate to the establishment of the overall enzyme-inhibitor equilibrium, shows that the apparent first-order rate constant k_{obs} varies linearly with D-Ala-P concentrations up to 880 μM. The inability to asymptotically approach the limiting value of k_{obs} at relatively high levels of D-Ala-P (**Figure II-4 B**) (lack of saturation) is consistent with the formation of a weak initial EI complex, suggesting that the tetrahedral phosphonate substituent of D-Ala-P is not a good replacement for the planar carboxylate group of substrate D-Ala. (**Figure II-4 A inset, Figure I-4 intermediate II**). To determine the minimal requirements and to assess the reversibility of inactivation, enzyme was pre-incubated with D-Ala-P in the presence or absence of MgATP, and then rapidly diluted 50-fold into assay buffer, within which residual enzyme activity was measured. The results of the rapid-dilution assay (**Figure II-4 C)** showed that MgATP was required to elicit the high affinity EI* complex. Enzyme and inhibitor, and enzyme and MgATP alone showed no significant loss of activity when compared to control samples (**Figure II-4 C**). This suggested that D-Ala-P binds primarily to the enzyme-MgATP complex, presumably to the binding site of donor D-alanine$_1$, and then either undergoes phosphorylation, similarly to what has been previously reported for aminoalkylphosphinate inhibitors[86, 87], a slow conformational change, or both.

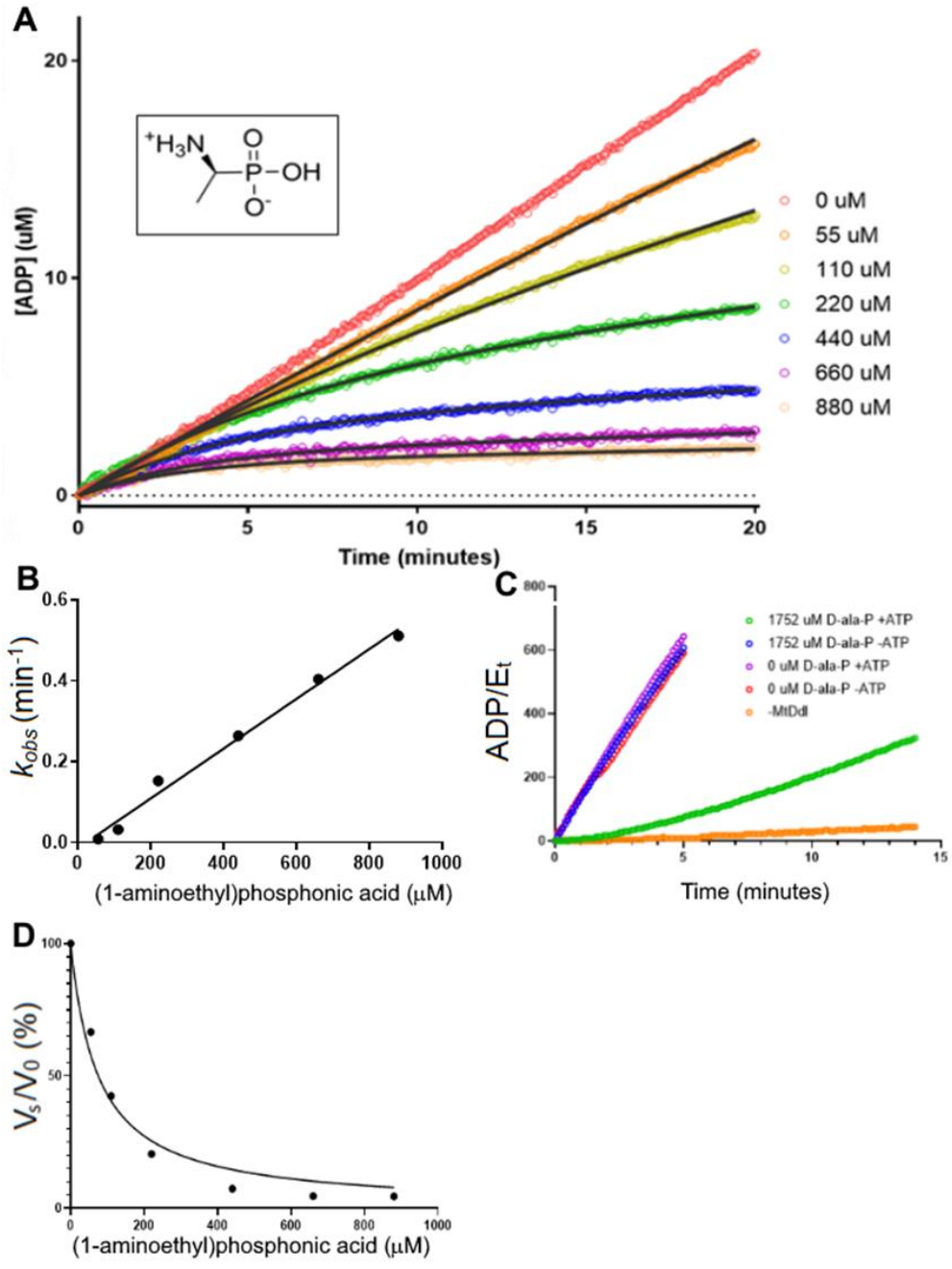

Figure II-4. Inhibition of MtDdl by 1-aminoethylphosphonic acid. A) Time-course of inhibition of *Mt*Ddl biosynthetic reaction at indicated concentrations of D-Ala-P, and with the structure of D-Ala-P in the inset. **B)** Replot of k_{obs} values vs. [D-Ala-P] determined by fitting data in A to (**eq. 2.4**). **C)** Reversibility of inhibition by D-Ala-P. **D)** Replot of normalized steady-state rate versus concentration of D-Ala-P fitted to (**eq. 2.3**).

Recovery of enzyme activity was slow, on the order of $1x\ 10^{-2}$ min^{-1}. Taken together, the value of the second-order rate constant $k_{inact}/K_{i,\ app}$ for the inactivation can be estimated to be $1x10^2$ $M^{-1}s^1$, which is within the same order-of-magnitude for the inactivation of *S. typhimurium* Ddl [85]. When considering the effect of a competing substrate, the value for the bimolecular rate constant can be extrapolated to approximately $1x10^3$ $M^{-1}s^{-1}$, which is much slower than a diffusion-limited process and may imply that there exist significant barriers for D-Ala-P binding to the enzyme. From plotting the relative activity as a function of D-Ala-P concentration, the overall dissociation constant of D-Ala-P from the enzyme (K_I^*) was determined to be 7.1 ± 0.9 μM (**Figure II-4 D**).

Inactivation by 3-amino-2-oxybutylphosphonate (3A2OBP)

To probe the potential binding and interactions of Ddl with other substrate analogs which may mimic the structures of reaction intermediates, we investigated the effects of 3A2OBP on Ddl catalysis. 3A2OBP (**Figure II-5 A, inset**) is a non-hydrolyzable mimic of the acyl-phosphate intermediate (**Figure I-4, Intermediate I**). 3A2OBP inhibition of the enzyme from *S. faecils* has been previously reported, however the mechanism of inhibition was not studied in detail[88]. In a similar fashion to D-Ala-P, 3A2OBP inhibited Ddl in a time-dependent manner (**Figure II-5 A**).

Additionally, the observed rates of inactivation did not display saturation at concentrations of 3A2OBP up to 1.6 mM, suggesting weak interactions in the initial EI complex formation (**Figure II-5 B**). Pre-incubation experiments showed that the

inactivation was reversible, and required the addition of MgADP (Figure II-5 **C**), indicating that the inhibitor bound to the enzyme-MgADP complex. The recovery of enzyme activity from a pre-formed complex of E-MgADP-3A2OBP was very similar to that of D-Ala-P, (k_{rev} on the order of 1x 10^{-2} min^{-1}). To further investigate the mechanism of inactivation, Ddl was treated with a range of 3A2OBP concentrations at several fixed concentrations of either D-alanyl-D-alanine (**Figure II-5 D**) or phosphate (**Figure II-5 E**). Variable concentrations of D-alanyl-D-alanine over an approximately 8-fold range had no significant effect on the apparent second-order rate constants of inactivation by 3A2OBP, indicating that the inactivator prevented binding of the dipeptide product. On the other hand, increasing the concentration of phosphate across an 8-fold concentration range had a substantial effect in lowering the apparent second-order rate constant of 3A2OBP inhibition.

The binding of 3A2OBP was further examined by monitoring the intrinsic tryptophan fluorescence of Ddl. Binding of the inhibitor to Ddl-MgADP was observed to increase the fluorescence intensity, suggesting that like D-alanine, binding of 3A2OBP to Ddl resulted in conformational changes (**Figure II-6**). From this experiment the overall dissociation constant for 3A2OBP was determined to be 6 ± 1 μM. The finding that 3A2OBP binds to the E-ADP complex (**Figure II-5 C, Figure II-6**) and that 3A2OBP is competitive versus phosphate (**Figure II-5 E**) indicates that phosphate is the second product released during catalysis. This is contradictory to what has been reported for the kinetic mechanisms of the Ddls from *M. tuberculosis* [67] and *S. typhimurium* [66],

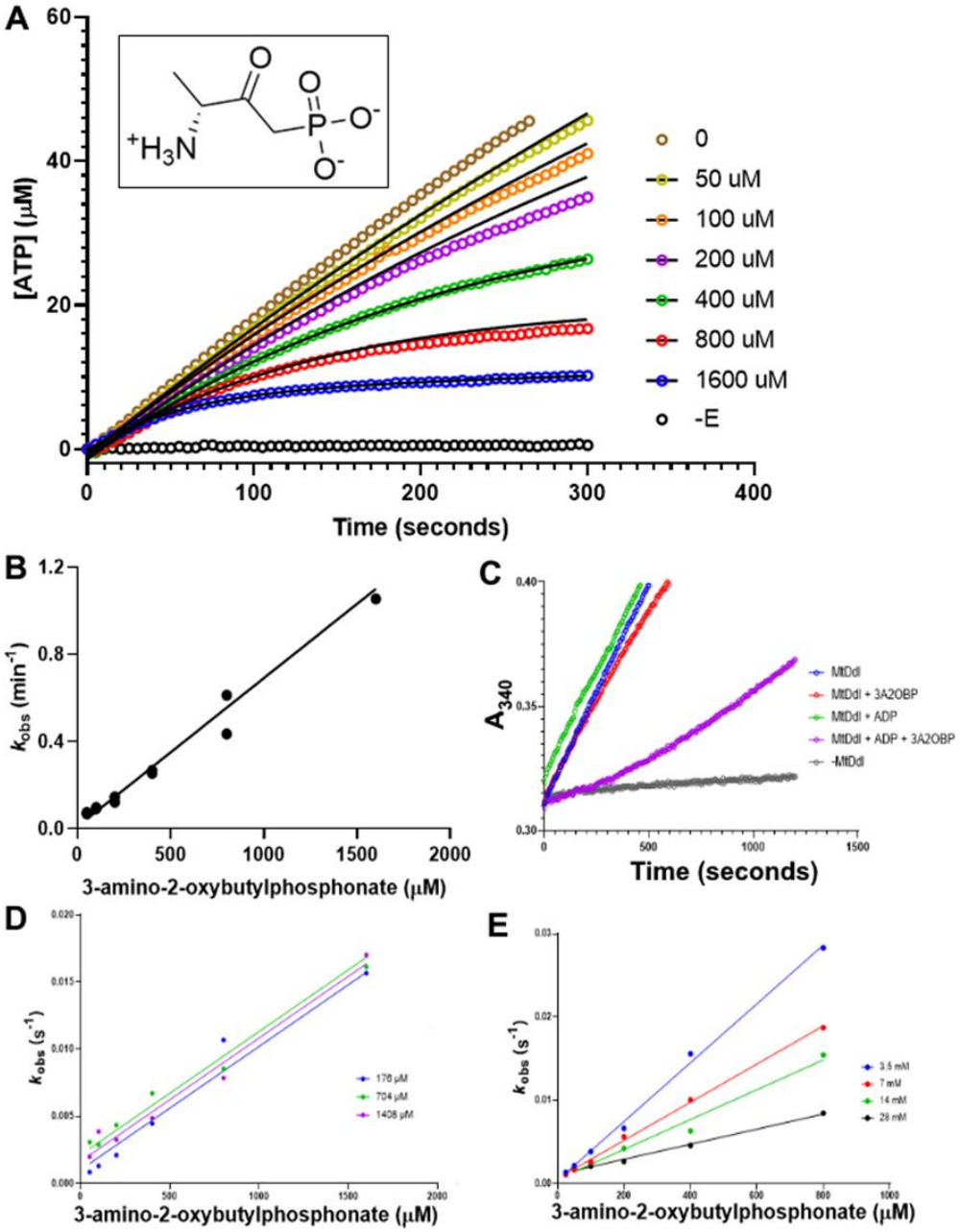

Figure II-5. Inhibition of *Mt*Ddl by 3-amino-2-oxybutylphosphonate. A) Representative time-course of *Mt*Ddl phosphorolysis inhibition by 0-1.6 mM 3A2OBP, structure of 3A2OBP in inset. **B)** Replot of k_{obs} vs. [3A2OBP] from data in **A** fitted to **(eq. 2.4). C)** Reversibility of inhibition by 3-amino-2-oxybutylphosphonate. Replot of k_{obs} values for inhibition of *Mt*Ddl by 3A2OBP at several concentrations of D-alanyl-D-alanine substrate **(D)** or phosphate substrate **(E).** Differences in slopes for data in (**D**) were determined to be insignificant. When fitted with slopes shared between datasets global $R^2 > 0.97$.

for which phosphate is proposed to be the first product released for the biosynthetic reaction. However, in both of these studies, the inability to observe uncompetitive patterns of phosphate versus MgATP at saturating levels of D-alanine (both the second and third substrate) implies a more complicated kinetic mechanism than the strictly ordered product release.

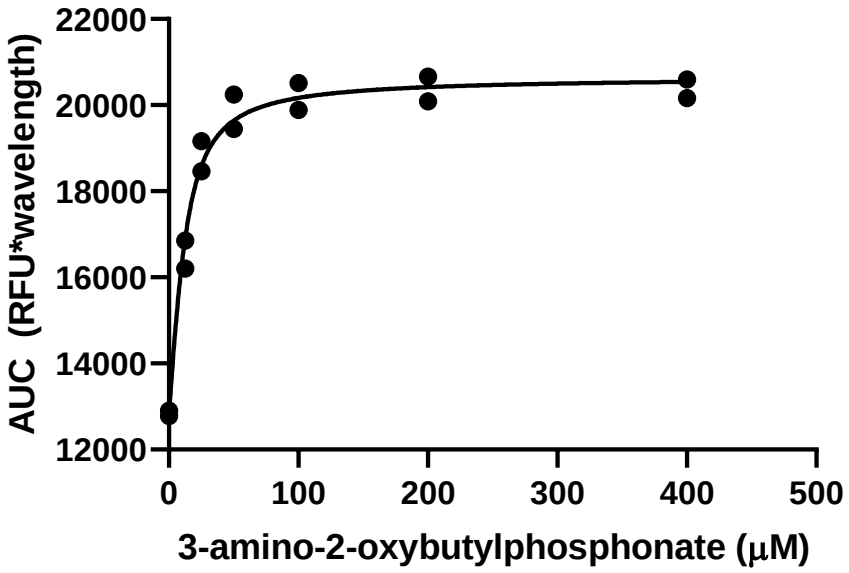

Figure II-6. Intrinsic tryptophan fluorescence of *Mt*Ddl is enhanced upon treatment with 3A2OBP. Fluorescence is enhanced by interaction of 3A2OBP with *Mt*Ddl-MgADP binary complex. Fitted to **(eq. 2.8).**

Positional Isotope Exchange (PIX)

To determine whether the inactivation of *Mt*Ddl by D-Ala-P and DCS is the result of an enzyme-catalyzed reversible phosphorylation of the two inhibitors, the ability of the compounds to catalyze positional isotope exchange of [γ-$^{18}O_4$] ATP [163, 164] was

examined. If either D-Ala-P or DCS is able to undergo a phosphoryl transfer from the γ-phosphate of γ-$^{18}O_4$-labelled ATP, and the β-phosphorus is able to freely rotate around the α-β bond, then the expected results should be an overall loss of γ-$^{18}O_4$ to γ-$^{16}O^{18}O_3$ to a final equilibrium of 1:2 (**S1**). Ddl was incubated with D-Ala-P and DCS such that the concentrations of enzyme and inhibitor were calculated to yield approximately a 1:1 ratio of E-MgATP and E-MgATP-I complexes. DCS was found to induce PIX at a rate that was more than twice that of the rate of exchange in its absence, $((5 \pm 1) \times 10^{-2}\ hr^{-1}$ vs $(12 \pm 1) \times 10^{-2}\ hr^{-1}$) (**Figure II-8)**, consistent with the reversible phosphorylation of enzyme-bound DCS by the γ-phosphate of ATP, which has been demonstrated with two different orthologous Ddl enzymes[78, 79]. It is likely the phosphorylation of DCS contributes to the potency, shifting the equilibrium away from the E-MgATP binary complex (**Figure II-7**).

The rate of PIX for D-Ala-P, when compared to the control (no compound), was not significantly different (**Figure II-8 A)**. In both cases the background rate of exchange was high, likely due to background hydrolysis of ATP, and the subsequent reverse reaction. This is supported by the formation of ADP (not shown), and the formation of the γ-$^{16}O_2{}^{18}O_2$ species at later time points (**Figure II-8 B-D)**.

The lack of observed PIX with added D-Ala-P does not necessarily eliminate the possibility of inhibitor phosphorylation. However phosphorylation of this inhibitor is very unlikely, especially when considering the much slower inactivation and reactivation

rates of D-Ala-P versus DCS. The same technique was unable to be applied to 3A2OBP as the γ-$^{18}O_4$-labelled ATP was an unsuitable probe for an inhibitor that structurally mimics intermediate I (**Figure I-4**) and binds to the Ddl-MgADP complex. The phosphonate compounds (D-Ala-P and 3A2OBP), as well as the antibiotic DCS all contain functional groups that mimic the α-amino group of D-alanine. While the methyl

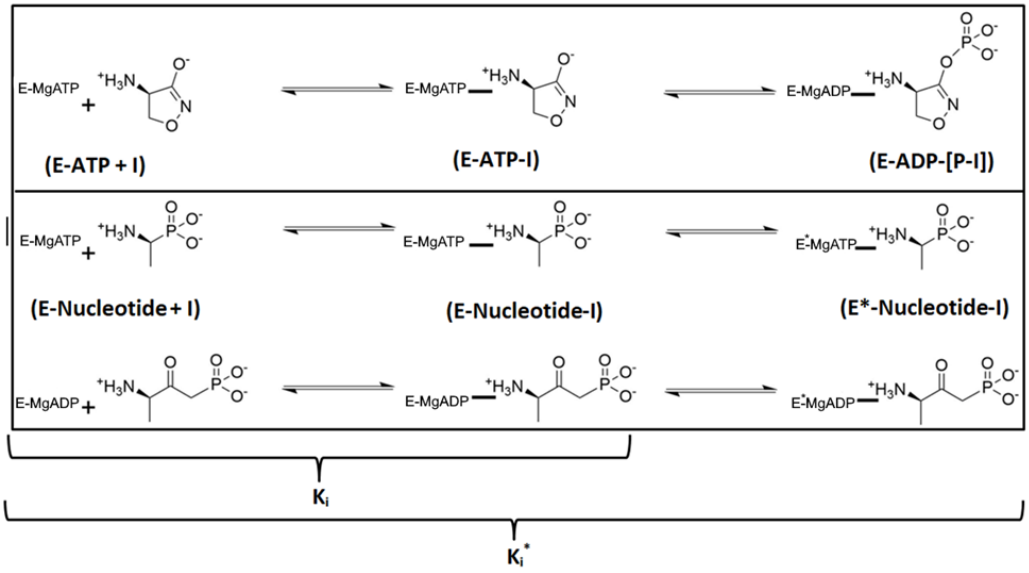

Figure II-7. Proposed Mechanism of inhibition of MtDdl by DCS, D-Ala-P, and 3A2OBP. All three compounds initially bind to an E-Nucleotide complex. In the case of DCS and D-Ala-P the nucleotide is ATP, whereas for 3A2OBP the nucleotide is ADP. DCS is then phosphorylated by the γ-phosphate of ATP to yield a phospho-DCS molecule and ADP. For 3A2OBP and D-Ala-P the enzyme undergoes a conformational change, pulling the overall equilibrium away from the free (non-inhibited) E-Nucleotide complex.

sidechain of the phosphonate compounds is identical to the physiological substrate, the structurally dissimilar cyclic group of DCS is evidently able to be accommodated in the active site. Inactivation of *Mt*Ddl by DCS has been observed by us (data not shown) and

others[77] to be rapid, occurring in the dead-time of a typical steady-state assay. In contrast, inactivation by D-Ala-P and 3A2OBP was slow and readily observed over the course of minutes in steady-state assays (**Figure II-4 A, Figure II-5 A**). Although the much more rapid inactivation rate of DCS compared to the phosphonate compounds,

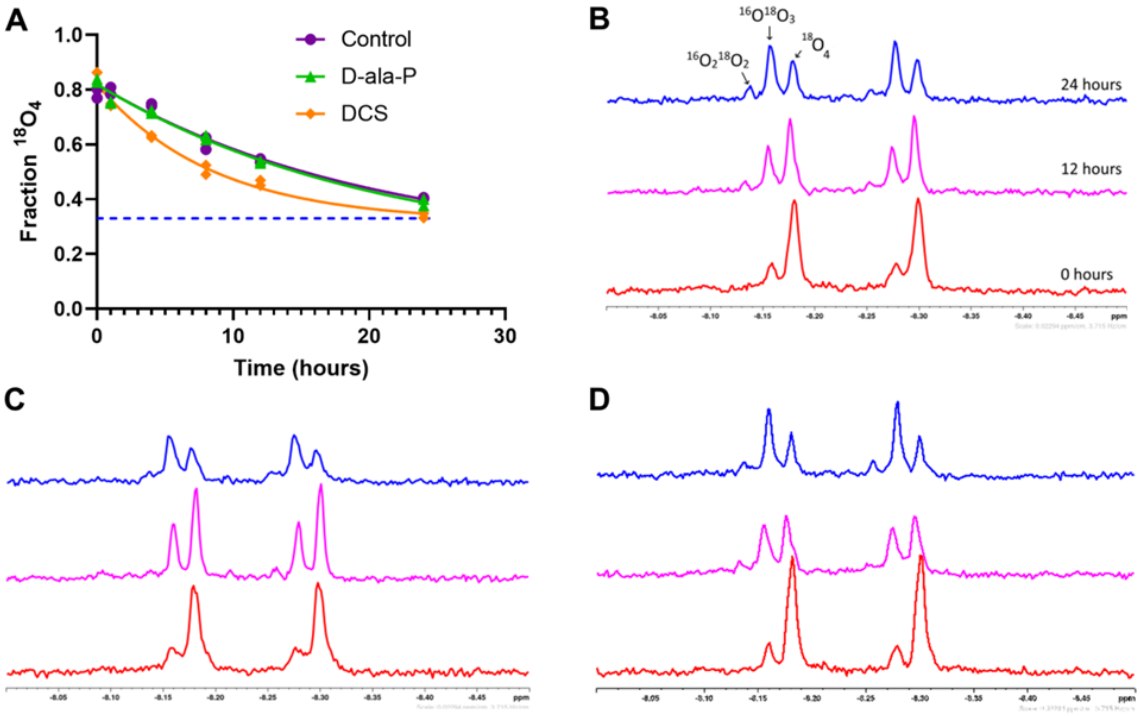

Figure II-8. Positional Isotope Exchange of γ-$^{18}O_4$-ATP. **A**) Plot of $^{18}O_4$ in the γ-phosphate position of MgATP versus time. MtDdl was treated with D-Ala-P, DCS, or compound-free (control). The dotted line represents theoretical equilibrium. The plotted values were determined from individual integrations of the γ-phosphate doublets (^{31}P NMR spectra) and fitted to **(eq. 2.9).** ^{31}P NMR spectra at indicated time points for compound-free control **(B),** D-Ala-P **(C),** and DCS **(D).**

D-Ala-P and 3A2OBP, cannot presently be explained, their modes of inactivation have several commonalities: 1) All three compounds appear to bind poorly to the initial EI complex, which is manifested by unsaturatable plots of k_{obs} vs. inhibitors at concentrations of inactivator much higher than the overall dissociation constant (K_I^*)

(**[77]**, **Figure II-4 B, Figure II-5 B).** 2) All three compounds exhibit reversible inhibition, and required nucleotide for binding (**[77]**, **Figure II-4 C, Figure II-5 C).** For DCS and D-Ala-P, binding to the E-MgATP complex provided evidence for inhibitor binding to the N-terminal site (D-Ala_1); as *Mt*Ddl conforms to an ordered kinetic mechanism (**Figure II-2 A-B, [67]**). 3) The binding of all three compounds increased the intrinsic fluorescence of *Mt*Ddl (**[67], Figure II-6, APPENDIX C**), and the observed fluorescence enhancement was similar to what occurs during catalysis (**Figure II-3 A**), indicating that binding of inhibitors to the enzyme induces conformational changes, presumably closure of the active site. 4) All three compounds displayed moderately potent inhibition with similar dissociation constants on the order of 1 μM, corresponding to respective ratios of $K_i^*/K_{M,D\text{-}ala1}$ of 0.010, 0.015, and 0.017 for DCS, 3A2OBP, and D-Ala-P; implying that binding of the inhibitor to enzyme captures signficantly greater binding energy than substrate D-alanine.

The weak initial binding, apparent conformational changes and overall relatively potent binding of DCS, D-Ala-P, and 3A2OBP can be described by the following model (**Figure II-7**): DCS, D-Ala-P, and 3A2OBP bind to the Ddl-nucleotide binary complex. The enzyme undergoes a conformational change, closing the active site and providing interactions to stabilize the catalytic intermediates. For D-Ala-P and 3A2OBP the phosphonate groups capture these interactions, stabilizing the EI^* complex. Conversely, DCS is phosphorylated by the γ-phosphate of MgATP yielding a phosphorylated product that apparently achieves faithful mimicry of the E-MgADP-D-Ala-phosphate complex.

Previous reports of inactivation/inhibition of Ddl by DCS have been entangled by contradictions: the enzyme from *M. tuberculosis* has been reported to either bind both D-alanine sites with equal affinity[67], bind both sites with different affinities [76], and bind exclusively to the C-terminal (acceptor) D-alanine site[77]. However in light of the apparent phosphorylation observed in this study and more recent studies of *E. coli* DdlB[79] and *Thermus thermophilus* Ddl[78], in which both presented evidence for DCS phosphorylation and binding primarily to the N-terminal (donor) site, we propose that binding of DCS to the N-terminal D-alanine site (D-alanine$_1$) comprises the main contribution of DCS inhibition of the clinically relevant *Mt*Ddl enzyme.

In summary, the work here has demonstrated the high degree of selectivity of D-alanine substrate analogs for *Mt*Ddl. The majority of compounds tested were unable to inhibit enzymatic catalysis significantly. The notable exceptions are the mimics of Intermediate I (3A2OBP) and II (D-Ala-P) of the catalytic cycle and the clinical antibiotic, D-cycloserine. All three of these inhibitors require nucleotide for binding and were of similar inhibitory potency. D-cycloserine was apparently reversibly phosphorylated in the active site of *Mt*Ddl, providing further evidence for a general mechanism of action of the antibiotic, one in which inhibition is primarily caused by binding to the N-terminal (donor) D-alanine site[78, 79].

CHAPTER III

KINETIC CHARACTERIZATION AND TRANSITION-STATE ANALOG INHIBITORS OF A HYPOXANTHINE-GUANINE PHOSPHORIBOSYLTRANSFERASE FROM *TRYPANOSOMA CRUZI*

Chagas disease, caused by the protozoa parasite *Trypanosoma cruzi*, primarily affects populations in Latin America where up to 8 million people are believed to be infected[165]. Current treatment for Chagas disease relies on the anti-parasitic drug benznidazole and to a lesser extent nifurtimox, both of which are replete with negative side effects and effective only in acute infections[166]. The severity of the side effects of these two drugs is so severe that treatment is often abandoned[96, 105]. Once the disease progresses into the chronic stage it is generally considered to be incurable and roughly a quarter of the victims will develop debilitating damage to the cardiovascular system [96, 99, 103-105].

Presumably in an adaptation for parasitism, *T. cruzi* like most other parasitic protozoa, are purine autotrophs which lack a functional *de novo* synthesis pathway for purine nucleotides[147]. Instead, the parasite relies on the utilization of pre-formed purines by the so-called salvage pathway, from which the nucleotide requirements of the organism are met. Hypoxanthine-guanine phosphoribosyltransferases (HGPRTs) are enzymes of the purine salvage pathway, catalyzing the formation of GMP and IMP from 5-phospho-α-D-ribose-1-diphosphate (PRPP) and the purines guanine and hypoxanthine,

respectively. Notably, IMP is positioned at the branching point of the salvage pathway, of which either IMP can be converted into GMP or AMP. The importance of HGPRTs for nucleotide synthesis in *T. cruzi* presents these enzymes as promising drug targets for the treatment of Chagas disease.

In this study we sought to develop transition-state analog inhibitors (TSAIs) of the HGPRT enzymes from *T. cruzi*. Our approach was highly influenced by the development of TSAIs for other *N*-glycotransferase enzymes, for which inhibitors of picomolar and/or nanomolar potency have been developed [167-172]. *T. cruzi* CL Brener has two pairs of genes encoding putative HGPRT activity. One of these pairs is identified by the non-Esmeraldo-like gene TcCLB.509693.70 (referred to here as TcA) and the Esmeraldo-like gene TcCLB.506457.30 (referred to here as TcC), which share a high degree (>98%) of amino-acid identity. Our results indicate that these two HGPRT genes are functionally identical, with both enzymes having essentially identical kinetic constants to what has been previously published for the TcA variant [173, 174]. This finding is consistent with the divergence between the two genes arising through random mutations that are not physiologically significant. The kinetics of TcC were examined in detail, and the enzyme was found to be kinetically more similar to human HGPRT [175] than *Plasmodium falciparum* hypoxanthine-guanine-xanthine phosphoribosyltransferase (HGXPRT)[176], with product release being the rate limiting step. TSAIs of *Pf*HGXPRT were found to be excellent inhibitors of the enzyme with the most potent

inhibitors binding with nearly picomolar affinity. The tight binding of Immucillin HP provided evidence for a transition state with significant S_N1 character.

Materials and Methods

Materials

Adenine, adenosine 5'-monophosphate, guanine, guanosine 5'-monophosphate, hypoxanthine, inosine 5'-monophosphate, 5-phospho-α-D-ribose-1-diphosphate (PRPP), magnesium chloride, ammonium acetate, imidazole, sodium phosphate (mono/di)basic, potassium phosphate (mono/di)basic, ethylenediaminetetraacetic acid (EDTA), sodium chloride, glycerol, tetrabutylammonium bisulfate, imidazole, 4-(2-hydroxyethyl)-1-piperazinepropanesulfonic acid (EPPS), *N*-[tris(hydroxymethyl)methyl]-3-aminopropanesulfonic acid (TAPS), 2-[4-(2-hydroxyethyl)piperazin-1-yl]ethanesulfonic acid (HEPES), xanthine oxidase, acetonitrile, and PEG-10000 were purchased from Sigma Aldrich/Sigma Millipore (Burlington, MA).

Expression and Purification of Typanosoma cruzi HGPRTs: TcC and TcA

The genome of *Trypanosoma cruzi* strain CL Brener encodes two putative hypoxanthine-guanine phosphoribosyltransferase (HGPRT) genes, one of these genes consist of two homologs: named herein TcA (TcCLB.509693.70) and TcC (TcCLB.506457.30), with 98% shared amino-acid identity. The coding sequences of each isoform were synthesized, and cloned into pET-28a(+) expression vector using NdeI and HindIII restriction sites (GenScript). Soluble expression of both TcA and TcC,

with N-terminal His-tags, was obtained in *Escherichia coli* C43(DE3) cells grown on TB media, in a shaker incubator at 37 °C and 180 RPM, in the presence of kanamycin (50 μg/mL). Cell cultures were grown until an OD_{660} of 0.4-0.6 was obtained, and induction was initiated by the addition of IPTG (final concentration 1 mM), and cell growth continued for 24 hours under the same conditions. Cells were harvested by centrifugation at 5000 RPM for 45 minutes (4 °C), and cell pellets were stored at -20 °C until purification.

Cell pellets were resuspended in lysis buffer containing 50 mM Na_2HPO_4/NaH_2PO_4 (pH 7.4) and 300 mM NaCl. Lysozyme was added to 0.2 mg/mL, and cells were disrupted by sonication (60% amplitude for 15 cycles of 10 seconds on and 59 seconds off). Cell lysates were then clarified by centrifugation (40000 x(g) for 45 minutes at 4 °C). Streptomycin sulfate was added to the clarified lysate to a final concentration of 1% (w/v), and after incubating at 4 °C for 30 minutes, the mixture was again clarified by centrifugation. The clarified supernatant was then dialyzed against buffer containing 50 mM sodium phosphate (pH 7.4) and 300 mM NaCl using 12-14k MWCO dialysis membranes (Spectrum Spectra/Por 4 regenerated cellulose). The dialysate was then applied to a column of approximately 10 mL of HisPur Ni-NTA resin, pre-equilibrated with lysis buffer containing 10 mM imidazole (equilibration buffer). The resin was washed with 5 column volumes of equilibration buffer, followed by 5 column volumes of wash buffer 1 (lysis buffer with 20 mM imidazole), followed by 2 column volumes of wash buffer 2 containing 50 mM imidazole. Protein was eluted with 15 column

volumes of elution buffer (lysis buffer with 300 mM imidazole), the first 2 CVs were later discarded. Approximately 150 mL of the elution fractions were dialyzed against 5x 2 L of buffer containing 50 mM EPPS, 500 mM ammonium sulfate, 50 mM L-arginine, and 50 mM L-glutamate (pH 8.3) at 4 °C. Protein was concentrated with a 10K MWCO spin concentrator (MilliporeSigma Amicon) and glycerol was added to a final concentration of 10% (v/v). Protein was flash-frozen with liquid nitrogen and stored at -20 °C.

Expression and Purification of Adenine Phosphoribosyltransferase (APRT1)

The coding sequence encompassing the adenine phosphoribosyltransferase gene from *Trypanosoma brucei* brucei (strain TREU927, Tbb927.7.1780) was synthesized and cloned into pET-28a(+) expression vector using NdeI and HindIII restriction sites (GenScript). Soluble expression of the recombinant protein with a N-terminal His-tag was observed in *Escherichia coli* C43(DE3) cells grown on TB media, in a shaker incubator at 37 °C and 180 RPM, in the presence of kanamycin (50 μg/mL). Cell cultures were grown until an OD_{660} of 0.4-0.6 was obtained, and induction was initiated by the addition of IPTG (final concentration 1 mM), and cell growth continued for 24 hours under the same conditions. Cells were harvested by centrifugation at 5000 RPM for 45 minutes (4 °C), and cell pellets were stored at -20 °C until purification.

Cell pellets were resuspended in lysis buffer (50 mM sodium phosphate (7.4) and 300 mM NaCl). Cells were disrupted by the addition of lysozyme (final concentration of 0.2 mg/mL), and the cell suspension was stirred for 30 minutes at 4 °C. Cells were then

disrupted by sonication (60% amplitude for 15 cycles of 10 seconds on and 59 seconds off), and the lysate was clarified by centrifugation. Streptomycin sulfate was added to a final concentration of 1% (w/v), and after incubating at 4 °C for 30 minutes, the mixture was again clarified by centrifugation. The clarified supernatant was then dialyzed against buffer containing 50 mM sodium phosphate (pH 7.4) and 300 mM NaCl using 12-14k MWCO dialysis membranes (Spectrum Spectra/Por 4 regenerated cellulose). The dialysate was then applied to a column of approximately 10 mL of HisPur Ni-NTA resin, pre-equilibrated with dialysis buffer containing 10 mM imidazole (equilibration buffer). The resin was washed with 5 column volumes of equilibration buffer, followed by 5 column volumes of wash buffer containing 20 mM imidazole, followed by 2 column volumes of wash buffer containing 50 mM imidazole. Protein was eluted with 15 column volumes of elution buffer (300 mM imidazole). Elution fractions were pooled and dialyzed against buffer containing 50 mM Tris (pH 8.0), 10 mM $MgCl_2$, and 2.5 mM DTT. Samples were filtered with a 5 μm syringe filter (PALL Acrodisc) and glycerol was added to a final volume of 10% (v/v). 25 mL of these samples were later dialyzed against 2x 2 L of buffer containing 50 mM sodium phosphate (pH 7.4), 0.1 mM DTT, and 1.4 mM $MgCl_2$ using a 12-14k MWCO dialysis membrane (Spectrum Spectra/Por 4 regenerated cellulose). The dialyzed sample was then concentrated using a 10K MWCO regenerated cellulose spin concentrator (MilliporeSigma Amicon). Protein samples were flash-frozen with liquid nitrogen and stored at -80 °C

Expression and Purification of adenine deaminase

The coding sequence of the zinc-dependent adenine deaminase from *Saccharomyces cerevisiae*, encoded by the gene aah1 (Uniprot P53909), was synthesized and cloned into a pET-28a(+)-TEV expression vector using NdeI and HindIII restriction sites (GenScript). Soluble expression of the recombinant protein with a N-terminal His-tag was observed in Escherichia coli BL21(DE3) cells, grown on TB media. Cell cultures were grown until an OD_{660} of 0.4-0.6 was obtained, and induction was initiated by the addition of IPTG (final concentration, 1 mM), and cell growth continued for 24h under the same conditions. Cells were harvested by centrifugation at 5000 RPM for 45 minutes (4 °C), and cell pellets were stored at -20 °C until purification.

5 g of wet cell paste was resuspended in Na_2HPO_4 50 mM, NaCl 300mM, pH 7.4 buffer (purification buffer), and stirred for 1 hour at 4 °C in presence of lysozyme (0.2mg/mL). Cells were disrupted by sonication (15 cycles of 10 seconds at 60% amplitude, with 1-min intervals), followed by centrifugation at 18,000 rpm for 45 min at 4°C. The supernatant was further diluted 1:1 in equilibration buffer (Na_2HPO_4 50 mM, NaCl 300 mM, pH 7.4, imidazole 10 mM), and then applied to a 10 mL Ni-NTA column (in Equilibration buffer (HisPur resin, ThermoFisher)) at room temperature. The bound His-tagged enzyme was washed with 5-10 column volumes (CV) of purification equilibration buffer in a stepwise gradient of imidazole 20 to 50 mM, followed by elution using 10 CVs of purification elution buffer in using (Na_2HPO_4 50 mM, NaCl 300mM, pH 7.4, a stepwise gradient of imidazole 300-600 mM). Fractions containing the purified (>95%) recombinant adenine deaminase, as determined by SDS-PAGE and

Coomassie Blue staining, were pooled, and dialyzed against HEPES 50 mM (pH 7.0), NaCl 300 mM, pH 7.0. Protein concentration was determined by measurement of A_{280} nm using an extinction coefficient of 40255 $M^{-1}cm^{-1}$ as determined from the primary sequence, assuming a molecular weight of 39,635 Da., and protein concentrations were confirmed by use of the Bradford assay [17]. Homogeneous protein (determined by Coomassie staining of SDS-PAGE gel) was stored at -80°C, in presence of 10% glycerol.

Kinetic Measurements for TcC and TcA

The absorbance spectra of the IMP, GMP, and XMP reaction products of the HGPRT-catalyzed biosynthetic reaction are sufficiently different from those of the substrates hypoxanthine, guanine, and xanthine as to provide a continuous spectrophotometric assay. Calibration curves were prepared from spectrophotometric data of reaction mixtures in which known concentrations of each base were obtained prior to their quantitative conversions to their respective NMPs by an excess of 5-phospho-α-D-ribose-1-diphosphate (PRPP) and 1 μM of HGPRT. All assays were measured in assay buffer containing 50 mM EPPS (pH 8.3) and 12 mM $MgCl_2$, unless otherwise noted. All kinetic data was measured with a SpectraMax M2 plate reader (Molecular Devices, San Jose, CA). Assays in the forward direction (NMP synthesis) were measured in Grenier Bio-One UV-Star 96-well microplates in a final volume of 250 μL. The absorbance of hypoxanthine was measured at 245 nm, for which the difference in extinction coefficient of the IMP product was determined to be 2039 $M^{-1}cm^{-1}$. The absorbance of guanine as

measured at 257 nm, for which the difference in extinction coefficient of the GMP product was determined to be 3957 $M^{-1}cm^{-1}$. The absorbance of allopurinol activity was measured at 272 nm, for which the difference in extinction coefficient of the riboside product was determined to be 1853 $M^{-1}cm^{-1}$. The absorbance of xanthine activity was measured simultaneously at 247 and 253 nm.

For the determination of kinetic constants, either PRPP or nucleobase was held at a fixed, saturating level and the other substrate was varied. Nucleobases (hypoxanthine and guanine) were varied between 3.3-100 μM with 1 mM fixed PRPP, PRPP was varied between 10-200 μM with 50 μM fixed concentrations of guanine or hypoxanthine. For the reverse direction, the reaction was monitored by following the formation of uric acid through coupling the formation of inosine monophosphate (IMP) to uric acid by xanthine oxidase. The conditions were essentially the same as the forward direction, except for the addition of 1.28 U/mL xanthine oxidase to the reaction. Enzyme activity was measured using Grenier Bio-One UV-Star 96-well microplates in a final assay volume of 250 μL. Uric acid formation was monitored at 293 nm using an extinction coefficient of 12,600 $M^{-1}cm^{-1}$. TcC concentration was varied between 11.4 and 45.6 nM.

Compound Screening, Dead-end, and product inhibitiom

Compounds were assessed for inhibitory potential by using conditions essentially identical to the kinetics measurements described above. For the forward reaction,

reaction mixtures containing 100 μM guanine, 12.5 nM TcC, 0-100 μM of test compound; reactions were initiated with the addition of1 mM PRPP; activity was measured for 1-2 minutes. For putative inhibitors assessed in the reverse direction, reaction mixtures contained 100 μM pyrophosphate and 42 nM TcC HGPRT, treated with 0.01-100 μM of test compound for **2**, **3**, **5**, and **7**, 0.001-10 μM of test compound for **9**, **4**, and **10**, and 0.01-10 μM of test compound for **1**, **6**, **8**, and **13**. Compounds **1**, **6**, **8**, and **13** were limited to less than 100 μM due to interference in kinetic measurements caused at higher concentrations. Reactions were initiated by the addition of IMP to 500 μM; activity was measured for 15-20 minutes.

Product inhibition studies of the forward reaction were conducted in assay mixtures containing 50 μM guanine, 10-200 μM PRPP, fixed concentrations of either GMP (0-60 μM) or IMP (0-120 μM), and 12.5 nM TcC HGPRT. Reactions were initiated by the addition of PRPP. Product and dead-end inhibition studies of the reverse reaction were conducted in assay mixtures containing 100 μM pyrophosphate and 25 nM TcC HGPRT. For product inhibition studies of PRPP, 0-3.0 μM PRPP was used and the reactions were initiated by the addition of 12.5-500 μM IMP. For dead-end inhibition studies with compound **1**, 0-1 μM of compound was tested in reactions initiated by the addition of 50, 71, or 500 μM IMP.

Analysis of Kinetic Data

Initial velocity data obtained at variable concentrations of a single substrate A at fixed concentrations of the other substrate were fitted to (**eq. 3.1**), in which *v* is the initial velocity,

$$\frac{v}{E_t} = \frac{k_{cat}A}{K_a + A} \tag{3.1}$$

E_t is the enzyme concentration, k_{cat} is the turnover number, A is the concentration of the variable substrate, and K_a is the apparent Michaelis constant. The fixed substrate was held at saturating concentrations (50 μM for nucleobases and 1 mM for PRPP), allowing for the simplication of kinetic data.

Initial velocity data obtained for the reverse reaction at variable concentrations of a single substrate A at changing-fixed concentrations of a second substrate B were fitted to (**eq. 3.2**), in which K_{ia} and K_a are the respective dissociation and Michaelis constants of substrate A, K_b is the Michaelis constant of substrate B.

$$\frac{v}{E_t} = \frac{k_{cat}AB}{K_{ia}K_b + K_bA + K_aB + AB} \tag{3.2}$$

Data obtained for product and dead-end inhibitor studies were first plotted in double-reciprocal form, and plots were inspected for slope and intercept effects resulting from the added inhibitor. Double-reciprocal data for plots containing intersecting lines were then fitted globally to (**eq. 3.3**), in which

$$Y = slope * (X - X_{cross}) + Y_{cross} \quad (3.3)$$

X_{cross} and Y_{cross} are the X and Y coordinates for the points of intersection.

Inhibition data which apparently conformed to competitive, non-competitive (mixed), or un-competitive inhibition were fitted to **eq. 3.4-3.6**, respectively, in which *v* is the initial velocity, V_{max} is the maximal velocity, A is the concentration of the variable substrate, K_a is the apparent Michaelis constant, I is the concentration of inhibitor, and K_{is} and K_{ii} are, respectively, the slope and intercept inhibition constants. Data that appeared competitive were also fitted to (**eq. 3.5**), describing non-competitive (mixed) inhibition. In all cases tested K_{ii} was at least one order-of-magnitude higher than K_i .

$$v = \frac{V_{max}A}{K_a(1 + \frac{I}{K_{is}}) + A} \quad (3.4)$$

$$v = \frac{V_{max}A}{K_a\left(1 + \frac{I}{K_{is}}\right) + A\left(1 + \frac{I}{K_{ii}}\right)} \quad (3.5)$$

$$v = \frac{V_{max}A}{K_a + A\left(1 + \frac{I}{K_{ii}}\right)} \quad (3.6)$$

For dead-end inhibitors that showed significant inhibition, the data were fitted to (**eq. 3.7**).

$$\frac{v_i}{v_0}\% = \frac{100}{1 + (\frac{IC_{50}}{I})^H} \quad (3.7)$$

where v_i is the enzyme activity at inhibitor concentration I, v_0 is the rate without inhibitor, and H is the Hill coefficient.

For inhibitors that were found to be competitive, the dissociation constant (K_I) was determined by use of the Cheng-Prussoff equation (**eq. 3.8**):

$$K_i = \frac{IC_{50}}{1 + (\frac{A}{K_a})} \quad (3.8)$$

Synthesis of Radiolabeled 5-Phospho-α-D-Ribose 1-Diphosphate

Samples of AMP, radiolabeled at [^{3}H-C1'], [^{14}C-C1'], [^{3}H-C5'], [^{14}C-C5'] were generous gifts from Professor Vern Schramm. Radiolabeled AMPs were converted into radiolabeled PRPPs by an enzymatic synthesis utilizing adenine phosphoribosyltransferase and adenine deaminase (**Figure III-1**) [176]. At room temperature in a 1.5 mL microcentrifuge tube was added buffer containing 50 mM potassium phosphate (pH 7.4), 1.4 mM $MgCl_2$, 1.4 mM pyrophosphate, 0.5 mM DTT, 35 μM purified APRT1, and approximately 0.2 mg/mL adenine deaminase. Approximately 50 μM of radiolabeled AMP was added last. After 15 minutes of incubation at room temperature, the reaction was quenched by the addition of EDTA, to a final concentration of 6.4 mM. The quenched reaction was filtered by centrifugation

using a micro centrifuge spin column (MilliporeSigma Amicon Ultra 0.5 mL 10k MWCO). The sample was then injected on to a 5-mL MonoQ anion exchange column (GE Lifescience) pre-equilibrated with deionized water. Material was eluted by a linear gradient (0-1.5 M) of ammonium acetate, and 2-mL fractions were collected. Fractions were analyzed by liquid scintillation counting after the addition of 25-50 μL of each fraction to 10 mL of Ultima Gold scintillation fluid. Chromatographic fractions that corresponded to PRPP were pooled together and diluted with water (3:4 water:sample). The radiolabeled PRPP sample was then frozen with liquid nitrogen, lyophilized to dryness, and then the residue was re-dissolved 3 mL of water. An aliquot was then removed for liquid scintillation counting, and the sample was again flash-frozen with liquid nitrogen and lyophilized to dryness. Dried samples were stored at -20 °C until needed.

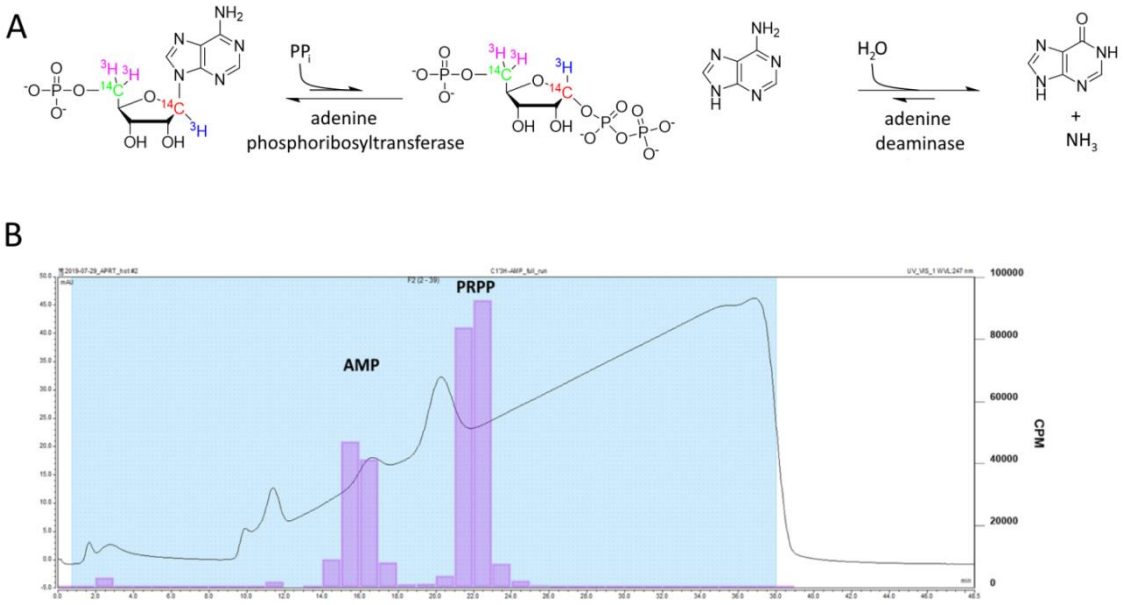

Figure III-1 Synthesis of radiolabeled PRPPs. A) [^{14}C-C5'] (green), [^{3}H-C5'] (magenta), [^{14}C-C1'] (red), and [^{3}H-C1'] (blue) radiolabeled AMPs were converted into their respective radiolabeled PRPPs by adenine phosphoribosyltransferase (APRT). The unfavorable pyrophosphorolysis was coupled to the favorable deamination of adenine to hypoxanthine by the enzyme adenine deaminase. **B)** Radiolabeled PRPP was synthesized from radiolabeled AMP and then purified by ion-exchange chromatography. CPM of fractions overlaid on top of HPLC trace (247 nm).

Measurement of Kinetic Isotope Effects

Isotope effects were measured by the method of internal competition, in which heavy (C1- labeled PRPP) and light (C5-labeled PRPP) were added together, and the ratio of heavy to light counts was compared in either the product (NMP) or the substrate (nucleobase). Reaction mixtures containing approximately 10 μM radiolabeled PRPP (^{3}H:^{14}C = 3:1 DPM), reaction buffer, and nucleobase (final concentration of 10-or 50 μM for hypoxanthine and 180 μM for allopurinol) were aliquoted into separate tubes. To the aliquots was added either TcC HGPRT to a final concentration of 100 nM or water. After incubation for 5 minutes, the reactions containing enzyme were quenched

by the addition of EDTA (14.3 mM final), while control samples without enzyme were quenched without any incubation. The quenched reactions were then filtered using a 10K MWCO microcentrifuge concentrator (MilliporeSigma Amicon Ultra 0.5 mL) and injected onto a Phenomenex 250 mm Luna C18 (5 μm) column pre-equilibrated with aqueous ion-pairing buffer (25 mM potassium phosphate (pH 6.0), 4 mM tetrabutylammonium bisulfate). The nucleotide products were separated from both remaining radiolabeled PRPP and other degradation products similarly to what has been previously described [176, 177]. Briefly, compounds were separated by a gradient of acetonitrile (0-30%). Fractions of 1 mL were collected, and aliquots were added to 10 mL of Ultima Gold scintillation fluid, followed by liquid scintillation counting. Samples were read for 10 minutes, and samples with more than 100 CPMs were evaluated for 10 x 10 min, in which a 0.5% 2CV cutoff was used. Radioactive counting was evaluated in two different channels: Channel A containing counts of 0-26 keV energy and Channel B containing counts of 26-1000 keV energy. Initial counts in substrate were measured in a mock reaction which contained no enzyme. After a fraction of the total substrate was converted to product, the counts in both residual substrate and formed product were measured. Counts per minute corresponding to ^{3}H and ^{14}C were calculated by the following relationship:

$$^{3}H\ counts = CPM_A - rCPM_B \qquad ^{14}C\ counts = CPM_B(1 + r) \tag{3.9}$$

Where *r* is the *ratio* of ^{14}C counts in channel A/channel B. The kinetic isotope effects were then calculated by using (**eq. 3.10**):

$$KIE_{\frac{V}{K}} = \frac{\log(1-f)}{\log(1-f\,R_p/R_0)} = \frac{\log(1-f)}{\log[(1-f)(R_s/R_0)]} \quad (3.10)$$

Where f is the fractional reaction, R_p is the ratio of heavy to light isotope in products, R_s is the ratio of heavy to light isotope in residual substrate, and R_0 is the initial ratio of heavy to light isotope in the substrate [178]. KIEs were measure in the product and residual substrate, for values of $f < 0.3$, the isotope effect was reported by the KIE measured on product formation, for $f \geq 0.3$, the isotope effect was reported by KIE measured on the residual substrate.

Effects of Viscosogens on the Kinetics of TcHGPRT

The effects of viscosity on the forward reaction of TcC HGPRT was determined by measuring kinetics with added 0-30% (w/v) glycerol (η_{rel} = 1-2.33). The kinematic (measured viscosity) of the reaction mixtures containing the viscosogens were measured using a Cannon-Fenske viscometer, and data were converted to dynamic viscosities (absolute viscosity, reflecting internal resistance of the fluid; product of kinematic viscosity and specific gravity). Kinetic data were collected in duplicate for each viscosogen for reaction mixtures containing 12.5 nM TcC HGPRT, 50 μM guanine, and 0-200 μM PRPP In assay buffer. Kinetic parameters were determined by fitting the results to (**eq. 3.1**).

Isotope Trapping

The specific radioactivity of preparative samples of [^{3}H-C5] PRPP was determined through titration and purification (**Figure III-2**). A master mix of 2.15 μM TcC, 2.18 x10^{3} CPM/μL of C5-^{3}H-PRPP, and reaction buffer was pipetted into 10-μL aliquots. To each aliquot was added 10 μL of hypoxanthine in reaction buffer, to a final concentration of 0-4 μM. After a brief incubation (<10 minutes), 480 μL of a mock chase solution was added containing 1.05 mM unlabeled PRPP in assay buffer. The reactions were quenched with the addition of 125 μL of 100 mM EDTA, and the quenched solutions were applied to an ion-exchange column (MonoQ, 5 mL); radiolabeled products were isolated as described above. Those fractions which eluted at the same retention time as IMP were pooled and lyophilized as described above in the description of the synthesis of radiolabeled PRPP. 10 mL Ultima Gold scintillation fluid was added to the lyophilized residues and the samples were analyzed by liquid scintillation. Sample quenching and disintegrations per minute were calculated by the tSIE parameter (external standard quench parameter) and referenced to a quench standard curve.

The isotope trapping (partitioning) experiment was performed closely to the method of Rose[179, 180]. TcC HGPRT was buffer exchanged (GE Healthcare, PD MidiTrap G-25) into assay buffer and concentrated prior to use. A pulse solution containing 6.23 μM [^{3}H-C5]PRPP, 10 μM TcC HGPRT, and reaction buffer was divided into 20 μL aliquots. To each pulse solution was added 480 μL of a chase solution containing 1.04 mM

unlabeled PRPP, 0-78 μM hypoxanthine, and buffer while rapidly mixing. The pulse-chase mixture was then quenched with 125 μL 100 mM EDTA, and placed on ice prior to purification of the radiolabeled products by ion-pairing HPLC as described above. Fractions containing IMP were then lyophilized, and radioactivity was determined by LSC. The amount of the radiolabeled EA* complex (HGPRT-PRPP*) present in the pulse mixtures was calculated by the dissociation constant of PRPP (0.8 ± 0.1 μM) and the number of DPM in the PRPP sample. The radioactivity in the sample from degradation products which co-eluted with IMP (in samples lacking hypoxanthine) was subtracted from the total counts. The data for the isotope trapping was fitted to a hyperbolic equation (**eq. 3.11**) approximating the commitment of the binary enzyme-PRPP complex to form labeled IMP at varying concentrations of hypoxanthine:

$$\frac{P^*}{EA^*} = \frac{T_{max} * B}{B_{50} + B} \tag{3.11}$$

Where "B" is the concentration of hypoxanthine in the pulse-chased solution, "B50" is the concentration of hypoxanthine to trap half of the maximal amount, and "T_{max}" is the maximal fraction of the binary complex trapped.

The commitment factor Cf is related to T_{max} by the following relationship:

$$C_f = \frac{T_{max}}{1 - T_{\max}} \tag{3.12}$$

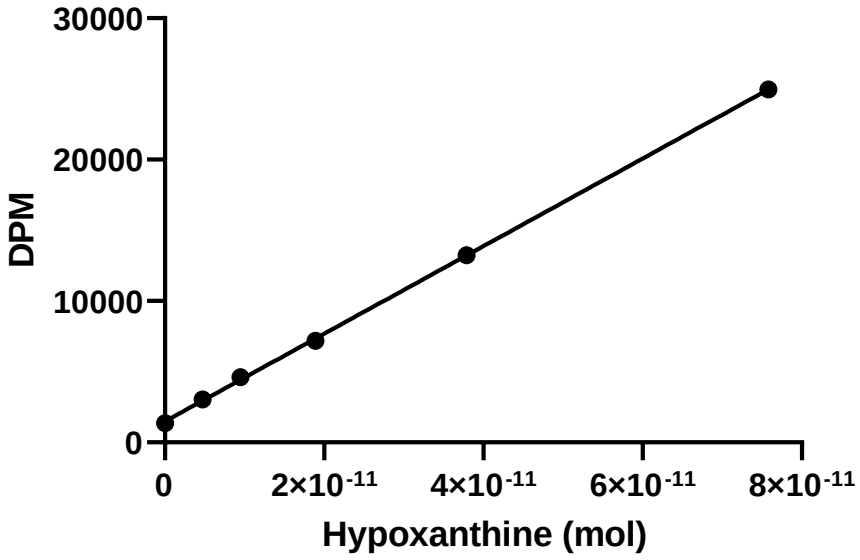

Figure III-2. Specific activity of [C5-^{3}H]-PRPP. TcC HGPRT was incubated with labeled PRPP and treated with a known amount of hypoxanthine. Radiolabeled product was purified and quantified by LSC.

Titration of Active Sites of TcHGPRT

Inhibitor **9** is a potent inhibitor of TcC HGPRT, and was used to titrate the active-site concentration of the enzyme. Initial velocities were obtained with (v_i) and without (v_0) inhibitor in reaction mixtures of the reverse reaction containing 100 μM pyrophosphate, 37.5 μM IMP, 0- 125 μM inhibitor **9,** and 25.8, 51.5, and 103 nM TcC HGPRT in a total volume of 150 μL. Reactions were initiated with the addition of TcC. Residual activity (v_i/v_0) was plotted as a function of **(9)** concentration and the data were fitted globally to (**eq. 3.13**).

$$\frac{V_i}{V_0}\% = V_0\left(1 - \frac{\left(a*E_t+I_t+\left(K_i\left(1+\frac{S}{K_M}\right)\right)\right) - \sqrt{\left(a*E_t+I+\left(K_i\left(1+\frac{S}{K_M}\right)\right)\right)^2 - 4*a*E_t*I_t}}{2*a*E_t}\right) \quad (3.13)$$

Where E_t is the concentration of total enzyme, a is the coefficient describing the fraction of active enzyme, and V_0 is the normalized activity of enzyme with no inhibitor.

Synthesis of inhibitors

1, **2**, **3**, **4**, **5**, **6**, **7**, **8**, **9**, **10**, **11**, **12**, **13** were generously provided by Professors Vern Schramm and Peter Tyler and were synthesized as previously described [169, 170, 172]

.

Results and Discussion

Kinetic characterization of TcA and TcC HGPRTs

Annotation of the genome from *Trypanosoma cruzi* revealed the presence of two genes encoding putative HGPRT activity. One of these genes, the non-Esmeraldo-like TcCLB.509693.70 (TcA), has a homolog, the Esmeraldo-like TcCLB.506457.30 (TcC), which share > 98% amino acid identity. To determine whether these two gene products are distinct from each other, the purine substrate specificity of both enzymes was examined. TcA HGPRT and TcC HGPRT were both found to be highly efficient ($k_{cat}/K_M \geq 1x10^5$ $M^{-1}s^{-1}$) at catalyzing *N*-ribosidic bond formation between 5-phospho-α-D-ribose 1-diphosphate (PRPP) and the 6-oxopurines: hypoxanthine and guanine (**Table III-1**, **Figure III-3**). Under our conditions, the kinetic constants were essentially identical to what has previously been reported for TcA HGPRT [173, 181].

Additionally, both HGPRTs were found to be functionally identical; with essentially identical catalytic efficiency for both GMP-forming and IMP-forming reactions, and neither enzyme catalyzed the formation of XMP (**Table III-1**).

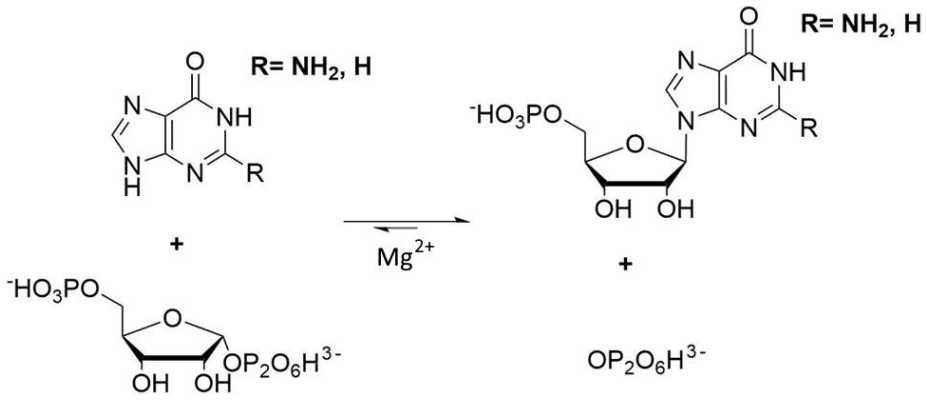

Figure III-3 Reaction catalyzed by hypoxanthine-guanine phosphoribosyltransferases (HGPRTs). An *N*-glycosidic bond is formed between N9 of 6-oxopurine and C1 of phosphoribosylpyrophosphate (PRPP) substrates. R=NH_2 for guanine, R=H for hypoxanthine.

Table III-1. 6-Oxopurine specificity of TcA and TcC. All kinetic data was measured at 37 °C. TcA activity was measured with 25 nM enzyme for GMP synthesis and 12.5 nM for IMP synthesis. TcC activity was measured with 12.5 nM enzyme for both GMP and IMP forming reactions. XMP formation was measured with 12.5 and 125 nM of both TcA and TcC. Kinetic data for GMP and IMP formation were fitted to (**eq. 3.1**).
N.D. = not detected.

Enzyme	Variable Substrate	Fixed Substrate	Apparent Kinetic Parameters		
			k_{cat} (s^{-1})	K_M (μM)	k_{cat}/K_M ($s^{-1}M^{-1}$)
TcA	Guanine (10-100 μM)	PRPP (1 mM)	14 ± 1	21 ± 5	(0.7 ± 0.2) x10^6
	Hypoxanthine (3.33-100 μM)	PRPP (1 mM)	32 ± 2	6 ± 2	(5 ± 2) x10^6
	Xanthine (10–100 μM)	PRPP (1 mM)	N.D.	N.D.	N.D.
TcC	Guanine (10-100 μM)	PRPP (1 mM)	16.3 ± 0.4	8 ± 1	(2.0 ± 0.2) x10^6
	Hypoxanthine (3.33-100 μM)	PRPP (1 mM)	14.8 ± 0.4	2.5 ± 0.6	(6 ± 1) x10^6
	Xanthine (10-100 μM)	PRPP (1 mM)	N.D.	N.D.	N.D

Kinetic Mechanism of TcC HGPRT.

The kinetic parameters for TcC HGPRT were further characterized. The bimolecular rate constant for PRPP for both the GMP-forming and IMP-forming reactions was found to be on the order of 1 x10^5 $M^{-1}s^{-1}$, providing further support for *bona fide* HGPRT activity (**Table III-2**). The kinetic constants for the reverse (IMP pyrophosphorolysis) reaction also matched closely with what has previously been reported for TcA HGPRT [181] and the kinetic data conformed to a sequential bi-bi mechanism (**Table III-2**, **Figure III-4**). The over 100-fold difference of values of k_{cat} for the forward (16.3 ± 0.4 s^{-1} (guanine), 14.8 ± 0.4 s^{-1} (hypoxanthine)) and reverse reactions (0.117 ± 0.002 s^{-1}) demonstrated that the biosynthetic reaction is highly favored and essentially irreversible.

Product inhibition of the forward reaction with IMP or GMP against varied concentrations of PRPP **(Table III-3, Figure III-5**, **B** and **C,** respectively) provided competitive patterns, as did product inhibition of the reverse reaction with PRPP against varied concentrations of IMP (**Table III-3**, **Figure III-5, A**). The apparent competitive patterns for all three cases provides evidence for an ordered kinetic mechanism, of which PRPP is the first substrate to bind and IMP is the last product released (**Figure III-6**). Additionally, the 7-deaza,8-aza analog of hypoxanthine: allopurinol, was assessed as an alternative substrate. Allopurinol was found to be a poor substrate with a second-order rate constant of $4.3 \pm 0.7 \times 10^3$, which reflects on both its Michaelis constant of 250 ± 40 μM and catalytic rate of $1.07 \pm 0.08\ s^{-1}$ (**Table III-2**). Allopurinol was previously reported as a poor substrate for TcA (k_{cat}/K_M of $5 \times 10^2\ M^{-1}s^{-1}$) [173] and the ribosylation of the purine analog is believed to play a role in the toxicity of the compound in Trypanosomastids[182].

Table III-2. Initial Velocity Studies of TcC Hypoxanthine-Guanine Phosphoribosyltransferase. Kinetic constants for the forward reaction are apparent (i.e. one substrate was varied at a fixed, saturating amount). When PRPP was varied in the forward direction, purine concentration was held fixed at 50 µM; when purine was varied in the forward direction, PRPP was held fixed at 1 mM. For GMP and IMP biosynthesis TcC concentration was 12.5 nM, for the synthesis of Allopurinol-MP the concentration of TcC was 200 nM. Kinetic data for forward reactions are fitted to (**eq. 3.1**). IMP phosphorolysis was measured with by varying the concentration of IMP between 31 µM and 1000 µM at several (12, 20, 30, 65, 250 µM) fixed concentrations of pyrophosphate. TcC concentration was varied between 11 and 46 nM. IMP pyrophosphorolysis data was fitted to (**eq. 3.2**).

Reaction	Variable Substrate	Fixed Substrate	Apparent Kinetic Parameters		
			k_{cat}/K_m (M^{-1}-s^{-1})	K_m (µM)	k_{cat} (s^{-1})
GMP Biosynthesis	Guanine (3.3-100 µM)	PRPP (1 mM)	(2.0 ± 0.2) x 10^6	8 ± 1	16.3 ± 0.4
	PRPP (10-200 µM)	Guanine (50 µM)	(5.2 ± 0.3) x 10^5	49 ± 3	25.4 ± 0.5
IMP Biosynthesis	Hypoxanthine (3.3-100 µM)	PRPP (1 mM)	(6 ± 1) x 10^6	2.5 ± 0.6	14.8 ± 0.4
	PRPP (10-200 µM)	Hypoxanthine (50 µM)	(4.3 ± 0.7) x 10^5	41 ± 4	17.7 ± 0.7
Allopurinol-MP Biosynthesis	Allopurinol (50-750 µM)	PRPP (1 mM)	(4.3 ± 0.7) x 10^3	250 ± 40	1.08 ± 0.07

Reaction	Variable Substrates	Initial Velocity Pattern	IMP (31-1000 µM)			
			k_{cat}/K_m (M^{-1}-s^{-1})	K_{IMP} (µM)	k_{cat} (s^{-1})	$K_{i,a\ IMP}$ (µM)
IMP Pyrophosphorolysis	PP_i vs. IMP	Intersecting	(3.1 ± 0.4) x 10^3	38 ± 5	0.117 ± 0.002	490 ± 80
			Pyrophosphate (12- 250 µM)			
			k_{cat}/K_m (M^{-1}-s^{-1})	K_{PPi} (µM)	k_{cat} (s^{-1})	
			(1.1 ± 0.1) x 10^4	11 ± 1	0.117 ± 0.002	

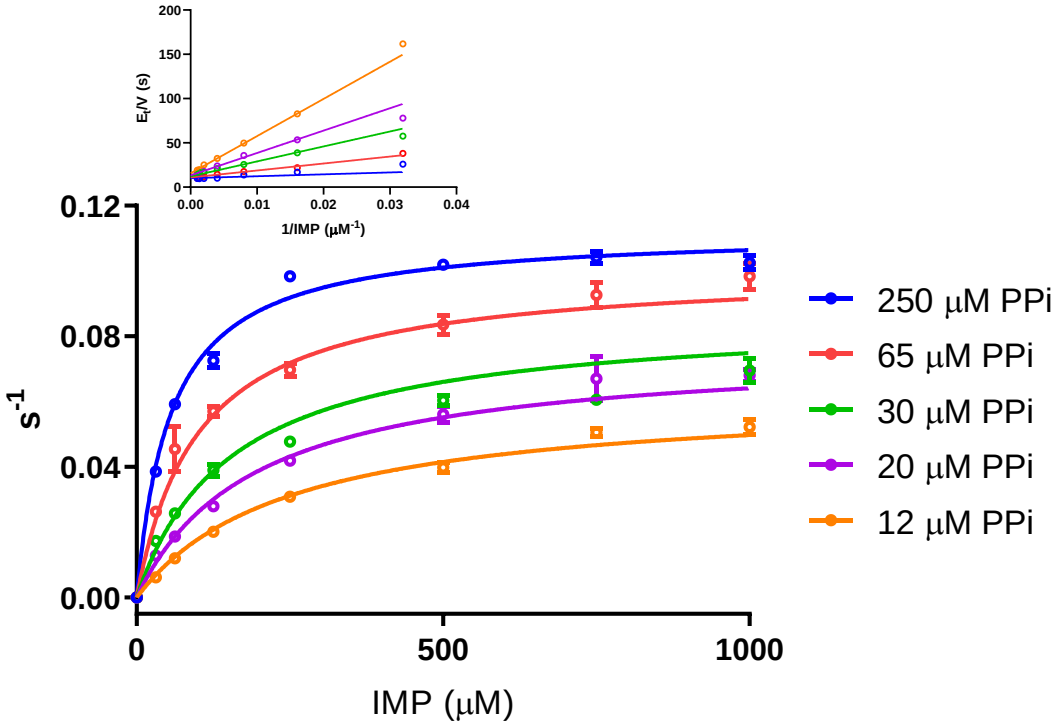

Figure III-4. Kinetic data for reverse reaction of TcC. The reaction was monitored by measuring uric acid formation by coupling the generation of hypoxanthine to xanthine oxidase at 37 °C. TcC was added to a final concentration of 11.4 nM (250 μM PP_i), 22.8 nM (65 μM PP_i), 30.0 nM (30 μM PP_i), 45.6 nM (20 and 12 μM PP_i). The concentration of IMP was varied between 31-1000 μM. Inset shows reciprocal plot (1/v vs. 1/IMP). Data fitted to (**eq. 3.2**), inset fitted to reciprocol.

Table III-3. Product and Dead-End Inhibition of TcC Hypoxanthine-Guanine Phosphoribosyltransferase. Product inhibition of the forward reaction with NMPs was measured with 0-120 μM of IMP or GMP versus 10-200 μM of PRPP with a fixed (50 μM) amount of purine. TcC HGPRT concentration was 12.5 nM and data were fitted to equations **3.4**, **3.5**, and **3.6**, representing competitive, non-competitive, and un-competitive models of inhibition, respectively. For both reactions an uncompetitive model of inhibition fit poorly; for the non-competitive model K_{ii} was at least an order-of-magnitude higher than K_{is}, therefore apparent kinetic parameters were determined by fitting the data to (**eq. 3.4**). For product and dead-end inhibition of IMP pyrophosphorolysis 25 nM of enzyme was used with a fixed (100 μM) concentration of pyrophosphate. For product inhibition by PRPP, IMP was varied between 12.5 and 500 μM against 0-3 μM of PRPP. Data were fitted to the same equations as the product inhibition in the forward reaction, for which the competitive model of inhibition (**eq. 3.4**) was determined to be the most accurate. For dead-end inhibition of IMP pyrophosphorolysis Immucillin-GP (**1**) was varied between 0.01-1 μM with several (50, 71, 500 μM) concentrations of IMP. A Dixon plot (**Figure III-5 D**) of the data indicated competitive inhibition (intersection in the second quadrant), apparent kinetic parameters were reported by fitting the data to the inverse of (**eq. 3.4**). C = competitive

Reaction	Variable Substrate	Inhibitor	Fixed Substrate	Inhibition Pattern	Apparent Kinetic Parameters	
					K_m (μM) of varied substrate	K_{is} (μM) of inhibitor
IMP Biosynthesis	PRPP (10-200 μM)	IMP (0-120 μM)	Hypoxanthine (50 μM)	C	42 ± 2	110 ± 10
GMP Biosynthesis	PRPP (10- 200 μM)	GMP (0-120 μM)	Guanine (50 μM)	C	40 ± 4	13 ± 1
IMP Pyrophosphorolysis	IMP (12.5-500 μM)	PRPP (0-3 μM)	PP_i (100 μM)	C	120 ± 20	0.8 ± 0.1
	IMP (50-500 μM)	Immucillin-GP (0.01-1 μM)	PP_i (100 μM)	C	54 ± 9	0.150 ± 0.020

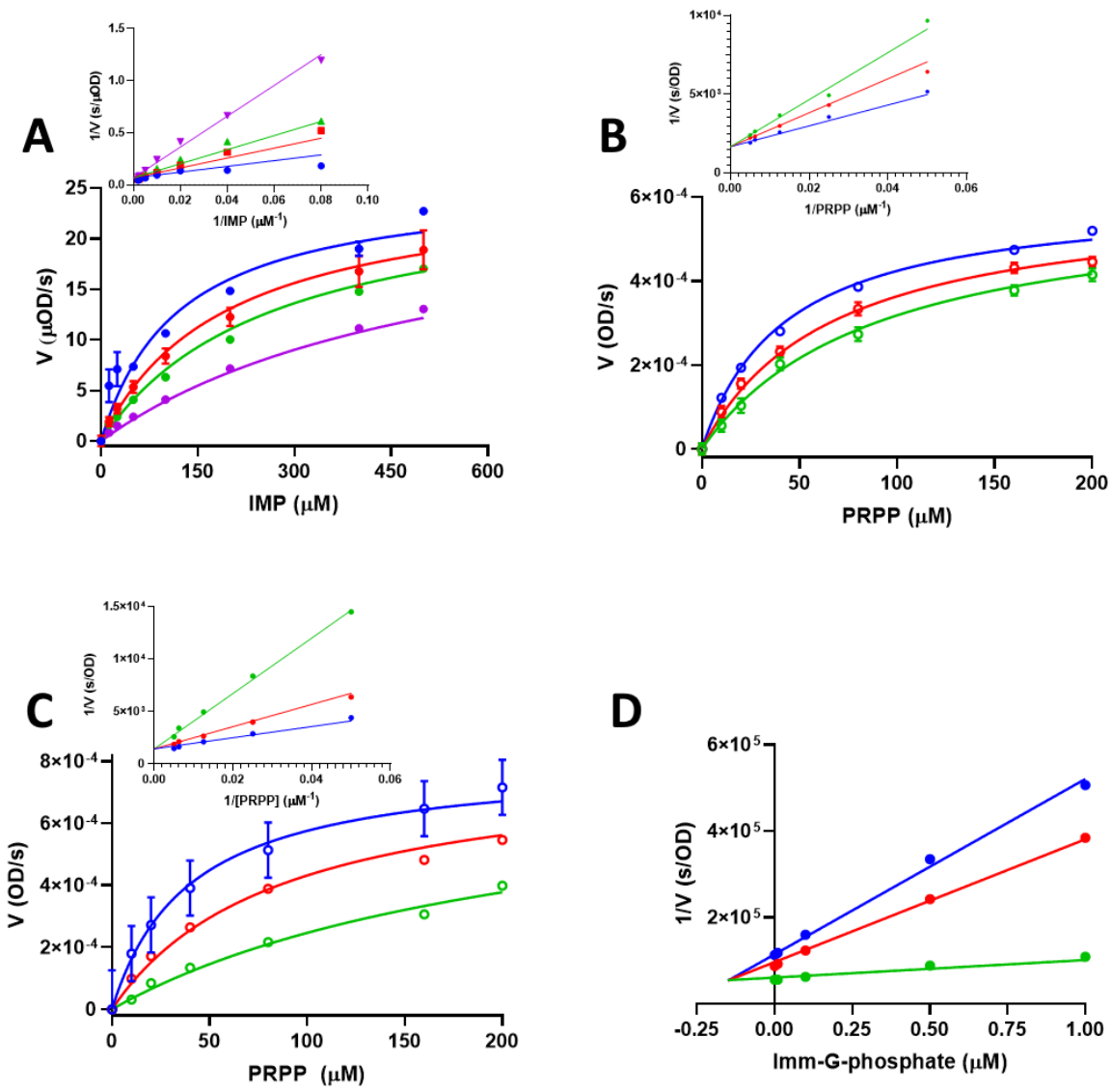

Figure III-5. Product and dead-end inhibition of TcC HGPRT. A) Product inhibition data (PRPP vs IMP) of the reverse reaction of TcC HGPRT with variable concentrations of IMP (12.5-500 µM) and changing-fixed concentrations of PRPP (0 µM (blue), 0.5 µM (red), 1 µM (green), 3 µM (purple). Fitting of the apparent competitive inhibition data to (**eq. 3.4**) produced values of K_{IMP} = 120 ± 20 µM and K_{is} PRPP = 0.8 ± 0.1 µM. **B)** Product inhibition data (IMP vs. PRPP) for the forward reaction of TcC HGPRT with variable concentrations of 0-200 µM PRPP and changing-fixed concentrations of product inhibitor IMP (0 µM (blue), 60 µM (red), 120 µM (green)). Fitting of the apparent competitive inhibition data to (**eq. 3.4**) produced values of K_{PRPP} = 42 ± 2 µM and K_{is} IMP = 110 ± 10 µM. **C)** Product inhibition data (GMP vs. PRPP) for the forward reaction of TcC HGPRT with variable concentrations of 0-200 µM PRPP

and changing-fixed concentrations of product inhibitor GMP (0 μM (blue), 60 μM (red), 120 μM (green)). Fitting of the apparent competitive inhibition data to (**eq. 3.4**) produced values of K_{PRPP} = 40 ± 4, and K_{is} GMP = 13 ± 1 μM. Insets in A-C are double-reciprocal plots (1/v vs. 1/substrate), indicating apparently intersecting lines on the Y-axis. **A-C** were also fitted to equations for non-competitive (mixed) and uncompetitive inhibition, (**eq. 3.5**) and (**eq. 3.6**), respectively. The data fit poorly to an uncompetitive model; for the non-competitive model K_{ii} was at least an order-of-magnitude higher than K_i for each data set. **D)** Dixon plot of Immucillin-GP (**1**) inhibition of the reverse reaction catalyzed by TcC HGPRT (25 nM) with IMP (50 μM (blue), 71 μM (red), 500 μM (green)) and 100 μM pyrophosphate. Data were fitted to the inverse of (**eq. 3.4**); K_{is} = 150 ± 20 nM, K_{IMP} = 54 ± 9 μM..

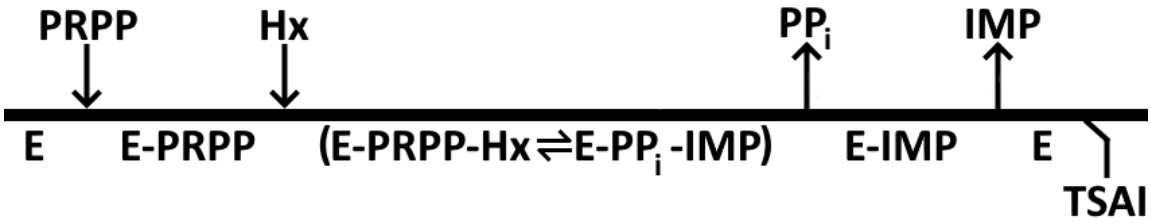

Figure III-6. Kinetic Mechanism of TcC HGPRT. Substrate binding is ordered with PRPP binding first, followed by hypoxanthine (Hx). Substrates are converted into products and then products are released, with pyrophosphate (PPi) release preceding inosine 5'-monophosphate (IMP) release. NMP-like transition-state analog inhibitors (TSAI) are competitive against IMP, binding to the free enzyme.

Kinetic Isotope Effects

In order to probe the structural features of the transition state for the reaction catalyzed by TcC HGPRT, we evaluated the kinetics of radiolabeled PRPP in which the anomeric proton [C1-^{3}H]PRPP and carbon ([C1-^{14}C]PRPP) were replaced, respectively, with tritium and ^{14}C [176]. We prepared two other (remote) radiolabeled samples of PRPP ([C5-^{3}H]PRPP and [C5-^{14}C]PRPP) which contain ^{1}H and ^{12}C at C1. One expects the

heavy isotopes at C5 to express a negligible isotope effect, and so the remote labels of ^{3}H and ^{14}C atoms at C5 provide a means to measure substrate turnover by radiometry when PRPP contains ^{1}H and ^{12}C at C1. The determination of values of the secondary tritium isotope effect ($^{\alpha\text{-}T}(V/K_{PRPP})$) and primary carbon isotope effect ($^{14}(V/K_{PRPP})$) on carbon-1 are obtained by measurement of the changes in the ratios of $^{3}H/^{14}C$ for purified, post-reaction samples of the remaining PRPP substrate or the NMP product.

The α-secondary tritium and primary carbon-14 kinetic isotope effects are reported in **Table III-4**. In all cases, the experimental KIEs, within statistical error, were either equal to or only slightly different from unity. However, the KIEs obtained by analysis of either the purified residual substrate or product (**Table III-4**) were in excellent agreement, despite their modest values, suggesting that these values represent accurate isotope effects. Upon averaging of the KIEs obtained from analysis of recovered radiolabeled substrate and product, values of $^{\alpha\text{-}T}(V/K_{PRPP})$ exhibited small, normal KIEs of 1.0075 ± 0.001 and 1.001 ± 0.004, respectively, at 10 μM (4x K_M) and 50 μM (20x K_M) fixed concentrations of hypoxanthine. The diminution of $^{\alpha\text{-}T}(V/K_{PRPP})$ to a value of 1.001 ± 0.004 at 50 μM hypoxanthine is consistent with an ordered bi-bi mechanism for TcC HGPRT, in which PRPP is the first substrate to bind, followed by hypoxanthine or other purine. For ordered bi-bi kinetic mechanisms, the value of the forward commitment factor (c_f), which describes the net partitioning of the EA* complex proceeding to EA*B and then products, versus the release of A* from the EA* complex,

contains a term for the concentration of the second substrate (B) in the expression for $^{\alpha\text{-}T}(V/K_{PRPP})$ (**eq. 3.14**). The relationship between c_f and the concentration of the second substrate is such that increasing concentrations of the second substrate (hypoxanthine) will increase the value of c_f ([183]). In other words, regardless of whether or not the bound PRPP contains protium or tritium at C1, it becomes trapped in the E-PRPP-hypoxanthine complex at high concentrations of hypoxanthine, resulting in the attenuation of the value of the intrinsic tritium isotope effect ($^{\alpha\text{-}T}k$) on the experimental values of $^{\alpha\text{-}T}(V/K_{PRPP})$.

$$^{\alpha-T}\left(\frac{V}{K_{PRPP}}\right) = \frac{^{\alpha-T}k + c_f[hypoxanthine]}{1 + c_f[hypoxanthine]} \tag{3.14}$$

$$^{14}\left(\frac{V}{K_{PRPP}}\right) = \frac{(^{14}k + c_f[hypoxanthine]}{1 + c_f[hypoxanthine]} \tag{3.15}$$

Another method used to unmask intrinsic kinetic isotope effects is to employ a poor substrate for which chemical steps may be rate-limiting, and therefore would express small forward commitment factors. Allopurinol, as discussed above, is a poor substrate for TcC HGPRT for which the value of k_{cat}/K_M is roughly 3 orders-of-magnitude lower than that of hypoxanthine or guanine. Interestingly, the value of $^{\square\text{-}T}(V/K_{PRPP})$ measured at 188 μM allopurinol (0.75x K_M) was near unity (0.98 (substrate) or 0.96 (product)), despite the fact that the E-PRPP-allopurinol complex is apparently less inclined to progress to products than its E-PRPP-hypoxanthine counterpart. The primary carbon-14

kinetic isotope effects were slightly inverse, $^{14}(V/K_{PRPP}) = 0.9933 \pm 0.0007$. The primary effect was again measured with a single sample containing 188 μM allopurinol, for which an apparent $^{14}(V/K_{PRPP})$ of unity was also observed (1.00 for product and substrate).

Although TcA [181] and most purine phosphoribosyltransferases [175, 184, 185] are also reported to have ordered-sequential kinetic mechanism, the suppression of experimental KIEs due to a high commitment to catalysis is only tenuously explained with the KIE data alone, as a KIE value of less than 1% approaches the limits of accurate detection for this technique. Furthermore, this explanation can only partially account for the lack of measurable KIEs for this enzyme, as evident by a lack of apparent KIEs for the poor substrate allopurinol- suggesting that other properties of the kinetic mechanism attenuate the involvement of chemistry on enzyme catalysis.

Table III-4. Kinetic Isotope Effects of PRPP Substrate for TcC HGPRT[a]. Kinetic isotope effects (KIEs) were measured with 100 nM of TcC and approximately 10 μM of radiolabeled PRPP substrate. Radioactivity of the product and residual substrate was collected in two channels, from which the relative amount of ^{14}C or ^{3}H in either the product or substrate was determined by (**eq. 3.9**). The KIE effect on the substrate or product was measured by (**eq. 3.10**). Bolded values indicate the more reliable of the two determinations, as indicated by the fraction of substrate conversion, *f*.
[a]The binding isotope effect (remote C5) is assumed to be negligible.

Heavy PRPP	Light PRPP	Purine Substrate	Fraction of Substrate Conversion (*f*)	[α-^{3}H]V/K_{PRPP} (substrate)	[α-^{3}H]V/K_{PRPP} (product)	[^{14}C]V/K_{PRPP} (substrate)	[^{14}C]V/K_{PRPP} (product)
C1-^{3}H	C5-^{14}C	Hypoxanthine (50 μM)	0.58-0.61	**1.000 ± 0.004**	1.001 ± 0.004		
C1-^{14}C	C5-^{3}H	Hypoxanthine (50 μM)	0.59-0.61			**0.9933 ± 0.0007**	0.9931 ± 0.0006
C1-^{3}H	C5-^{14}C	Hypoxanthine (10 μM)	0.64-0.70	**1.008 ± 0.001**	1.008 ± 0.001		

Rate-limiting step and commitment to catalysis

In order to better understand the small values of KIEs for the reaction catalyzed by TcC HGPRT, we investigated the effects of added viscosogens on the kinetic parameters of the effect of viscosity on the apparent catalytic rate, V_{Max}, was measured. The viscosogen glycerol was used. Microviscosogens such as glycerol generally increase the microviscosity of the solution, affecting the rate of diffusional steps, such as the binding and desorption of small ligands to enzymes [186-188]. Increasing fixed-levels of glycerol proportionally decreased the initial velocity data in reaction mixtures which contained a fixed guanine concentration of 50 μM and variable concentrations of PRPP (10-200 μM). Fitting of these data to (**eq. 3.1**) provided the viscosity-dependent values of the kinetic parameters V_{max} and V_{max}/K_{PRPP}. Normalized values of $(V_{max}/K_{PRPP})/(V_{max}/K_{PRPP})_\eta$ and $V_{max}/(V_{max})_\eta$ were than plotted vs. the relative viscosity (η_{rel}). While plots of $(V_{max}/K_{PRPP})/(V_{max}/K_{PRPP})_\eta$ vs. η_{rel} were refractory to interpretation, fitting of $V_{max}/(V_{max})_\eta$ vs. η_{rel} conformed to linear plots (**Figure III-7**) in which a slope of $0.95 \pm 0.13\ \eta_{rel}^{-1}$ was obtained for glycerol. An absence of a viscosity effect on V_{max} would suggest that chemical steps are rate-limiting for TcC HGPRT, but the near-unity slopes for plots of glycerol as a viscosogen indicates the post-chemistry release of product is rate-limiting.

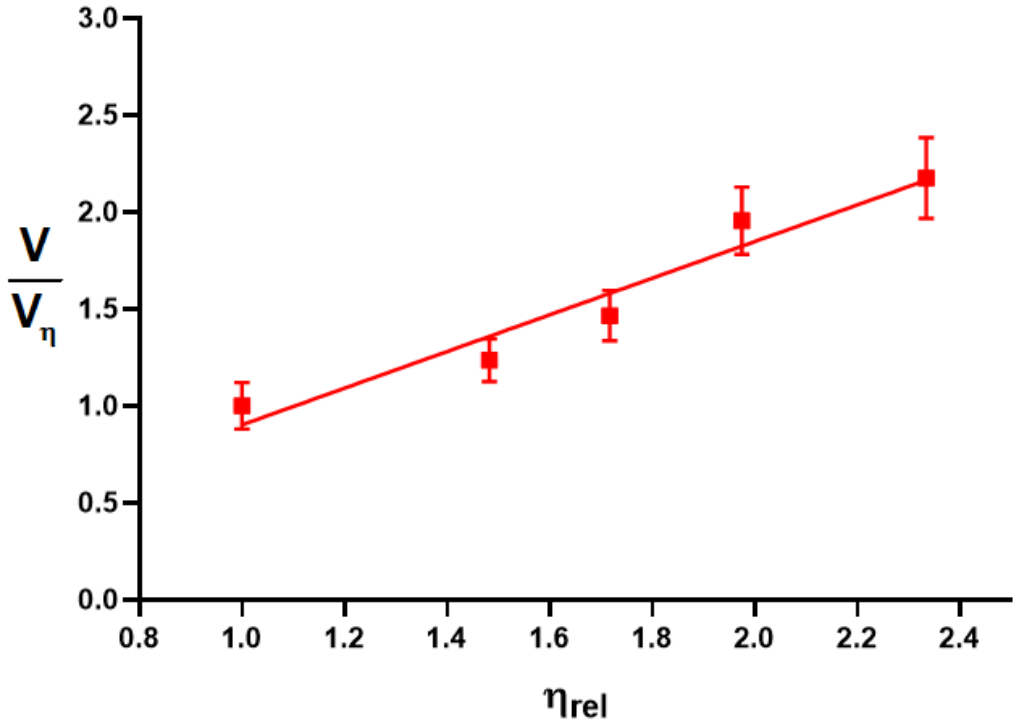

Figure III-7. Effect of viscosity on the catalytic rate of TcC HGPRT. Apparent maximal velocities were obtained from plots of initial velocity vs. variable concentrations of PRPP 0 -200 μM PRPP containing 50 μM guanine, 12.5 nM TcHGPRT, 0-30% (w/v) glycerol (η_{rel} = 1-2.33) Fitting the data to a line produced a slope that was determined to be 0.95 ± 0.1 η^{-1}.

This finding is in accord with what has been observed with human HGPRT [175], in what was perhaps the most exhaustive kinetics study of any phosphoribosyltransferase enzyme to date. Xu *et al.* found that both products (PP_i and IMP) are released from enzyme at least an order-of-magnitude slower than the chemical step (phosphoribosyl transfer), and that the rate of IMP release was about half that of pyrophosphate. The viscosity data for TcC HGPRT suggests that like the human enzyme, product release largely comprises the rate-limiting step.

We utilized the isotope partitioning method of Rose[179, 180] to assess the forward commitment to catalysis of the substrate PRPP. Here a preformed solution of enzyme and radiolabeled PRPP (a "pulse" solution) is mixed with a panel of "chase" solutions containing a large excess of unlabeled PRPP and variable concentrations of hypoxanthine, followed by rapid quenching of the reaction to ensure few turnover events. The dependence of the formation of radiolabeled IMP (P*) (relative to the concentration of the initial E-PRPP* complex) on the concentration of hypoxanthine provides quantitation on the amount of PRPP* trapped in the E-PRPP* (low hypoxanthine) and E-PRPP*-hypoxanthine (high hypoxanthine) complexes.

For TcC HGPRT the formation of radiolabeled IMP (IMP^*) increased with increasing concentration of hypoxanthine to a limiting value for $IMP^*/E\text{-}PRPP^*$ of 0.69 ± 0.03, which describes the rate of IMP formation relative to desorption of $PRPP^*$, and corresponds to a commitment factor of approximately 2.2 ± 0.1 (**Figure III-8**). The inability to trap the entire E-PRPP ("EA^*") complex as product IMP is likely caused by two contributing factors: 1) release of PRPP from the ternary complex and 2) the formation of dead-end complexes. PRPP has been proposed to be released from the ternary complex (E-PRPP-Purine, "EAB") of human[175] and *T. cruzi* [181] enzymes, which implies a degree of randomness in the kinetic mechanisms. Dissociation from the ternary complex prevents complete trapping of the E-PRPP complex, even at very high levels of purine (k_7, **Figure III-9**). The formation of the dead-end E-pyrophosphate-purine complex has also been documented for both human[175] and *T. cruzi*[181]

HGPRTs. The formation of this catalytically-incompetent complex as well as other potential dead-end complexes from PRPP degradation products (ribose-5-phosphate, ribose-5-phosphate-1,2-cyclic phosphate)[189] caused a reduction in the apparent amount of EA^* complex that is trapped[180]. Indeed, PRPP degradation became more prominent at the much higher enzyme concentrations required for the isotope trapping experiment (unpublished observation).

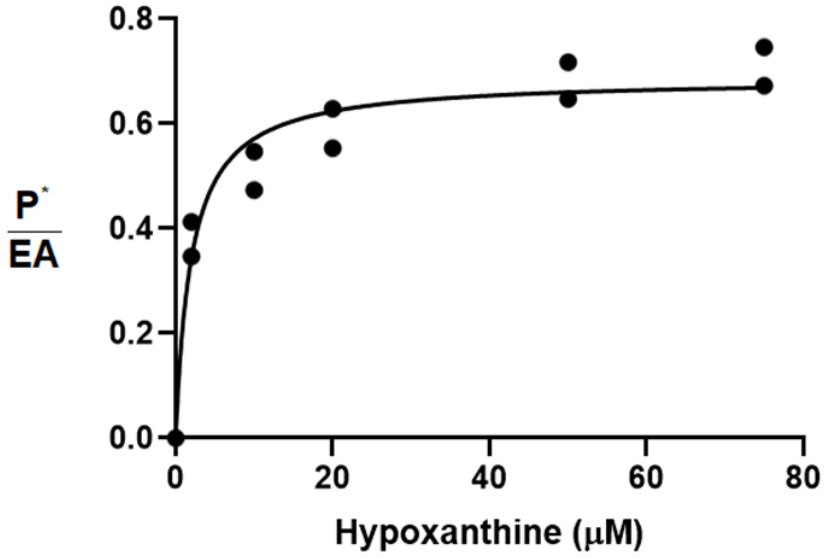

Figure III-8. Isotope trapping of binary complex with hypoxanthine. TcC HGPRT was incubated with [C5-^{3}H]-PRPP in the pulse solution, and combined with chase solutions containing variable concentrations of hypoxanthine (0-75 μM final) and an excess of unlabeled PRPP (1 mM final) , followed by rapid quenching with EDTA. Product [C5'-3H]-IMP was then purified and quantified. The maximal amount of [C5'-^{3}H]-IMP product (P*) trapped provided a ratio of (IMP*/E-PRPP*) that was calculated to be 0.69 ± 0.03

Although both the release of purine from the ternary complex and the formation of dead-end complexes reduce the overall amount of labeled PRPP trapped as product, it is important to note that these two factors have two different implications. The release of purine from the ternary complex is an event that does in fact reduce the commitment of the PRPP substrate to catalysis. On the other hand, the reduction in apparent trapping from dead-end complexes is due to a reduction of the E-PRPP complex and through sequestration of hypoxanthine. This results in a lower concentration of catalytically competent EA^* than the concentration determined of EA^* determined by calculation, which results in an arifactual reduction in P^*/EA^*. Therefore the commitment factor of 2.2 ± 0.1 should be understood as a lower limit.

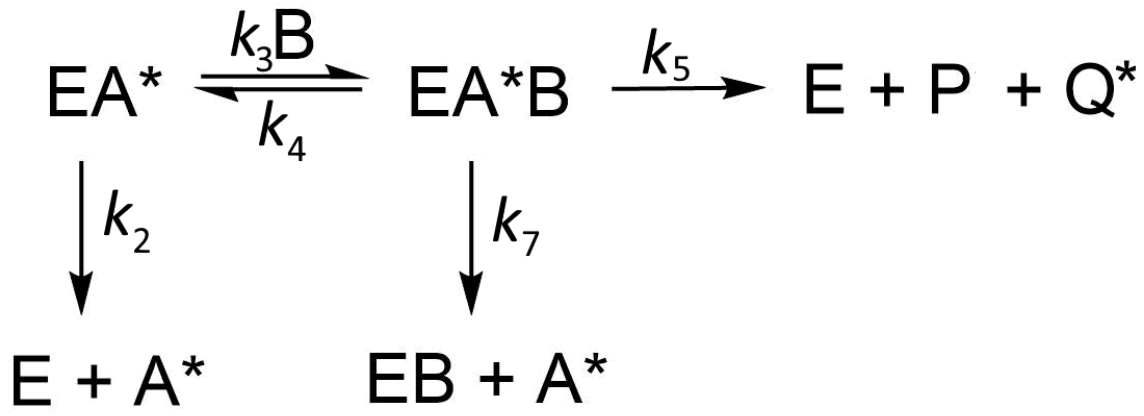

Figure III-9. Partitioning of radiolabeled binary (enzyme-PRPP) complex in chase solution. E=enzyme, A*=[C5-^{3}H]-PRPP, B = hypoxanthine, P = pyrophosphate, Q*= radiolabeled IMP. The experimental conditions are designed such that the dissociation of radioactive material from the binary and ternary complexes is essentially irreversible in the chase solution.

Overall, these results show that TcC HGPRT is kinetically very different from the HGXPRT from *P*. *falciparum*. This finding was initially surprisingly, given the superimposability of the tertiary structures of both enzymes [167, 190] (**Figure III-10**). Kinetic characterization of *Pf*HGXPRT has shown that the rate-limiting step of its catalytic cycle is binding of PRPP to the free enzyme, presumably due to concomitant isomerization of the enzyme [184, 191]. Once activated (isomerized), the enzyme is partially rate-limited by catalysis, and the second-order rate constant for PRPP is approximately 2 orders-of-magnitude lower than that of TcC HGPRT (10^3 M^{-1} vs 10^5 $M^{-1}s^{-1}$)[184, 191](**Table III-2**). *Pf*HGXPRT is also reported to be extraordinarily uncommitted to catalysis, with PRPP dissociating from the ternary complex approximately 1000 times for every successful turnover [176]. Conversely, TcC HGPRT is kinetically very similar to human HGPRT: both are rate limited by product release, have second-order values of V/K_{PRPP} (or k_{cat}/K_{PRPP}) on the order of 10^5 $M^{-1}s^{-1}$, and are highly committed.[175].

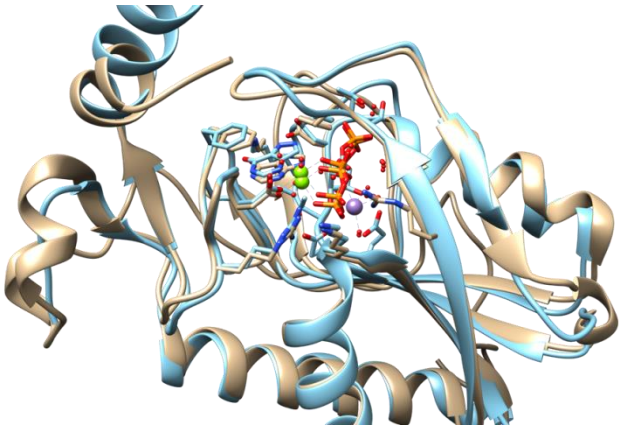

Figure III-10 Overlay of *Trypanosoma cruzi* HGPRT and *Plasmodium falciparum* HGXPRT. *T. cruzi* HGPRT (TcA) (blue, 1TC2) in complex with PRPP and allopurinol. *P. falciparum* HGXPRT (tan, 3OZF) in complex with hypoxanthine and pyrophosphate. The ternary structures of both enzymes are highly similar, with the active sites being superimposable. Image generated in Chimera 1.13 using the MatchMaker function.

Putative transition state analog inhibitors

Lacking an experimental model for the transition-state of *N*-ribosyltransferase reaction catalyzed by TcC HGPRT, the enzyme was tested against phosphate and phosphonate derivatives of inhibitors for related purine nucleoside phosphorylase [192, 193] and purine phosphoribosyltransferase enzymes[167]. Perhaps the most striking observation is that a two-atom replacement of IMP to form (**2**) (**Figure III-11**) resulted in a compound with a K_i/K_M of roughly 1 x10^{-3}. The tight binding of (**2**) to the enzyme is likely due to replacement of the endocyclic oxygen of ribose with nitrogen, which presumably mimics the putative oxocarbenium formed on the ribose ring during the transition state, and is compelling evidence for an S_N1-like mechanism.

There are several other observations worth noting regarding the relationship between structure and inhibitory potency (K_i). The acyclic forms of ImmGP (**1**) and ImmHP (**2**), (**6**) and (**7**) respectively, show a roughly 3-fold increase in K_i, indicating that the 2' and 3' hydroxyl groups contribute to binding. The addition of hydroxyl groups which are comparable to the 2' hydroxyl of the ribose ring in compounds (**9**) and (**4**) results in a roughly 100-fold decrease in the K_i value. Additionally the (S)-enantiomer (**4**) binds roughly 100-fold tighter than the (R) enantiomer (**5**), which demonstrates a strong preference for the chirality in this position. The lack of significant inhibition by (**11**) was surprising. We propose that the difference in bond angles between the methylene of the phosphonate (**11**) and the oxygen of the phosphoester (**2**) alters the positioning of the phosphonate of (**11**) such that the compound is no longer readily accommodated in the active site. The placement of the 5'-equivalent phosphate appears to be affected differently on the acyclic inhibitors, where the phosphonate (**4**) binds to the enzyme significantly tighter than the phosphate (**8**). Consistent with the importance of phosph(on)ate groups in the 5'-equivalent position, the non-phosph(on)ate compound (**12**) shows no significant inhibition. Additionally, the analog with the deaza-xanthine base (**13**) showed no appreciable inhibition, which is consistent with the kinetic data in this study (**Table III-1**) and with what has previously been published[181].

In conclusion, the genome for *T. cruzi* is annotated as having two genes encoding enzymes with HGPRT activity, one of these genes is comprised of two homologs: the non-Esmeraldo-like TcA (TcCLB.509693.70) and the Esmeraldo-like TcC

(TcCLB.506457.30). Both enzymes were found to be essentially identical and consistent with having HGPRT activity (**Table III-1**). Despite the structural similarities of *T. cruzi* HGPRT with the HGXPRT enzyme from *P. falciparum* (**Figure III-10**), the two enzymes are kinetically quite different. *Pf*HGXPRT was previously reported to have large KIEs with very low commitment to catalysis[176], whereas for TcC the experimentally measured KIEs were negligible (**Table III-4**), in part due to chemistry not contributing to the rate-limiting step(s) (**Figure III-7**) and high commitment to catalysis (**Figure III-8**). TcC is kinetically much more similar to human HGPRT[175], which was previously reported to have essentially identical kinetic behavior (limited by product release, high commitment to catalysis). Even though the transition-state of the reaction catalyzed by TcC was unable to be elucidated by KIE measurements, the tight binding of compounds such as Immucillin-HP (**2**) and –GP (**1**) provides compelling evidence for the formation of an oxocarbenium in the transition state and supports and S_N1-like mechanism.

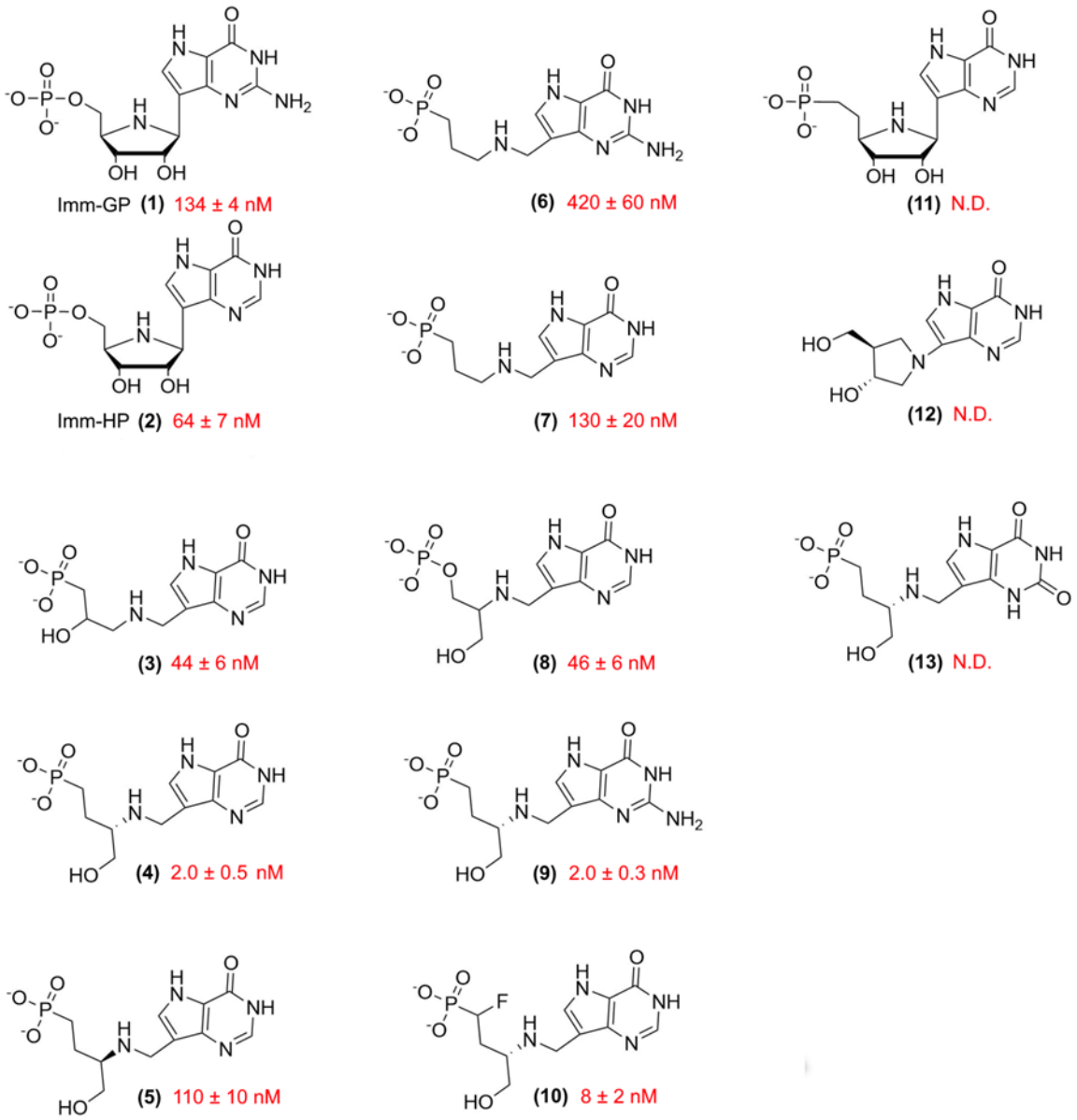

Figure III-11 Putative transition-state analogs of TcC. Dissociation constants shown in red. N.D. = not determined, IC_{50} > 10 μM.

CHAPTER IV

CONCLUSIONS AND FUTURE DIRECTIONS

Analogs of D-alanine and catalytic intermediates as inhibitors of D-alanine:D-alanine ligase from *Mycobacterium tuberculosis*

Worldwide, tuberculosis remains the leading cause of death by an infectious disease. The enzyme D-alanine:D-alanine ligase is a target of the second-line antibiotic D-cycloserine (DCS). The use of DCS is limited, in part due to the negative side-effects associated with the drug. We therefore investigated whether alternative D-alanine analogs could provide the inhibitory effects of DCS while potentially avoiding the negative side effects. A small library of compounds was developed (**Table II-2),** the design of which was largely influenced by previous work with glutamine synthetase [83, 84, 194, 195] and Ddl[66, 81, 85, 88, 89, 160, 196]. Surprisingly, most of the D-alanine analogs failed to demonstrate significant inhibition of the enzyme *in vitro*. The two notable exceptions were 1-aminoethylphosphonate and 3-amino-2-oxybutyl-phosphonate, phosphonate mimics of the putative catalytic intermediates. As shown in chapter II, both compounds were comparable to the antibiotic DCS *in vitro*, however *in vivo* potency is doubtful as both previously failed to inhibit bacterial growth in culture [88, 196]. The lack of whole cell efficacy may be due to poor cell penetration; while apparently DCS is able to be imported by D-alanine/glycine transport systems[196]. Positional isotope exchange (PIX) experiments provided some evidence for the phosphorylation of DCS in the enzyme active site of *Mt*Ddl, which may be a general

mechanism of inhibition by the antibiotic [78, 79]. In contrast, PIX provided no evidence for the phosphorylation of 1-aminoethylphosphonate, contradicting the putative mechanism of inhibition for the compound [85].

Overall, the design of compounds targeting the D-alanine binding site has proved difficult, owing largely to the stringency of substrate specificity for Ddl enzymes, as originally reported by Francis Neuhaus[63, 64, 159]. Secondly, the translation of potent *in vitro* inhibitors to potent bactericidal agents has also proved to be challenging. This is perhaps most dramatically exemplified by the failure of the aminkalkylphosphinate series of inhibitors to elicit a potent whole-cell response, despite the most potent in this class of Ddl inhibitors having enzyme-inhibitor complex half-lives of much greater than one day[82]. An alternate strategy may be to develop compounds that target the ATP site, such as the ellipticine-derivative of Kovač *et al* [91]. It may be possible to develop similar derivatives which simultaneously retain whole-cell activity and engage the D-alanine binding site to allow for specificity of Ddl inhibition.

Kinetic characterization and transition-state analog inhibitors of a hypoxanthine-guanine phosphoribosyltransferase from *Trypanosoma cruzi*

Chagas Disease is endemic to Latin America, where it disproportionally affects those living in poverty. The current treatments for the disease are toxic and ineffective against the chronic stages. The etiological agent of Chagas disease is *T. cruzi*. Like most other parasitic protozoa, *T. cruzi* relies on the salvage of purines from the host. A critical

enzyme for purine salvage is hypoxanthine-guanine phosphoribosyltransferase, which forms GMP and IMP from PRPP and the respective nucleobases. We sought to characterize the features of the transition state of *T. cruzi* HGPRTs by the use of isotopically labeled substrates in a series of KIE experiments. The experimentally-derived model of the transition-state could then be used to assist in the development of inhibitors that are structural analogs of the transition-state. In our work, which is detailed in chapter III, we have found that the two variants (TcA and TcC) of one pair of HGPRT genes are functionally identical, with both enzymes catalyzing GMP and IMP formation, but not the formation of XMP. The results of the KIE experiments showed that both the α-secondary and primary effects are attenuated. Reducing the commitment to catalysis by decreasing the concentration of purine or using a poor substrate analog of the purine was unable to successfully unmask the isotope effects. Further characterization of the enzyme revealed that chemistry was not significantly rate-limiting, and that the natural substrates are highly committed to catalysis. These findings have shown that kinetically, this enzyme is much more similar to human HGPRT[175], than the HGXPRT enzyme from *Plasmodium falciparum*[176, 184, 191].

Although we were unsuccessful in probing the transition-state through KIE experiments, a small panel of putative transition-state analogs was screened against the enzyme, the most potent of which was shown to have near picomolar affinity. Analysis of the structural-activity relationship of the compounds, such as Immucillin-HP and Immucillin-GP, provided compelling evidence for a transition-state with significant S_N1

character. Although isotopic effects are useful to uncover the chemical mechanisms of enzymes, they are not a requirement. For example, the formation of a carbenium ion intermediate in the reaction catalyzed by yeast isopentenyl pyrophosphate isomerase is supported by the tight binding of tertiary amine derivatives of the natural substrate, isopentenyl pyrophosphate [197, 198]. On the other hand, isotopic effects can potentially uncover more detail about the transition-state than what is afforded by the assessment of structural-activity relationships with putative transition-state analogs. Subtle differences in the transition-states between orthologous enzymes may be useful in the design of TSAI with selectivity. Although it is unclear what kind of side-effects would be expected of short-term exposure to HGPRT inhibitors, congenital deficiency of HGPRT activity in humans results in gouty arthritis, and in extreme cases, the neurological disease Lesch Nyhan.

For these reasons, one may still be able to rationalize the continued investigation of isotope effects for *T. cruzi* HGPRTs, although clearly not in the biosynthetic direction. The ideal approach may be to use alternative substrates in the reverse direction (bond breaking between *N*9 and C1'), where presumably chemistry is more rate-limiting and commitment is reduced. Indeed, this approach has been highly successful in the studies of PNP enzymes, for which the phosphorolysis reaction was replaced with arsenolysis[199-201], and for orotate phosphoribosyltransferase, for which pyrophosphate was replaced by phosphonoacetate[202].

REFERENCES

1. Comas, I., et al., *Out-of-Africa migration and Neolithic coexpansion of Mycobacterium tuberculosis with modern humans.* Nature Genetics, 2013. **45**(10): p. 1176-1182.

2. WHO, *Global tuberculosis report 2020.* Geneva: World Health Organization., 2020.

3. Sturgill-Koszycki, S., et al., *Lack of acidification in Mycobacterium phagosomes produced by exclusion of the vesicular proton-ATPase.* Science, 1994. **263**(5147): p. 678-681.

4. Crowle, A.J., et al., *Evidence that vesicles containing living, virulent Mycobacterium tuberculosis or Mycobacterium avium in cultured human macrophages are not acidic.* Infection and Immunity, 1991. **59**(5): p. 1823-1831.

5. De Chastellier, C., et al., *Implication of phagosome-lysosome fusion in restriction of Mycobacterium avium growth in bone marrow macrophages from genetically resistant mice.* Infection and Immunity, 1993. **61**(9): p. 3775-3784.

6. Moraco, A.H. and H. Kornfeld, *Cell death and autophagy in tuberculosis.* Seminars in Immunology, 2014. **26**(6): p. 497-511.

7. Lee, J., M. Hartman, and H. Kornfeld, *Macrophage Apoptosis in Tuberculosis.* Yonsei Medical Journal, 2009. **50**(1): p. 1.

8. Seki, M., et al., *Tuberculosis: A persistent unpleasant neighbour of humans.* 2021(1876-035X (Electronic)).

9. Houben, R.M.G.J. and P.J. Dodd, *The Global Burden of Latent Tuberculosis Infection: A Re-estimation Using Mathematical Modelling.* PLOS Medicine, 2016. **13**(10): p. e1002152.

10. WHO, *Latent tuberculosis infection.* Geneva: World Health Organization., 2018.

11. CDC. *Treatment for TB Disease*. 2016 [cited 2021; Available from: https://www.cdc.gov/tb/topic/treatment/tbdisease.htm.

12. Belanger, A.E., et al., *The embAB genes of Mycobacterium avium encode an arabinosyl transferase involved in cell wall arabinan biosynthesis that is the target for the antimycobacterial drug ethambutol.* Proceedings of the National Academy of Sciences, 1996. **93**(21): p. 11919-11924.

13. Mikusova, K., et al., *Biogenesis of the mycobacterial cell wall and the site of action of ethambutol.* Antimicrobial Agents and Chemotherapy, 1995. **39**(11): p. 2484-2489.

14. Johnsson, K., D.S. King, and P.G. Schultz, *Studies on the Mechanism of Action of Isoniazid and Ethionamide in the Chemotherapy of Tuberculosis.* Journal of the American Chemical Society, 1995. **117**(17): p. 5009-5010.

15. Dessen, A., et al., *Crystal structure and function of the isoniazid target of Mycobacterium tuberculosis.* Science, 1995. **267**(5204): p. 1638-1641.

16. Quemard, A., et al., *Binding of Catalase-Peroxidase-Activated Isoniazid to Wild-Type and Mutant Mycobacterium tuberculosis Enoyl-ACP Reductases.* Journal of the American Chemical Society, 1996. **118**(6): p. 1561-1562.

17. Quemard, A., et al., *Enzymic Characterization of the Target for Isoniazid in Mycobacterium tuberculosis.* Biochemistry, 1995. **34**(26): p. 8235-8241.

18. Rawat, R., A. Whitty, and P.J. Tonge, *The isoniazid-NAD adduct is a slow, tight-binding inhibitor of InhA, the Mycobacterium tuberculosis enoyl reductase: Adduct affinity and drug resistance.* Proceedings of the National Academy of Sciences, 2003. **100**(24): p. 13881-13886.

19. Rozwarski, D.A., *Modification of the NADH of the Isoniazid Target (InhA) from Mycobacterium tuberculosis.* Science, 1998. **279**(5347): p. 98-102.

20. Campbell, E.A., et al., *Structural Mechanism for Rifampicin Inhibition of Bacterial RNA Polymerase.* Cell, 2001. **104**(6): p. 901-912.

21. Hartmann, G., et al., *The specific inhibition of the DNA-directed RNA synthesis by rifamycin.* Biochimica et Biophysica Acta (BBA) - Nucleic Acids and Protein Synthesis, 1967. **145**(3): p. 843-844.

22. Scorpio, A. and Y. Zhang, *Mutations in pncA, a gene encoding pyrazinamidase/nicotinamidase, cause resistance to the antituberculous drug pyrazinamide in tubercle bacillus.* Nature Medicine, 1996. **2**(6): p. 662-667.

23. Gopal, P., et al., *Pyrazinamide triggers degradation of its target aspartate decarboxylase.* Nature Communications, 2020. **11**(1).

24. Mahapatra, S., et al., *N Glycolylation of the Nucleotide Precursors of Peptidoglycan Biosynthesis of Mycobacterium spp. Is Altered by Drug Treatment.* Journal of Bacteriology, 2005. **187**(7): p. 2341-2347.

25. Raymond, J.B., et al., *Identification of the namH Gene, Encoding the Hydroxylase Responsible for the N-Glycolylation of the Mycobacterial Peptidoglycan*.* Journal of Biological Chemistry, 2005. **280**(1): p. 326-333.

26. Wietzerbin-Falszpan, J., et al., *Isolation and mass spectrometric identification of the peptide subunits of mycobacterial cell walls.* Biochemical and Biophysical Research Communications, 1970. **40**(1): p. 57-63.

27. Lavollay, M., et al., *The Peptidoglycan of Stationary-Phase Mycobacterium tuberculosis Predominantly Contains Cross-Links Generated by l,d-Transpeptidation.* Journal of Bacteriology, 2008. **190**(12): p. 4360-4366.

28. Mcneil, M., M. Daffe, and P.J. Brennan, *Evidence for the nature of the link between the arabinogalactan and peptidoglycan of mycobacterial cell walls.* Journal of Biological Chemistry, 1990. **265**(30): p. 18200-18206.

29. Vilkas, E., et al., *Occurrence of a galactofuranose disaccharide in immunoadjuvant fractions of Mycobacterium tubercolosis (cell walls and wax D).* Biochimica et Biophysica Acta (BBA) - General Subjects, 1973. **297**(2): p. 423-435.

30. McNeil, M., et al., *Demonstration that the galactosyl and arabinosyl residues in the cell-wall arabinogalactan of Mycobacterium leprae and Myobacterium tuberculosis are furanoid.* Carbohydrate Research, 1987. **166**(2): p. 299-308.

31. Daffe, M., P.J. Brennan, and M. Mcneil, *Predominant structural features of the cell wall arabinogalactan of Mycobacterium tuberculosis as revealed through characterization of oligoglycosyl alditol fragments by gas chromatography/mass spectrometry and by 1H and 13C NMR analyses.* Journal of Biological Chemistry, 1990. **265**(12): p. 6734-6743.

32. Bhamidi, S., et al., *The Identification and Location of Succinyl Residues and the Characterization of the Interior Arabinan Region Allow for a Model of the Complete Primary Structure of Mycobacterium tuberculosis Mycolyl Arabinogalactan.* Journal of Biological Chemistry, 2008. **283**(19): p. 12992-13000.

33. Bhamidi, S., et al., *Detailed Structural and Quantitative Analysis Reveals the Spatial Organization of the Cell Walls of in Vivo Grown Mycobacterium leprae and in Vitro Grown Mycobacterium tuberculosis.* Journal of Biological Chemistry, 2011. **286**(26): p. 23168-23177.

34. Mcneil, M., M. Daffe, and P.J. Brennan, *Location of the mycolyl ester substituents in the cell walls of mycobacteria.* Journal of Biological Chemistry, 1991. **266**(20): p. 13217-13223.

35. Watanabe, M., et al., *Separation and characterization of individual mycolic acids in representative mycobacteria.* Microbiology, 2001. **147**(7): p. 1825-1837.

36. Brown, E.D., et al., *MurA (MurZ), the enzyme that catalyzes the first committed step in peptidoglycan biosynthesis, is essential in Escherichia coli.* Journal of bacteriology, 1995. **177**(14): p. 4194-4197.

37. Marquardt, J.L., et al., *Cloning and sequencing of Escherichia coli murZ and purification of its product, a UDP-N-acetylglucosamine enolpyruvyl transferase.* Journal of Bacteriology, 1992. **174**(17): p. 5748-5752.

38. Zhu, J.-Y., et al., *Functional Consequence of Covalent Reaction of Phosphoenolpyruvate with UDP-N-acetylglucosamine 1-*

Carboxyvinyltransferase (MurA). Journal of Biological Chemistry, 2012. **287**(16): p. 12657-12667.

39. Krekel, F., et al., *Determination of the pKaValue of C115 in MurA (UDP-N-Acetylglucosamine Enolpyruvyltransferase) from Enterobacter cloacae.* Biochemistry, 2000. **39**(41): p. 12671-12677.

40. Dhalla, A.M., et al., *Steady-State Kinetic Mechanism of Escherichia coli UDP-N-Acetylenolpyruvylglucosamine Reductase.* Biochemistry, 1995. **34**(16): p. 5390-5402.

41. Benson, T.E., et al., *Overexpression, purification, and mechanistic study of UDP-N-acetylenolpyruvylglucosamine reductase.* Biochemistry, 1993. **32**(8): p. 2024-2030.

42. Mahapatra, S., D.C. Crick, and P.J. Brennan, *Comparison of the UDP-N-Acetylmuramate:l-Alanine Ligase Enzymes from Mycobacterium tuberculosis andMycobacterium leprae.* Journal of Bacteriology, 2000. **182**(23): p. 6827-6830.

43. Pratviel-Sosa, F., D. Mengin-Lecreulx, and J. Heijenoort, *Over-production, purification and properties of the uridine diphosphate N-acetylmuramoyl-l-alanine: d-glutamate ligase from Escherichia coli.* European Journal of Biochemistry, 1991. **202**(3): p. 1169-1176.

44. Michaud, C., et al., *Over-production, purification and properties of the uridine-diphosphate-N-acetylmuramoyl-l-alanyl-d-glutamate: meso-2,6-diaminopimelate ligase from Escherichia coli.* European Journal of Biochemistry, 1990. **194**(3): p. 853-861.

45. Duncan, K., J. Van Heijenoort, and C.T. Walsh, *Purification and characterization of the D-alanyl-D-alanine-adding enzyme from Escherichia coli.* Biochemistry, 1990. **29**(9): p. 2379-2386.

46. Barreteau, H., et al., *Cytoplasmic steps of peptidoglycan biosynthesis.* FEMS Microbiology Reviews, 2008. **32**(2): p. 168-207.

47. Strych, U., et al., *Purification and preliminary crystallization of alanine racemase from Streptococcus pneumoniae.* BMC Microbiol, 2007. **7**: p. 40.

48. Neuhaus, F.C., *The Enzymatic Synthesis of D-Alanyl-D-alanine.* The Journal of Biological Chemistry, 1962. **237**(3): p. 778.

49. Takayama, K. and D.S. Goldman, *Enzymatic Synthesis of Mannosyl-1-phosphoryl-decaprenol by a Cell-free System of Mycobacterium tuberculosis.* Journal of Biological Chemistry, 1970. **245**(23): p. 6251-6257.

50. Kaur, D., P.J. Brennan, and D.C. Crick, *Decaprenyl Diphosphate Synthesis in Mycobacterium tuberculosis.* Journal of Bacteriology, 2004. **186**(22): p. 7564-7570.

51. Higashi, Y., J.L. Strominger, and C.C. Sweeley, *Structure of a lipid intermediate in cell wall peptidoglycan synthesis: a derivative of a C55 isoprenoid alcohol.* Proceedings of the National Academy of Sciences, 1967. **57**(6): p. 1878-1884.

52. Geis, A. and R. Plapp, *Phospho-N-acetylmuramoyl-pentapeptide-transferase of Escherichia coli K12 Properties of the membrane-bound and the extracted and partially purified enzyme.* Biochimica et Biophysica Acta (BBA) - Enzymology, 1978. **527**(2): p. 414-424.

53. Pless, D.D. and F.C. Neuhaus, *Initial Membrane Reaction in Peptidoglycan Synthesis.* Journal of Biological Chemistry, 1973. **248**(5): p. 1568-1576.

54. Al-Dabbagh, B., et al., *Catalytic mechanism of MraY and WecA, two paralogues of the polyprenyl-phosphate N-acetylhexosamine 1-phosphate transferase superfamily.* Biochimie, 2016. **127**: p. 249-257.

55. Crouvoisier, M., D. Mengin-Lecreulx, and J. Van Heijenoort, *UDP-N-acetylglucosamine:N-acetylmuramoyl-(pentapeptide) pyrophosphoryl undecaprenolN-acetylglucosamine transferase fromEscherichia coli: overproduction, solubilization, and purification.* FEBS Letters, 1999. **449**(2-3): p. 289-292.

56. Mengin-Lecreulx, D., et al., *The murG gene of Escherichia coli codes for the UDP-N-acetylglucosamine: N-acetylmuramyl-(pentapeptide) pyrophosphoryl-undecaprenol N-acetylglucosamine transferase involved in the membrane steps of peptidoglycan synthesis.* Journal of Bacteriology, 1991. **173**(15): p. 4625-4636.

57. Ruiz, N., *Bioinformatics identification of MurJ (MviN) as the peptidoglycan lipid II flippase inEscherichia coli.* Proceedings of the National Academy of Sciences, 2008. **105**(40): p. 15553-15557.

58. Mohammadi, T., et al., *Identification of FtsW as a transporter of lipid-linked cell wall precursors across the membrane.* The EMBO Journal, 2011. **30**(8): p. 1425-1432.

59. Sham, L.-T., et al., *MurJ is the flippase of lipid-linked precursors for peptidoglycan biogenesis.* Science, 2014. **345**(6193): p. 220-222.

60. Taguchi, A., et al., *FtsW is a peptidoglycan polymerase that is functional only in complex with its cognate penicillin-binding protein.* Nature Microbiology, 2019. **4**(4): p. 587-594.

61. Hett, E.C., M.C. Chao, and E.J. Rubin, *Interaction and Modulation of Two Antagonistic Cell Wall Enzymes of Mycobacteria.* PLoS Pathogens, 2010. **6**(7): p. e1001020.

62. Filippova, E.V., et al., *Crystal structures of the transpeptidase domain of the Mycobacterium tuberculosis penicillin-binding protein PonA1 reveal potential mechanisms of antibiotic resistance.* The FEBS Journal, 2016. **283**(12): p. 2206-2218.

63. Neuhaus, F.C., *The Enzymatic Synthesis of d-Alanyl-d-alanine.* Journal of Biological Chemistry, 1962. **237**(3): p. 778-786.

64. Neuhaus, F.C. and J.L. Lynch, *The Enzymatic Synthesis of D-Alanyl-D-alanine. III. On the Inhibition of D-Alanyl-D-alanine Synthetase by the Antibiotic D-Cycloserine*.* Biochemistry, 1964. **3**(4): p. 471-480.

65. Neuhaus, F.C., *The Enzymatic Synthesis of d-Alanyl-d-alanine.* Journal of Biological Chemistry, 1962. **237**(10): p. 3128-3135.

66. Mullins, L.S., et al., *Kinetic Evidence for the Formation of D-Alanyl Phosphate in the Mechanism of D-Alanyl-D-alanine Ligase.* The Journal of Biological Chemistry, 1990. **256**(16): p. 8993.

67. Prosser, G.A. and L.P.S.d. Carvalho, *Kinetic mechanism and inhibition of Mycobacterium tuberculosis D-alanine:D-alanine ligase by the antibiotic D-cycloserine.* FEBS Journal, 2013. **280**: p. 1150.

68. Healy, V.L., et al., *D-Ala-D-X Ligase: Evaluation of D-alanyl phosphate intermediate by MIX, PIX, and rapid quench.* Chemistry & Biology, 2000. **7**: p. 505.

69. Kitamura, Y., et al., *Structure ofD-alanine-D-alanine ligase fromThermus thermophilusHB8: cumulative conformational change and enzyme–ligand interactions.* Acta Crystallographica Section D Biological Crystallography, 2009. **65**(10): p. 1098-1106.

70. WHO, *WHO operational handbook on tuberculosis Module 4: treatment - drug resistant tuberuclosis treatment*. 2020, Geneva: World Health Organization.

71. Halouska, S., et al., *Metabolomics Analysis Identifiesd-Alanine-d-Alanine Ligase as the Primary Lethal Target ofd-Cycloserine in Mycobacteria.* Journal of Proteome Research, 2014. **13**(2): p. 1065-1076.

72. Prosser, G.A. and L.P.S. De Carvalho, *Metabolomics Reveald-Alanine:d-Alanine Ligase As the Target ofd-Cycloserine inMycobacterium tuberculosis.* ACS Medicinal Chemistry Letters, 2013. **4**(12): p. 1233-1237.

73. Nakatani, Y., et al., *Role of Alanine Racemase Mutations in Mycobacterium tuberculosisd-Cycloserine Resistance.* Antimicrobial Agents and Chemotherapy, 2017. **61**(12).

74. Chen, J., et al., *Identification of novel mutations associated with cycloserine resistance in Mycobacterium tuberculosis.* Journal of Antimicrobial Chemotherapy, 2017. **72**(12): p. 3272-3276.

75. Awasthy, D., et al., *Alanine racemase mutants of Mycobacterium tuberculosis require d-alanine for growth and are defective for survival in macrophages and mice.* Microbiology, 2012. **158**(2): p. 319-327.

76. Bruning, J.B., et al., *Structure of the Mycobacterium tuberculosis D-Alanine:D-Alanine Ligase, a Target of the Antituberculosis Drug D-Cycloserine.* Antimicrobial Agents and Chemotherapy, 2011. **55**: p. 291.

77. Prosser, G.A. and L.P.S.d. Carvalho, *Reinterpreting the Mechanism of Inhibition of Mycobacterium tuberculosis D-Alanine:D-Alanine Ligase by D-Cycloserine.* Biochemistry, 2013. **52**: p. 7145.

78. Pederick, J.L., et al., *d-Alanine–d-alanine ligase as a model for the activation of ATP-grasp enzymes by monovalent cations.* Journal of Biological Chemistry, 2020. **295**(23): p. 7894-7904.

79. Batson, S., et al., *Inhibition of D-Ala:D-Ala ligase through a phosphorylated form of the antibiotic D-cycloserine.* Nature Communications, 2017. **8**(1).

80. De Chiara, C., et al., *d-Cycloserine destruction by alanine racemase and the limit of irreversible inhibition.* Nature Chemical Biology, 2020. **16**(6): p. 686-694.

81. Lacoste, A.-M., et al., *Inhibition ofd-alanyl-d-alanine ligase in different bacterial species by amino phosphonic acids.* Current Microbiology, 1979. **2**(2): p. 113-117.

82. Parsons, W.H., et al., *Phosphinc Acid Inhibitors of D-Alanyl-D-alanine Ligase.* Journal of Medicinal Chemistry, 1988. **31**: p. 1772.

83. Colanduoni, J.A. and J.J. Villafrance, *Inhibition of Escherichia coli Glutamine Synthetase by Phosphothricin.* Bioorganic Chemistry, 1986. **14**: p. 163.

84. Rowe, W.B., R.A. Ronzio, and A. Meister, *Inhibition of Glutamine Synthetase by Methionine Sulfoximine. Studies on Methionin Sulfoximine Phosphate.* Biochemistry, 1969. **8**: p. 2674.

85. Duncan, K. and C.T. Walsh, *ATP-Dependent Inactivation and Slow Binding Inhibition of Salmonella typhimurium D-Alanine:D-Alanine Ligase (ADP) by (1-aminoalkyl)phosphinate and Aminophosphonate Analogues of D-Alanine.* Biochemistry, 1988. **27**: p. 3709.

86. Mcdermott, A.E., et al., *Rotational resonance determination of the structure of an enzyme-inhibitor complex: phosphorylation of an (aminoalkyl)phosphinate inhibitor of D-alanyl-D-alanine ligase by ATP*. Biochemistry, 1990. **29**(24): p. 5767-5775.

87. Fan, C., et al., *D-alanine:D-Alanine Ligase: Phosphonate and Phosphinate Intermediates with Wild Type and the Y216F Mutant.* Biochemistry, 1997. **36**: p. 2531.

88. Chakravarty, P.K., et al., *(3-Amino-2-oxoalkyl)phosphonic acids and their analogs as novel inhibitors of D-alanine:D-alanine ligase.* Journal of Medicinal Chemistry, 1989. **32**(8): p. 1886-1890.

89. Lacoste, A., et al., *Time-dependent inhibition of Streptococcus faecalisd-alanine: d-alanine ligase by α-aminophosphonamidic acids.* European Journal of Medicinal Chemistry, 1991. **26**(3): p. 255-260.

90. Hrast, M., et al., *Function of thed-Alanine:d-Alanine Ligase Lid Loop: A Molecular Modeling and Bioactivity Study.* Journal of Medicinal Chemistry, 2012. **55**(15): p. 6849-6856.

91. Kovač, A., et al., *Discovery of New Inhibitors ofd-Alanine:d-Alanine Ligase by Structure-Based Virtual Screening†.* Journal of Medicinal Chemistry, 2008. **51**(23): p. 7442-7448.

92. WHO. *Neglected tropical diseases*. 2012; Available from: https://www.who.int/news-room/q-a-detail/neglected-tropical-diseases.

93. Freitas, E.C., et al., *Analysis of the seroprevalence of and factors associated with Chagas disease in an endemic area in Northeastern Brazil.* Revista da Sociedade Brasileira de Medicina Tropical, 2017. **50**(1): p. 44-51.

94. WHO. *Chagas disease (American trypanosomiasis)*. Available from: https://www.who.int/health-topics/chagas-disease#tab=tab_1.

95. Bern, C., et al., *Chagas Disease in the United States: a Public Health Approach.* Clinical Microbiology Reviews, 2019. **33**(1).

96. Bern, C., *Chagas' Disease.* New England Journal of Medicine, 2015. **373**(5): p. 456-466.

97. Echeverria, L.E. and C.A. Morillo, *American Trypanosomiasis (Chagas Disease).* Infectious Disease Clinics of North America, 2019. **33**(1): p. 119-134.

98. Kribs-Zaleta, C., *Estimating Contact Process Saturation in Sylvatic Transmission of Trypanosoma cruzi in the United States.* PLoS Neglected Tropical Diseases, 2010. **4**(4): p. e656.

99. Rassi, A., A. Rassi, and J. Marcondes De Rezende, *American Trypanosomiasis (Chagas Disease).* Infectious Disease Clinics of North America, 2012. **26**(2): p. 275-291.

100. Docampo, R., *Sensitivity of parasites to free radical damage by antiparasitic drugs.* Chemico-Biological Interactions, 1990. **73**(1): p. 1-27.

101. Edwards, D.I., *Nitroimidazole drugs-action and resistance mechanisms I. Mechanism of action.* Journal of Antimicrobial Chemotherapy, 1993. **31**(1): p. 9-20.

102. Caldas, I.S., E.G. Santos, and R.D. Novaes, *An evaluation of benznidazole as a Chagas disease therapeutic.* Expert Opinion on Pharmacotherapy, 2019. **20**(15): p. 1797-1807.

103. Perez-Molina, J.A., et al., *Use of benznidazole to treat chronic Chagas' disease: a systematic review with a meta-analysis.* Journal of Antimicrobial Chemotherapy, 2009. **64**(6): p. 1139-1147.

104. Morillo, C.A., et al., *Randomized Trial of Benznidazole for Chronic Chagas' Cardiomyopathy.* New England Journal of Medicine, 2015. **373**(14): p. 1295-1306.

105. Urbina, J.A. and R. Docampo, *Specific chemotherapy of Chagas disease: controversies and advances.* Trends in Parasitology, 2003. **19**(11): p. 495-501.

106. Dias, J., A. Silveira, and C. Schofield, *The impact of Chagas disease control in Latin America: a review.* Memórias do Instituto Oswaldo Cruz, 2002. **97**(5): p. 603-612.

107. Shapiro, T.A. and P.T. Englund, *The structure and replication of kinetoplast DNA.* (0066-4227 (Print)).

108. Liang, X.-H., et al., *trans and cis Splicing in Trypanosomatids: Mechanism, Factors, and Regulation.* Eukaryotic Cell, 2003. **2**(5): p. 830-840.

109. Vanhamme, L. and E. Pays, *Control of gene expression in trypanosomes.* Microbiological reviews, 1995. **59**(2): p. 223-240.

110. Souza, W.D., *A short review on the morphology of Trypanosoma cruzi: from 1909 to 1999.* Memórias do Instituto Oswaldo Cruz, 1999. **94**(suppl 1): p. 17-36.

111. Nájera, C.A., et al., *Mixed signals – how Trypanosoma cruzi exploits host-cell communication and signaling to establish infection.* Journal of Cell Science, 2021. **134**(5): p. jcs255687.

112. Dorta, M.L., et al., *Ca2+ signal induced by Trypanosoma cruzi metacyclic trypomastigote surface molecules implicated in mammalian cell invasion.* Molecular and Biochemical Parasitology, 1995. **73**(1-2): p. 285-289.

113. Manque, P.M., et al., *Cell Adhesion and Ca2+ Signaling Activity in Stably Transfected Trypanosoma cruzi Epimastigotes Expressing the Metacyclic Stage-Specific Surface Molecule gp82.* Infection and Immunity, 2003. **71**(3): p. 1561-1565.

114. Fernandes, M.C., et al., *Trypanosoma cruzi subverts the sphingomyelinase-mediated plasma membrane repair pathway for cell invasion.* Journal of Experimental Medicine, 2011. **208**(5): p. 909-921.

115. Fernandes, M.C. and N.W. Andrews, *Host cell invasion byTrypanosoma cruzi: a unique strategy that promotes persistence.* FEMS Microbiology Reviews, 2012. **36**(3): p. 734-747.

116. Tyler, K.M., et al., *Responsive microtubule dynamics promote cell invasion by Trypanosoma cruzi.* Cellular Microbiology, 2005. **7**(11): p. 1579-1591.

117. Pessoa, C.C., et al., *Trypanosoma cruzi Differentiates and Multiplies within Chimeric Parasitophorous Vacuoles in Macrophages Coinfected with Leishmania amazonensis.* Infection and Immunity, 2016. **84**(5): p. 1603-1614.

118. De Souza, W., T.M.U. De Carvalho, and E.S. Barrias, *Review onTrypanosoma cruzi: Host Cell Interaction.* International Journal of Cell Biology, 2010. **2010**: p. 1-18.

119. Ferri, G. and M.M. Edreira, *All Roads Lead to Cytosol: Trypanosoma cruzi Multi-Strategic Approach to Invasion.* Frontiers in Cellular and Infection Microbiology, 2021. **11**.

120. Gonzales-Perdomo, M., P. Romero, and S. Goldenberg, *Cyclic AMP and adenylate cyclase activators stimulate Trypanosoma cruzi differentiation.* Experimental Parasitology, 1988. **66**(2): p. 205-212.

121. El-Sayed, N.M., *The Genome Sequence of Trypanosoma cruzi, Etiologic Agent of Chagas Disease.* Science, 2005. **309**(5733): p. 409-415.

122. Buschiazzo, A., et al., *The Crystal Structure and Mode of Action of Trans-Sialidase, a Key Enzyme in Trypanosoma cruzi Pathogenesis.* Molecular Cell, 2002. **10**(4): p. 757-768.

123. Scudder, P., et al., *Enzymatic characterization of beta-D-galactoside alpha 2,3-trans-sialidase from Trypanosoma cruzi.* Journal of Biological Chemistry, 1993. **268**(13): p. 9886-9891.

124. Parodi, A.J., et al., *Identification of the gene(s) coding for the trans-sialidase of Trypanosoma cruzi.* The EMBO Journal, 1992. **11**(5): p. 1705-1710.

125. Previato, J., et al., *Incorporation of sialic acid into Trypanosoma cruzi macromolecules. A proposal for a new metabolic route.* Molecular and Biochemical Parasitology, 1985. **16**(1): p. 85-96.

126. Schenkman, S., et al., *A novel cell surface trans-sialidase of trypanosoma cruzi generates a stage-specific epitope required for invasion of mammalian cells.* Cell, 1991. **65**(7): p. 1117-1125.

127. Tomlinson, S., et al., *Role of sialic acid in the resistance of Trypanosoma cruzi trypomastigotes to complement.* (0022-1767 (Print)).

128. Almeida, I.C., et al., *Lytic anti-α-galactosyl antibodies from patients with chronic Chagas' disease recognize novel O-linked oligosaccharides on mucin-like glycosyl-phosphatidylinositol-anchored glycoproteins of Trypanosoma cruzi.* Biochemical Journal, 1994. **304**(3): p. 793-802.

129. Schenkman, S., et al., *Mucin-like glycoproteins linked to the membrane by glycosylphosphatidylinositol anchor are the major acceptors of sialic acid in a reaction catalyzed by trans-sialidase in metacyclic forms of Trypanosoma cruzi.* Molecular and Biochemical Parasitology, 1993. **59**(2): p. 293-303.

130. Freitas-Junior, L.H.G., M.R.S. Briones, and S. Schenkman, *Two distinct groups of mucin-like genes are differentially expressed in the developmental stages of Trypanosoma cruzi.* Molecular and Biochemical Parasitology, 1998. **93**(1): p. 101-114.

131. Buscaglia, C.A., et al., *The Surface Coat of the Mammal-dwelling Infective Trypomastigote Stage of Trypanosoma cruzi Is Formed by Highly Diverse Immunogenic Mucins.* Journal of Biological Chemistry, 2004. **279**(16): p. 15860-15869.

132. Pereira-Chioccola, V.L., et al., *Mucin-like molecules form a negatively charged coat that protects Trypanosoma cruzi trypomastigotes from killing by human anti-alpha-galactosyl antibodies.* Journal of Cell Science, 2000. **113**(7): p. 1299-1307.

133. Di Noia, J.M., et al., *The Trypanosoma cruzi Mucin Family Is Transcribed from Hundreds of Genes Having Hypervariable Regions.* Journal of Biological Chemistry, 1998. **273**(18): p. 10843-10850.

134. Pollevick, G.D., et al., *Trypanosoma cruzi Surface Mucins with Exposed Variant Epitopes.* Journal of Biological Chemistry, 2000. **275**(36): p. 27671-27680.

135. Sampei, G.-I., et al., *Crystal structures of glycinamide ribonucleotide synthetase, PurD, from thermophilic eubacteria.* The Journal of Biochemistry, 2010. **148**(4): p. 429-438.

136. Aimi, J., et al., *De novopurine nucleotide biosynthesis: cloning of human and avian cDNAs encoding the trifunctional glycinamide ribonucleotide synthetase-aminoimidazole ribonucleotide synthetase-glycinamide ribonucleotide transformylase by functional complementation inE.c.* Nucleic Acids Research, 1990. **18**(22): p. 6665-6672.

137. Eichinger, L., et al., *The genome of the social amoeba Dictyostelium discoideum.* Nature, 2005. **435**(7038): p. 43-57.

138. Minet, M.L. and F.O. Lacroute, *Cloning and sequencing of a human cDNA coding for a multifunctional polypeptide of the purine pathway by complementation of the ade2-101 mutant in Saccharomyces cerevisiae.* Current Genetics, 1990. **18**(4): p. 287-291.

139. Rayl, E.A., B.A. Moroson, and G.P. Beardsley, *The Human purH Gene Product, 5-Aminoimidazole-4-carboxamide Ribonucleotide Formyltransferase/IMP Cyclohydrolase.* Journal of Biological Chemistry, 1996. **271**(4): p. 2225-2233.

140. Mueller, E.J., et al., *N5-Carboxyaminoimidazole Ribonucleotide: Evidence for a New Intermediate and Two New Enzymic Activities in the de Novo Purine Biosynthetic Pathway of Escherichia coli.* Biochemistry, 1994. **33**(8): p. 2269-2278.

141. Kratzer, J.T., et al., *Evolutionary history and metabolic insights of ancient mammalian uricases.* Proceedings of the National Academy of Sciences, 2014. **111**(10): p. 3763-3768.

142. Johnson, R.J., et al., *Lessons from comparative physiology: could uric acid represent a physiologic alarm signal gone awry in western society?* Journal of Comparative Physiology B, 2009. **179**(1): p. 67-76.

143. Hammond, D.J. and W.E. Gutteridge, *Purine and pyrimidine metabolism in the trypanosomatidae.* Molecular and Biochemical Parasitology, 1984. **13**(3): p. 243-261.

144. Fernandes, J.F. and O. Castellani, *Nucleotide and polynucleotide synthesis in Trypanosoma cruzi. I. Precursors of purine compounds.* Experimental Parasitology, 1958. **7**(2): p. 224-235.

145. Gutteridge, W.E. and M. Gaborak, *A re-examination of purine and pyrimidine synthesis in the three main forms of Trypanosoma cruzi.* International Journal of Biochemistry, 1979. **10**(5): p. 415-422.

146. Ceron, C.R., et al., *Purine Metabolism in Trypanosomatids.* The Journal of Protozoology, 1979. **26**(3): p. 479-483.

147. Berens, R.L., et al., *Purine metabolism in Trypanosoma cruzi.* Molecular and Biochemical Parasitology, 1981. **3**(3): p. 187-196.

148. Davies, M.J., A.M. Ross, and W.E. Gutteridge, *The enzymes of purine salvage in Trypanosoma cruzi, Trypanosoma brucei and Leishmania mexicana.* Parasitology, 1983. **87**(2): p. 211-217.

149. Miller, R.L., et al., *Nucleoside hydrolases from Trypanosoma cruzi.* Journal of Biological Chemistry, 1984. **259**(8): p. 5073-5077.

150. Cohn, C.S. and M. Gottlieb, *The acquisition of purines by trypanosomatids.* Parasitology Today, 1997. **13**(6): p. 231-235.

151. Boswell-Casteel, R.C. and F.A. Hays, *Equilibrative nucleoside transporters—A review.* Nucleosides, Nucleotides and Nucleic Acids, 2017. **36**(1): p. 7-30.

152. Landfear, S.M., et al., *Nucleoside and Nucleobase Transporters in Parasitic Protozoa.* Eukaryotic Cell, 2004. **3**(2): p. 245-254.

153. M., S., *Drugs and Transporters in Kinetoplastid Protozoa*, in *Advances In Experimental Medicine And Biology*. 2008, Springer New York. p. 22-32.

154. De Koning, H.P., C.J. Watson, and S.M. Jarvis, *Characterization of a Nucleoside/Proton Symporter in ProcyclicTrypanosoma brucei brucei.* Journal of Biological Chemistry, 1998. **273**(16): p. 9486-9494.

155. Finley, R.W., D.A. Cooney, and J.A. Dvorak, *Nucleoside uptake in Trypanosoma cruzi: analysis of a mutant resistant to tubercidin.* Molecular and Biochemical Parasitology, 1988. **31**(2): p. 133-140.

156. Yew, W.W., et al., *Adverse Neurological Reactions in Patients with Multidrug-Resistant Pulmonary Tuberculosis After Coadministration of Cycloserine and Ofloxacin.* Clinical Infectious Diseases, 1993. **17**(2): p. 288-289.

157. Schade, S. and W. Paulus, *D-Cycloserine in Neuropsychiatric Diseases: A Systematic Review.* International Journal of Neuropsychopharmacology, 2016. **19**(4): p. pyv102.

158. Lambert, M.P. and F.C. Neuhaus, *Mechanism of d-Cycloserine Action: Alanine Racemase from Escherichia coli W1.* Journal of Bacteriology, 1972. **110**(3): p. 978-987.

159. Neuhaus, F.C. and J.L. Lynch, *Studies on the inhibition of D-alanyl-D-alanine synthetase by the antibiotic D-cycloserine.* Biochem Biophys Res Commun, 1962. **8**: p. 377-82.

160. Ellsworth, B.A., N.J. Tom, and P.A. Bartlett, *Synthesis and evaluation of inhibitors of bacterial d-alanine: d-alanine ligases.* Chemistry & Biology, 1996. **3**(1): p. 37-44.

161. Meek, T.D., K.A. Johnson, and J.J. Villafrance, *Escherichia coli Glutamine Synthetase. Determination of Rate-Limiting Steps by Rapid Quench and Isotope Partitioning Experiments.* Biochemistry, 1982. **21**: p. 2158.

162. Pham, T.V., et al., *Mechanism-based inactivator of isocitrate lyases 1 and 2 from Mycobacterium tuberculosis.* Proceedings of the National Academy of Sciences, 2017. **114**(29): p. 7617-7622.

163. Raushel, F.M. and J.J. Villafranca, *Positional Isotope Exchange.* Critical Reviews in Biochemistry, 1988. **23**(1): p. 1.

164. Rose, I.A., *Positional Isotope Exchange Studies of Enzyme Mechanisms.* Advances in Enzymology and Related Areas of Molecular Biology, 1979. **50**: p. 361.

165. CDC. *Parasites - American Trypanosomiasis (also known as Chagas Disease).* Available from: https://www.cdc.gov/parasites/chagas/gen_info/detailed.html#intro.

166. Braga, M.S., et al., *Persistent infections in chronic Chagas' disease patients treated with anti-Trypanosoma cruzi nitroderivatives.* Revista do Instituto de Medicina Tropical de São Paulo, 2000. **42**(3): p. 157-161.

167. Hazleton, Keith Z., et al., *Acyclic Immucillin Phosphonates: Second-Generation Inhibitors of Plasmodium falciparum Hypoxanthine- Guanine-Xanthine Phosphoribosyltransferase.* Chemistry & Biology, 2012. **19**(6): p. 721-730.

168. Kicska, G.A., et al., *Transition State Analogue Inhibitors of Purine Nucleoside Phosphorylase from Plasmodium falciparum.* Journal of Biological Chemistry, 2002. **277**(5): p. 3219-3225.

169. Schramm, V.L., et al., *Transition-state analogs as inhibitors of the human and malarial hypoxanthine-guanine phosphoribosyltransferases.* Nature Structural Biology, 1999. **6**(6): p. 582-587.

170. Evans, G.B., et al., *Azetidine Based Transition State Analogue Inhibitors ofN-Ribosyl Hydrolases and Phosphorylases.* Journal of Medicinal Chemistry, 2008. **51**(4): p. 948-956.

171. Clinch, K., et al., *Third-Generation Immucillins: Syntheses and Bioactivities of Acyclic Immucillin Inhibitors of Human Purine Nucleoside Phosphorylase.* Journal of Medicinal Chemistry, 2009. **52**(4): p. 1126-1143.

172. Clinch, K., et al., *Acyclic phosph(on)ate inhibitors of Plasmodium falciparum hypoxanthine-guanine-xanthine phosphoribosyltransferase.* Bioorganic & Medicinal Chemistry, 2013. **21**(17): p. 5629-5646.

173. Allen, T.E. and B. Ullman, *Molecular characterization and overexpression of the hypoxanthine-guanine phosphoribosyltransferase gene from Trypanosoma cruzi.* Molecular and Biochemical Parasitology, 1994. **65**(2): p. 233-245.

174. Eakin, A.E., et al., *Hypoxanthine phosphoribosyltransferase from Trypanosoma cruzi as a target for structure-based inhibitor design: crystallization and inhibition studies with purine analogs.* Antimicrobial Agents and Chemotherapy, 1997. **41**(8): p. 1686-1692.

175. Xu, Y., et al., *Kinetic Mechanism of Human Hypoxanthine−Guanine Phosphoribosyltransferase: Rapid Phosphoribosyl Transfer Chemistry†.* Biochemistry, 1997. **36**(12): p. 3700-3712.

176. G. Ducati, R., R. S. Firestone, and V. L. Schramm, *Kinetic Isotope Effects and Transition State Structure for Hypoxanthine-Guanine-Xanthine Phosphoribosyltransferase from Plasmodium falciparum.* Biochemistry, 2017. **56**(48): p. 6368-6376.

177. Contreras-Sanz, A., et al., *Simultaneous quantification of 12 different nucleotides and nucleosides released from renal epithelium and in human urine samples using ion-pair reversed-phase HPLC.* Purinergic Signalling, 2012. **8**(4): p. 741-751.

178. Paul F. Cook , W.W.C., *Enzyme Kinetics and Mechanism*. 2007: Garland Science Publishing.

179. Rose, I.A., E.L. O'Connell, and S. Litwin, *Determination of the Rate of Hexokinase-Glucose Dissociation by the Isotope-trapping Method.* The Journal of Biological Chemistry, 1974. **249**: p. 5163.

180. Rose, I.A., *The isotope trapping method: Desorption rates of productive E·S complexes*, in *Methods in Enzymology*, D.L. Purich, Editor. 1980, Academic Press. p. 47-59.

181. Wenck, M.A., et al., *Steady-state kinetics of the hypoxanthine phosphoribosyltransferase from Trypanosoma cruzi.* Biochimica et Biophysica Acta (BBA) - Proteins and Proteomics, 2004. **1700**(1): p. 11-18.

182. Marr, J.J. and R.L. Berens, *Pyrazolopyrimidine metabolism in the pathogenic trypanosomatidae.* Molecular and Biochemical Parasitology, 1983. **7**(4): p. 339-356.

183. Cook, P.F. and W.W. Cleland, *Mechanistic deductions from isotope effects in multireactant enzyme mechanisms.* Biochemistry, 1981. **20**(7): p. 1790-1796.

184. Roy, S., et al., *Kinetic mechanism of Plasmodium falciparum hypoxanthine-guanine-xanthine phosphoribosyltransferase.* Molecular and Biochemical Parasitology, 2015. **204**(2): p. 111-120.

185. Bashor, C., et al., *Kinetic Mechanism of Adenine Phosphoribosyltransferase from Leishmania donovani†.* Biochemistry, 2002. **41**(12): p. 4020-4031.

186. Nakatani, H. and H.B. Dunford, *Meaning of diffusion-controlled association rate constants in enzymology.* The Journal of Physical Chemistry, 1979. **83**(20): p. 2662-2665.

187. Cerjan, C. and R.E. Barnett, *Viscosity dependence of a putative diffusion-limited reaction.* The Journal of Physical Chemistry, 1972. **76**(8): p. 1192-1195.

188. Brouwer, A.C. and J.F. Kirsch, *Investigation of diffusion-limited rates of chymotrypsin reactions by viscosity variation.* Biochemistry, 1982. **21**(6): p. 1302-1307.

189. Meola, M., et al., *The catalytic effect of Mg2+ and imidazole on the decomposition of 5-phosphoribosyl-α-1-pyrophosphate in aqueous solution.* Journal of Inorganic Biochemistry, 2003. **93**(3-4): p. 235-242.

190. Focia, P.J., S.P. Craig, and A.E. Eakin, *Approaching the Transition State in the Crystal Structure of a Phosphoribosyltransferase†,‡.* Biochemistry, 1998. **37**(49): p. 17120-17127.

191. Roy, S., et al., *Slow ligand-induced conformational switch increases the catalytic rate in Plasmodium falciparum hypoxanthine guanine xanthine phosphoribosyltransferase.* Molecular BioSystems, 2015. **11**(5): p. 1410-1424.

192. Miles, R.W., et al., *One-Third-the-Sites Transition-State Inhibitors for Purine Nucleoside Phosphorylase.* Biochemistry, 1998. **37**(24): p. 8615-8621.

193. A. Taylor, E., et al., *Acyclic Ribooxacarbenium Ion Mimics as Transition State Analogues of Human and Malarial Purine Nucleoside Phosphorylases.* Journal of the American Chemical Society, 2007. **129**(22): p. 6984-6985.

194. Rao, S.L.N. and A. Meister, *In vivo formation of methionine sulfoximine phosphate, a protein-bond metabolite of methionine sulfoximine.* Biochemistry, 1972. **11**(7): p. 1123-1127.

195. Ronzio, R.A. and A. Meister, *Phosphorylation of methionine sulfoximine by glutamine synthetase.* Proceedings of the National Academy of Sciences, 1968. **59**(1): p. 164-170.

196. Parsons, W.H., et al., *Phosphinic acid inhibitors of D-alanyl-D-alanine ligase.* Journal of Medicinal Chemistry, 1988. **31**(9): p. 1772-1778.

197. Reardon, J.E. and R.H. Abeles, *Mechanism of action of isopentenyl pyrophosphate isomerase: evidence for a carbonium ion intermediate.* Biochemistry, 1986. **25**(19): p. 5609-5616.

198. Reardon, J.E. and R.H. Abeles, *Time-dependent inhibition of isopentenyl pyrophosphate isomerase by 2-(dimethylamino)ethyl pyrophosphate.* Journal of the American Chemical Society, 1985. **107**(13): p. 4078-4079.

199. Lewandowicz, A. and V.L. Schramm, *Transition State Analysis for Human and Plasmodium falciparum Purine Nucleoside Phosphorylases.* Biochemistry, 2004. **43**(6): p. 1458-1468.

200. Silva, R.G., et al., *Arsenate and Phosphate as Nucleophiles at the Transition States of Human Purine Nucleoside Phosphorylase.* Biochemistry, 2011. **50**(13): p. 2701-2709.

201. Kline, P.C. and V.L. Schramm, *Purine nucleoside phosphorylase. Catalytic mechanism and transition-state analysis of the arsenolysis reaction.* Biochemistry, 1993. **32**(48): p. 13212-13219.

202. Tao, W., C. Grubmeyer, and J.S. Blanchard, *Transition State Structure of Salmonella typhimurium Orotate Phosphoribosyltransferase†.* Biochemistry, 1996. **35**(1): p. 14-21.

APPENDIX A

LIPID II STRUCTURE

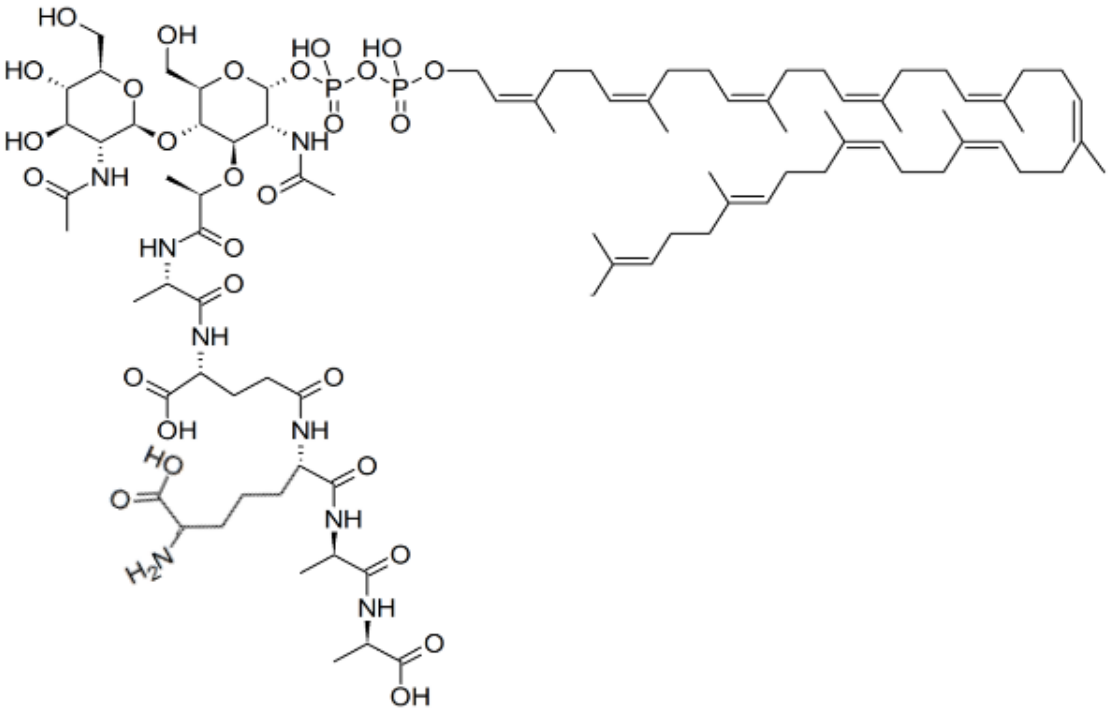

Lipid II shown with C50 and *N*-acetylmuramic acid (MurNAc)

APPENDIX B

SCRAMBLING OF GAMMA-[$^{18}O_4$]-ATP IN PIX

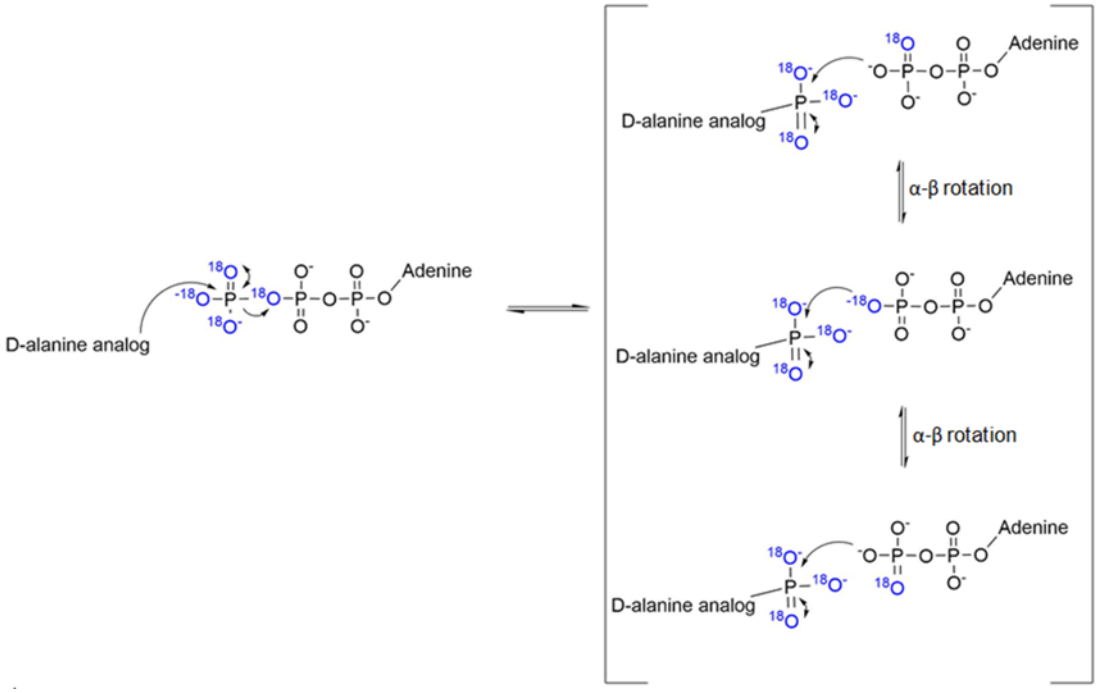

D-alanine or related analog is phosphorylated in the enzyme active site by ATP. If the β-phosphate is able to freely rotate around the α-β bond in the active site, the back reaction will yield a single [$^{18}O_4$]-γ-ATP for every two [$^{16}O^{18}O_3$]-γ-ATP molecules formed.

APPENDIX C

INTRINSIC TRYPTOPHAN FLUORESCENCE OF MTDDL-ATP COMPLEX

TREATED WITH 1-AMINOETHYLPHOSPHONATE

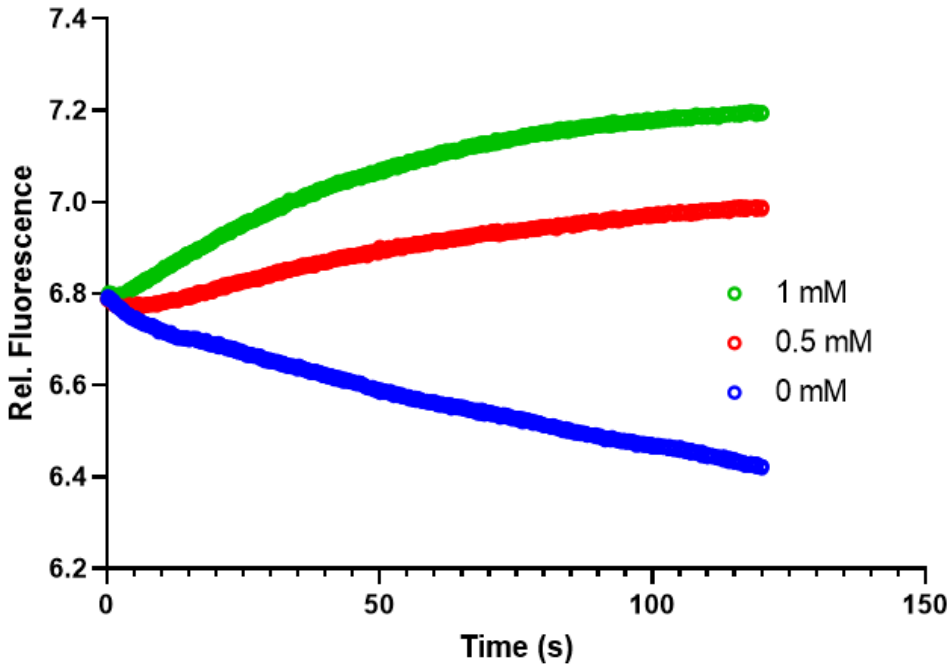

Concentration of 1-aminoethylphosphonate displayed in the figure legend. Photobleaching dominates signal.

APPENDIX D

REPRESENTATIVE CPM DISTRIBUTION FOR ION-PAIRING PURIFICATION

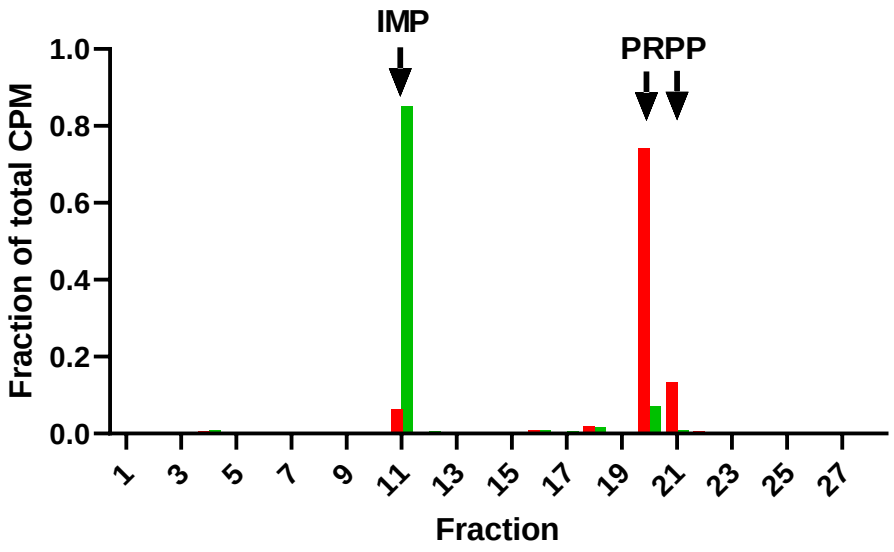

TcC HGPRT was incubated with [C1-^{14}C]PRPP and 50 μM hypoxanthine under conditions that resulted in high conversion (green) or low conversion (red) of substrate PRPP into product IMP.

APPENDIX E

ACTIVE SITE TITRATION OF TCC HGPRT

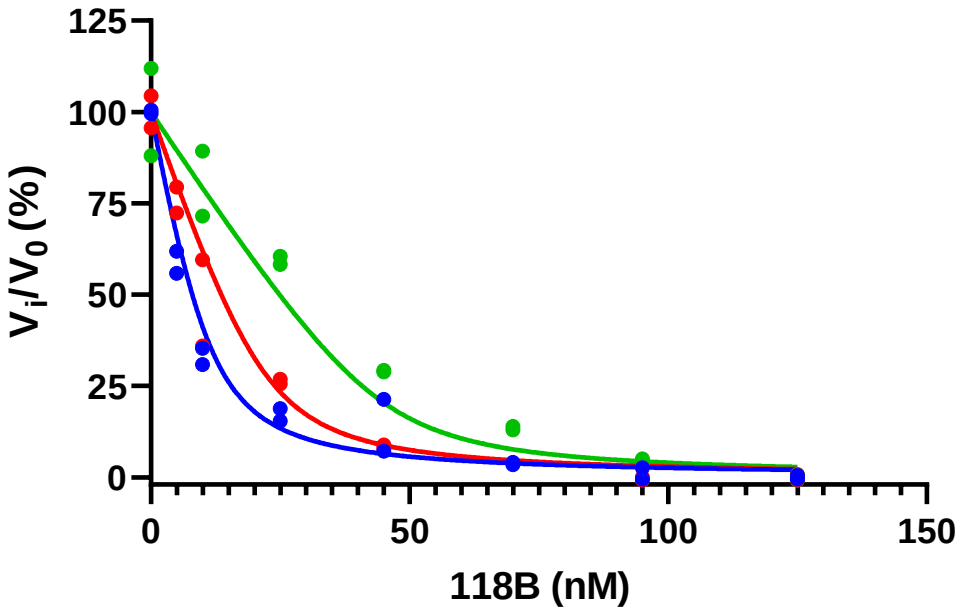

TcC HGPRT activity was measured with 25.8 nM (blue), 51.5 nM (red), or 103 nM (green) TcC treated with 0-125 nM of compound (**9**). Residual activity was fitted to (**eq. 3.10**) to yield an active-site fraction of (a) of= 0.48 ± 0.04.

APPENDIX F

INHIBITION OF TCC HGPRT

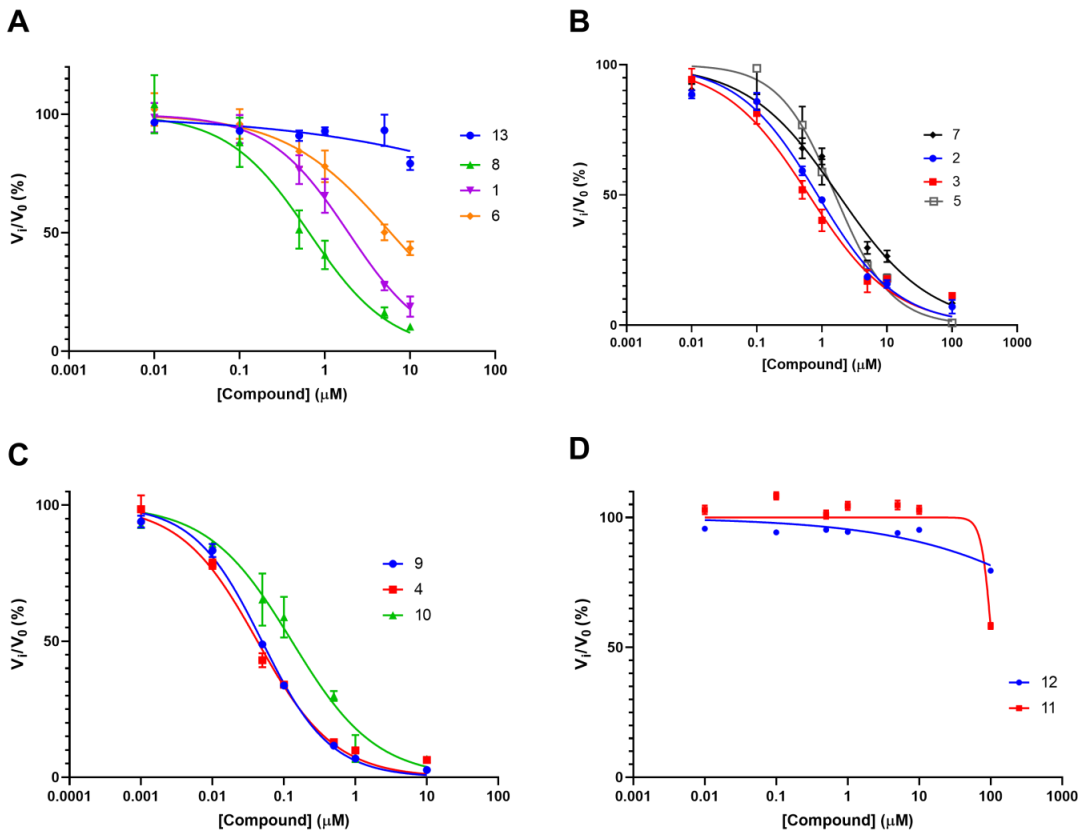

A-C Inhibition of IMP pyrophosphorolysis, measured with 42 nM TcC, 100 μM phosphate, and 500 μM IMP at 37 °C. **A)** Compounds tested between 0.01-10 μM. **B)** Compounds tested between 0.01-100 μM. **C)** Compounds tested between 0.001-10 μM. **D)** Inhibition of GMP synthesis of TcC treated with 0.01-100 μM of compound, measured with 12.5 nM of TcC, 1 mM PRPP, and 100 μM guanine at 37 °C. Legends indicated compounds tested. All data fitted to (**eq. 3.7**).

APPENDIX G

EFFECT OF GLYCEROL ON V/K FOR PRPP WITH TCC HGPRT

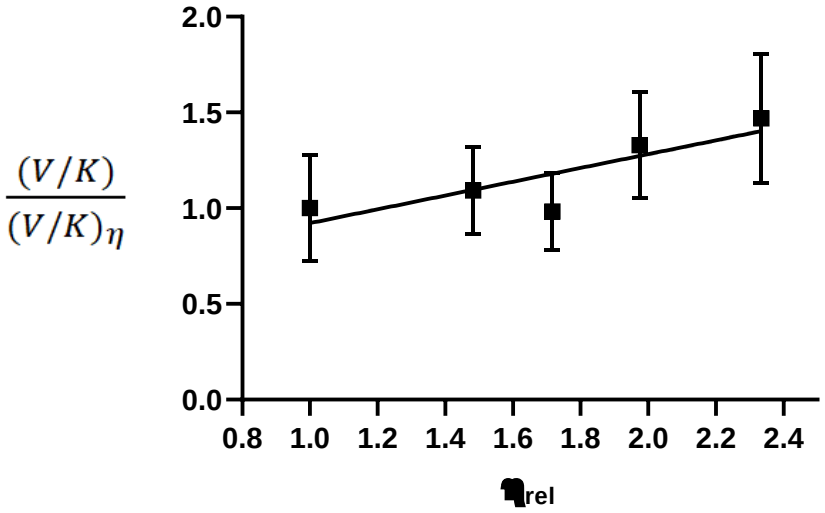

Apparent maximal velocities and Michaelis constants were obtained from plots of initial velocity vs. variable concentrations of 0 -200 μM PRPP containing 50 μM guanine, 12.5 nM TcHGPRT, 0-30% (w/v) glycerol (η_{rel} = 1-2.33) Fitting the data to a line produced a slope that was determined to be 0.4 ± 0.1 η^{-1} and a Y-intercept of 0.6 ± 0.2. Propagation of error on both V and *K* make the data refractory to interpretation.